TECHNISCHE UNIVERSITÄT WIEN

DISSERTATION

# Influence of Non-Superconducting Additions on the Pinning Behavior in $MgB_2$ Wires and Bulk Samples -a Comparative Study

ausgeführt zum Zwecke der Erlangung des akademischen Grades eines Doktors der technischen Wissenschaften unter der Leitung von

Ao. Univ. Prof. Dipl.-Ing. Dr. techn. Michael REISSNER

E138

Institut für Festkörperphysik

eingereicht an der Technischen Universität Wien

Fakultät für Physik

von

Saleh MOHAMMAD MSc

Matr.-Nr 0327353

Jahngasse 14/21

1050 Wien

Wien, am März 2008 Unterschrift

# Zusammenfassung

Ziel dieser Arbeit war das Studium des Einflusses verschiedener Substitutionen auf das Pinningverhalten von $MgB_2$ Drähten mittels Untersuchung der kritischen Stromdichten und magnetischer Relaxationen. Drähte mit unterschiedlicher Konzentration von SiC Beimengungen, sowie mit gleicher Konzentration aber unterschiedlichen Verbindungen (SiC, $B_4C$, $Al_2O_3$) wurden in einem Vibrationsmagnetometer gemessen. Die Ergebnisse werden mit jenen von Bulk-Proben verglichen, welche ohne und mit Substitution von Al und SiC hergestellt wurden, um den Einfluss des Herstellungsprozesses zu erfassen.

Die Feld- und Temperaturabhängigkeit der kritischen Stromstärke wurde mittels verschiedener Pinning Modelle analysiert. Aus der Zeitabhängigkeit des magnetischen Momentes wurden die mittlere effektive Aktivierungsenergie, Aktivierungs-energieverteilungen sowie der Zusammenhang zwischen Aktivierungsenergie und Stromdichte bestimmt und im Modell kollektiven Pinnings interpretiert.

Die Analyse der Pinningkraft weist stark auf Korngrenzen – Pinning als Hauptmechanismus hin. Aus der Temperaturabhängigkeit der kritischen Stromdichte wurde auf Δ/ Pinning als wahrscheinlichstem Prozess geschlossen.

Die Analyse der Relaxationsmessungen deutet ebenfalls auf 2D – Pinning hin.

**To my parents whose unconditional love has always been my strength**

# ACKNOWLEDGMENTS

I am thankful to God Almighty for all His blessings and kindness.

I would like to express my sincere appreciations and gratitude to my supervisor Ao. Univ.Prof. Dr. Michael Reissner for his continuous guidance, encouragement and support during my study in the Institute of Solid State Physics. He always has patiently and gently kept me on track.

Many thanks to Dr. Pavol Kovac and I. Husek of Slovakian Academy of Sciences, Bratislava for the $MgB_2$ wires preparation and to Dr. Ernst Bauer for two of the bulk samples. Thanks to Dr. Andrey Prokofiev and Mrs. Vanda Peter for the support in X-ray investigation and sample preparation and to Mrs. Monika Waas for providing the SEM pictures.

My special thanks go also to all people of the Institute of Solid State Physics who helped me continually.

My colleagues from Pakistan, Kamran Ali, Nasir Mehmood, Tahir Ali, Rao Tahir and Mohammad Atif I want to thank them for their support and nice company.

I am obliged to the Higher Education Commission of Pakistan for the financial support during the entire study period in Austria and to the Austrian Exchange Services OÄD team for their sincere services all the way long. I am thankful to Principal and staff of PPS/C Peshawar for the grant of the study leave.

I wish to acknowledge the moral support of my friends Dr. Shah Khusro, Dr. Abdul Bais, Atta-ur- Rahman, Rashid Ahmad, Hammad Hassan, Fakhr-e-Alam and Rehanullah. I am fortunate to have friends like Joher Ali who always has extended his utmost help when needed. A lot of prayers for my deceased uncle Shahbaz Khan who was very kind and was a source of inspiration for me.

I am grateful to all family members for their cooperation during this period, especially to Jehad Ali for taking care of all the matters at home.

Finally, I would like to extend my appreciations to my wife who was patient and kind enough to support and encourage me and to take very good care of our children Azlan and Hassan.

# Table of Contents

## Abstract

The aim of this work was to study the influence of different additions on flux pinning behavior of $MgB_2$ wires by investigation of the critical current density and magnetic relaxation. Wires with different concentration of SiC and with same concentration but different additives (SiC, $B_4C$, $Al_2O_3$) were measured in a vibrating sample magnetometer. The results are compared with those obtained from bulk samples prepared without and with substitution of Al and SiC to study the effect of preparation process.

The field and temperature dependence of the critical current density is analyzed in terms of different pinning models. From the time dependence of the magnetic moment, the mean effective activation energy, activation energy distributions and the current-energy relation were determined and interpreted in terms of collective pinning theory.

The analysis of pinning force strongly supports the grain boundary pinning as the main mechanism. From the temperature dependence of critical current density it is concluded that $\Delta l$ core pinning is most probable.

The analysis of the relaxation measurements also favors 2D pinning.

# Chapter1 Introduction

The discovery of superconductivity in metallic $MgB_2$ [Nag01] got high attention of the scientific community because of the highest $T_c$ ever found for non-cuprate superconductors. Until then the highest superconducting transition in metallic compounds was known to be 33 K for non Cu oxide superconductors [Tan91], which for long time also was believed to be the BCS limit for such materials. The simple structure, large coherence length, absence of weak links, two gap superconductivity, easy and cheap preparation and availability are some of the attractive points to focus on this material. In the last seven years roughly more than 2500 studies appeared with an average of 1 per day including some excellent reviews [e.g. Buz01, Maz03, Mur05, Dou05, Eis07]

Many of the characteristics and behaviors of $MgB_2$ have been experimentally observed and theoretically explained. Despite of the enormous work on this material there are still open questions like the investigations of new routes to improve pinning, how to avoid the strong field dependence of the critical current density, the granularity and anisotropy etc. Both theoretical and experimental work is under way to bring $MgB_2$ into the market, where it is expected to be able to replace for example the expensive classical Nb based superconductors in high magnetic field applications.

The critical current density $J_c$ in $MgB_2$ is reported to decrease rapidly with magnetic field which is considered to be due to the lower value of upper critical field $H_{c2}$ [Eis07] and the presence of only weak pinning centers. Different techniques have been reported to improve $J_c$ in magnetic fields, some of which include chemical doping, mechanical alloying, irradiation and magnetic shielding. Amongst these methods, the most widely used method is doping of various particles and compounds which either result in substitution at Mg or B sites or then appear as inclusions to act as additional pinning centers. Many elements have been tried for substitution at Mg site in which Zr, Ti and Al were found to be more effective. Doping with Zr and Ti resulted in an improvement of $J_c$ at low fields, while Al causes a $J_c$ improvement at low field along with a decrease in $T_c$.

The other way of particle doping is substitution at B site which is considered to be more effective as superconductivity is believed to be in the B lattice. Elements reported for substitution at the B site include C, O, F, Si, and Be in which C and O substitution have shown higher $H_{c2}$ at low temperature and improved $J_c$ at high fields [Mur05, Sol03].

Various compound were also used for doping in to $MgB_2$ including SiC [Dou02], $Y_2O_3$ [Wan04], $SiO_2$ [Mat03], $Li_2CO_3$, $NaCO_3$ [Ued04] in which SiC doping has shown to improve both $J_c$ and $B_{irr}$ as well as $H_{c2}$. Dou et al [Dou05] have investigated the effect of SiC substitution reporting a significant improvement on $J_c(B)$ dependence.

Large efforts have been undertaken to produce wires and tapes for future applications.

There are several studies on bulk materials concerning the pinning behavior on chemically doped samples in more detail than only by measuring the field and temperature dependence of the critical current density, but only very few such investigations on wires and tapes. A conclusive comparison of the reported results is difficult, because the pinning behavior is strongly dependent on the preparation conditions like sintering temperature, purity of starting material, chosen sheath material for the wires etc.

In the present work a systematic investigation of the pinning behavior is carried out both on $MgB_2$ wires with different additives, but also on some bulk samples. All wires had the same Nb-sheath and were prepared exactly in the same way, thus allowing to figure out only the effect of substitution.

In one of the $MgB_2$ wire series, the influence of different concentration of SiC inclusions on the pinning behavior was investigated. In order to study the substitution effect of different additives on the pinning behavior, a second series of $MgB_2$ wires was investigated using different additives (SiC, $B_4C$, $Al_2O_3$) while their concentration was kept constant.

In a third series three $MgB_2$ compounds were investigated. One with 10% SiC substitution, one with 8% Al substitution and one without any additive. The first one was intended to allow a comparison of a bulk with a wire sample of same substitution state. A comparison of the first and the second one allows information about difference by substitution on Mg or B site. The third one is the reference to all the others which have some additives incorporated.

Beside the field and temperature dependence of the critical current density magnetic relaxation measurements were performed on all investigated samples. During the latter method the time dependence of the magnetic moment at constant field and temperature is reported. Such measurements usually allow a deeper insight into the pinning mechanisms.

One further motivation for this work was the fact that it is not clear if the pinning behavior in $MgB_2$ compounds resembles more the one in classical metallic superconductors or in the high temperature superconductors. As different analyses are used for both cases, a critical comparison of these methods in case of $MgB_2$ is attempted.

## 1.1 Crystallographic and electronic structure of $MgB_2$

The structure of $MgB_2$ had been studied long before its discovery as superconductor [Nag01]. It crystallizes in the structure, which is similar to graphite. It consists of hexagonal honey-comb-like planes of boron atoms separated by planes of magnesium atoms with magnesium centered above and below the boron hexagon [Mur05] (Fig. 1.1).

Mg is at the center of the hexagonal prism of boron atoms at a distance of 2.5 Å. Each B atom is surrounded by three other B atoms forming equilateral triangles at distances of $a/1.732$ while the Mg atoms are separated by one lattice constant $c$ [Mur05]. In $AlB_2$ type structure the lattice parameters $a$ and $c$ are typically in the range of 3.0-3.2 Å and 3.0-3.4 Å respectively, while $MgB_2$ has average values ($a$ = 3.08 Å, $c$ = 3.51 Å) [Jor01, Oik02, Pra01, Nis01, Lee01, Vog01, Gon01].

In graphite each carbon atom is surrounded by three other carbon atoms forming strong σ-bonds while the fourth valance electron moves above and below the plane to form π-bonds. In case of $MgB_2$ the in-plane σ-bonds are not always occupied due to less valance electrons than in carbon and thus the lattice vibration can form strong electron pairs causing superconductivity in this material as reported by many groups before and after its discovery as superconductor [Nag01].

The two imperfectly filled σ-bands cause the observed 2D properties while 3D behavior is due to electrons and holes along the π-bands [Kar01, An01, Maz03].

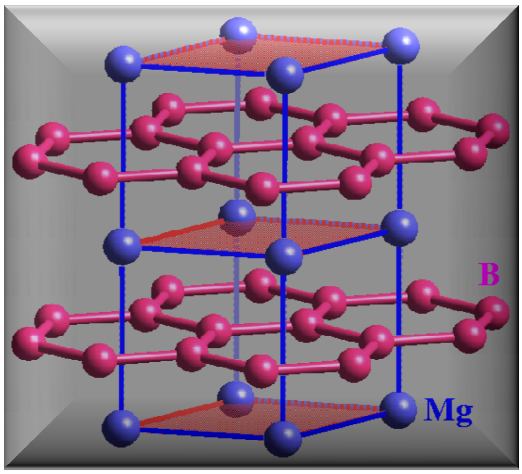


**Figure 1.1 Crystal structure of $MgB_2$ [Mur05].**

The existence of the two bands give rise to two gaps, a large one in the σ-bands and a small gap in the π-band due to different electron-phonon coupling in these bands.

There are several experimental results indicating the presence of the second gap in $MgB_2$ e.g. specific heat measurements [Bou01, Bou01b, Wan01, B], photoemission spectroscopy [Tsu01, Tsu03, Sou03] and scanning tunneling microscopy [Sha01, Kar01]. From these and other experimental results the two energy gaps were found to range from 1.7 to 2.8 meV in case of the Δπ-gap and from 6.2 to 10 meV for the Δσ-gap.

## 1.2 Comparison with other superconductors

On the basis of some of the properties $MgB_2$ resembles low temperature superconductors with a very high transition temperature $T_c$. These properties include isotope effect [Hin01, Bud01b], linear temperature dependence of upper critical field with a positive curvature near $T_c$ [Bud01a] and a decrease of $T_c$ (onset) with increasing field [Lee01, Xu01]. On the other hand the temperature dependence of penetration depth λ(T), the sign reversal of Hall coefficient near $T_c$ [Jin01] and the layered structure show similarities of $MgB_2$ with high $T_c$ superconductors.

**Table 1.1 Comparison of superconducting parameters of $MgB_2$ [Buz01] with YBCO, BSCCO and $Nb_3Sn$ [Cyr91].**

| Parameters | $MgB_2$ | $YBa_2Cu_3O_7$ | $Bi_2Sr_2Ca_2Cu_3O_{10}$ | $Nb_3Sn$ |
|---|---|---|---|---|
| $T_c$ (K) | 39 | 90 | 110 | 18 |
| Upper critical field $H_{c2}(0)$//ab (T) | 14-39 | 150 | 250 | 24 |
| Upper critical field $H_{c2}(0)$//c (T) | 2-24 | 40 | 30 | 24 |
| Coherence length $\xi_{ab}(0)$ (nm) | 3.7-12 | 1.5 | 1.4 | 3 |
| Coherence length $\xi_c(0)$ (nm) | 1.6-3.6 | 0.4 | 0.2 | 3 |
| Penetration depth $\lambda_{ab}(0)$ (nm) | 85-180 | 150 | 200 | 80 |
| Penetration depth $\lambda_c(0)$ (nm) | 0.4-16 | 600 | 1000 | 80 |
| Ginzburg-Landau parameter κ | 26 | 52 | 70 | 45 |

Some of the basic superconducting properties of $MgB_2$ [Buz01] in comparison with YBCO, BSCCO and Nb3Sn are given in Table 1.1. Some controversies about the mechanism of superconductivity in $MgB_2$ still remain unresolved but most of the scientific community supports the BCS mechanism of superconductivity in $MgB_2$.

Although the cuprate superconductors have higher transition temperatures than $MgB_2$, their applications are limited due to short coherence lengths resulting in a sharp decrease of $J_c$ with field, high anisotropy which needs grain alignment for application and their rare and comparatively expensive constituents. $MgB_2$ on the other hand has well connected grains large coherence length, low anisotropy and inexpensive constituents. $MgB_2$ can be used in liquid hydrogen (≈20 K) or in cryocoolers which is cheap compared to widely used metallic superconductors like $Nb_3Sn$ using expensive liquid helium for operation.

## 1.3 Preparation

One of the important advantages of $MgB_2$ is its easy availability as it was discovered half century before its discovery as superconductor [Nag01]. $MgB_2$ has been prepared as bulk, film, and single crystalline material but also as wires and tapes. For films typical methods are pulsed laser deposition, Mg diffusion and magnetron sputtering [Buz01]. Single crystals are prepared with solid-liquid reaction and vapor transport methods.

Mg diffusion method [Can01] can also be used for bulks, wire and tapes where Mg and B are heated in Nb or Ta tubes and heat treated up to 900°C. Hot isostatic pressing (HIP) is also reported [Fre01] to be suitable for bulks and wires.

For wires and tapes, the most popular method is the powder in tube (PIT) method. In this method there are two routes. One is to fill a metal tube with reacted powder of $MgB_2$ (known as ex-situ reaction) [Gra03], while the second is to put Mg and B powder in metal tube and let it react to $MgB_2$ afterwards (known as in-situ reaction). The metal tubes are drawn to wires or cold-worked to tapes, followed by heat treatment between 600 and $1000^0$C.

The critical current density of pure bulk $MgB_2$ can also be improved by changing the crystallinity [Buz01]. Poor crystallinity results in higher $H_{c2}$, the pinning force can be enhanced by decreasing the grain size and $J_c$ can be increased by increasing the density.

In case of wires and tapes one has to take into account, that Mg is very volatile and reactive. Therefore suitable metals should be used for sheathing to avoid degradation of superconductivity. As pointed out by Wang et al. [Wan04] that in the choice of sheathing material, one has to look on compatibility, ductibility, thermal and electrical conductivity

and cost of the metals to be used. There are very few metals which were found insoluble and which do not form intermetallic compounds with $MgB_2$. These include Ag, Cu, Fe, Mo, Ni, Nb, V, Ta, Hf, W and stainless steel. Amongst these sheath materials Fe has been reported to have given best field performance and $J_c$ value [Jin01b, Sol01, Wan01, Suo01] however Fe was reported to form an interface layer as a result of its reaction with $MgB_2$ [Kov02, Kov03]. Schlachter et al [Sch06] have described that a conductive metal can be added as buffer layer to the sheath composite which acts as parallel shunt in order to improve thermal stability.

The Nb has been reported [Gol01, Fen03, Kov06] to be one of the least reactive metals with Mg or B and therefore is suitable for using it as sheathing metal.

## 1.4 Pinning Mechanism

$MgB_2$ is a type 2 superconductor, which is charactized by two critical fields. Below the lower critical field $H_{c1,}$ the superconductor is in a field free region called Meissner phase, where the sample is shielded from external fields by supercurrents flowing along the surface of the sample. This field is rather low. At fields higher than $H_{c1,}$ flux enters the superconductor in quantized form, known as flux lines or vortices [Abrikosov]. A vortex carries one flux quantum. It can be considered to consist of a normal conducting core separated by supercurrents from the superconducting matrix. The diameter of such flux line is determined by the coherence length. These vortices repel each other with a force similar to the Lorentz force of electro-dynamics thus forming a hexagonal lattice [Abr57, Fri63]. The higher the external field, the higher the density of the flux lines. If the density reaches a value that vortices overlap, superconductivity is lost. The appropriate field is the upper critical field $H_{c2}$. In real superconductors interaction takes place between flux lines and pinning centers (normalconducting regions like defects, dislocations, precipitates, grain boundaries etc) due to a gain in the condensation energy if a flux line goes through a pinning center. As a result of this interaction, the vortices are trapped at the pinning centers as long as the pinning forces are larger than the driving force, which is due to the fact that new flux lines, which are formed at the surface by an increase of the external field, force the others to go into the interior of the superconductor. As a result a gradient in the flux line density, and therefore in the field distribution appears. This field gradient determines the current density in the superconductor. If the pinning force equals the driving force the maximum current density is reached. The superconductor is in the critical state, the respective current is called critical current density $J_c$ [Bea62, Bea64]. Smallest energy inputs like thermal activation, quantum tunneling or mechanical energy can free the flux lines from the pinning centers, thus leading to a reduction of the field gradient

and therefore of the current density. This process is known as relaxation and manifests itself in a reduction of the magnetic moment which is proportional to $J_c$. The measurement of the time dependence of the magnetic moment for different temperatures and fields gives the possibility to investigate the pinning mechanisms active in the sample. Relaxation measurements are therefore a good method to complement direct transport measurements of $J_c$.

In the critical state one can write

$$J_c(B) \times B = -F_p(B) \qquad 1.1$$

where $F_p(B)$ is the pinning force per unit volume exerted by the vortices on each other, $B$ the spatially average induction field and $J_c$ is the critical current density.

According to Dew-Hughes [Dew74], there are two types of pinning centers. The first one is known as Δκ pinning which arises from small changes in Ginzburg-Landau parameter κ due to a change in normal state resistivity, compositional fluctuations, non-uniform distribution of dislocations or martensite transformations. The second one is the so-called 'normal pinning' which is due to the presence of non-superconducting particles. These pinning centers give rise to two kinds of pinning interactions namely magnetic interaction and core interaction. Magnetic interaction takes place if the size and spacing of pinning centers are larger than the penetration depth $\lambda$ of the superconductor, however if the size or spacing of pinning center is smaller than $\lambda$ then the interaction is said to be core interaction. The pinning force $F_p(h)$, with $h = H/H_{c2}$, in case of magnetic and core interaction and for different geometry of the pinning centers are given in Table 1.2 [Dew74].

Point pinning centers are those whose dimensions are smaller than the inner spacing of flux line, *d.* A point pining center can interact with only one flux line. Surface pinning centers are those in which two of their dimensions are greater than *d,* which includes grain boundaries, staking faults, dislocation arrays, and twin boundaries etc. They have a strong influence when the surface is parallel to the direction of Lorentz force. For volume pins, all dimensions are greater than *d* e.g. large precipitates and thick walls dislocations.

**Table 1.2 Pinning interactions with their respective pinning functions after Dew-Hghes [Dew 74]**

| Type of interaction | Geometry of pinning center | Type of pinning center | Pinning function | Position of maximum |
|---|---|---|---|---|
| magnetic | volume | normal | ~ $h^{0.5}$ (1-$h$) | 0.33 |
| | | ΔK | ~ $h^{0.5}$ (1-2$h$) ΔK | 0.17 |
| core | volume | normal | ~ $(1-h)^2$ | - |
| | | ΔK | ~ $h$ (1-$h$) ΔK | 0.5 |
| | surface | normal | ~ $h^{0.5}$ $(1-h)^2$ | 0.2 |
| | | ΔK | ~ $h^{1.5}$ (1-$h$) ΔK | 0.6 |
| | point | normal | ~ $h$ $(1-h)^2$ | 0.33 |
| | | ΔK | ~ $h^2$ (1-$h$) ΔK | 0.67 |

The high value of the Ginzburg-Landau parameter κ found or $MgB_2$ (Tab. 1.1) suggests that core interaction is the dominant pinning mechanism in this superconductor. There are two types of core pinning known, namely $\Delta T_c$ and $\Delta l$ pinning. $\Delta T_c$ pinning is due to the variation of $\kappa$ caused by the disorder in the transition temperature while $\Delta l$ pinning is due to the variation in mean free path $l$. Griessen et al [Gri94] have reported $\Delta l$ pinning as the dominant mechanism in $YBa_2Cu_3O_7$ and $YBa_2Cu_3O_7$ films. Making investigation on bulk $MgB_2$ samples Qin et al [Qin02] have concluded that $\Delta T_c$ is the dominant pinning mechanism. The same was reported by Prischepa et al [Pri03] for $MgB_2$ thin films. On the other hand, Yaun et al [Yau05] have reported that in carbon doped samples synthesized under ambient pressure $\Delta T_c$ pinning seems to be dominant, whereas the same samples synthesized under high pressure show $\Delta l$ pinning at low temperature and $\Delta T_c$ pinning at high temperature. Another study on $MgB_2$ thin films on the basis of a $J_c(T)$ analysis reports on a superposition of both $\Delta T_c$ and $\Delta l$ pinning [Xu03].

As mentioned relaxation measurements can also be used to study the flux pinning mechanism in $MgB_2$. The normalized relaxation rate in $MgB_2$ has been reported to be smaller than in high temperature superconductors [Mar04, Wen01, Jin03, Fen03, Mum01] which means the pinning is stronger than in HTS.

In 1962 Anderson suggested that the hopping of vortices out of their pinning sites is triggered by thermal activation [And62] according to an Arrhenius relation $\tau = \tau_0 exp\left(\frac{U}{KT}\right)$ where $\tau_0$ is the hopping attempt time and $U$ the effective activation energy which increases monotonically with time resulting in a logarithmic time dependence of magnetization. Thermally activated flux motion causes a decrease in effective activation energy and therefore $U$ is a decreasing function of current density. The dependence of

activation energy on current density is very important to study the vortex dynamics of the superconductors, because its special dependence is proposed from theory according to different pinning mechanisms. Anderson and Kim [And62,64] assumed a linear $U(J)$ relation with a single value of activation energy. An extension of this theory replaces the mean effective barrier by a spectrum of activation energies [Hag89].

The assumption of a linear $U(J)$ leads to an unphysical V-notch shape pinning potential [Bea69]. For a realistic pinning potential, the $U(J)$ relation is non-linear. Maley et al [Mal90] have proposed a method to determine the $U(J)$ relation from relaxation measurements without any prior assumption. The Anderson-Kim behavior is obtained by the tangent on the $U(J)$ curve at the current density, defined by the field and temperature applied during the measurement. The extrapolation of this tangent to $J = 0$ gives $U_0$ which can largely differ from the real value if the $U(J)$ relation is non linear.

For randomly distributed weak pinning centers, collective pinning theory can be usd to interpret the $U(J)$ relation. Here it is assumed that flux lines are elastic, and that the volume of the moving flux line bundle change with current density.

Only few papers are reporting on relaxation measurements on $MgB_2$. Most of them deal with bulk compounds. A clear picture of pinning could not be drawn up to now. Contradictory results are obtained from analyses which are based on strong pinning models as introduced for explaining pinning in classical metallic superconductors like $Nb_3Sn$, and from analyses which are used to describe the weak pinning behavior in high temperature superconductors.

In this work a systematic study on $MgB_2$ wires was performed. The aim was twofold. On the one hand the influence of different substitutions on critical current density and pinning was investigated, on the other hand different models explaining field, temperature, and time dependence of the magnetic moment used to get information about possible pinning mechanisms were performed. The obtained results are compared with those obtained from bulk samples.

# Chapter 2: Experimental

## 2.1 Samples

### 2.1.1 Preparation methods

Three series of samples in the shape of wires and bulk with and without particle addition were prepared. The first series contains $MgB_2$ wires with Nb sheaths with different concentration (0 wt%, 3 wt%, 10 wt%, 20 wt%) of SiC inclusions. In the second series the concentration of different additives (SiC, $B_4C$ and $Al_2O_3$) was held constant (10 wt%). In the third series three bulk samples, one pure $MgB_2$, one with 8 wt% Al and one with 10% SiC were combined. The investigated samples with their symbolic representation are given in Table 2.1.

All Nb sheathed wires under study were prepared using in-situ PIT techniques. Commercially available Mg (99.8% Alfa Aesar) of particle size about 20 micrometer, B (99% Alfa Aesar) with particle size of 1 micrometer and SiC (0 wt%, 3 wt%, 10 wt%, 20 wt%), $B_4C$ (10 wt%), $Al_2O_3$ (10 wt%) nano particles were put into niobium tubes with 3 mm inner diameter (ID) and 4.5 mm outer diameter (OD) and were mixed by ball milling for 30 minutes. The relation of core to sheath was approximately 1:2. The tube was closed and drawn by rotary swaging to around 3 mm in diameter followed by subsequent two axial rolling into rectangular wires of 1 mm size. Heat treatment was carried out in highly pure flowing Ar at 650$^{o}$C for about 30 minutes followed by furnace cooling to room temperature.

In case of bulk samples a thick wire with 10 wt% SiC addition, was prepared in the same way as the $MgB_2$/Nb wires, but the diameter of the Nb tube was large (2.4 mm) so that the superconducting properties of the core can be assumed to be more like bulk than wire.

**Table 2.1 $MgB_2$/Nb wires and bulk samples with nano particles additions.**

| Sample | Compounds | Label |
|---|---|---|
| 1 | $MgB_2$/Nb Wire Reference | 0% SiC |
| 2 | $MgB_2$/Nb Wire +3% SiC | 3% SiC |
| 3 | $MgB_2$/Nb Wire +10% SiC | 10% SiC |
| 4 | $MgB_2$/Nb Wire +20% SiC | 20% SiC |
| 5 | $MgB_2$/Nb Wire +10% $B_4C$ | 10% $B_4C$ |
| 6 | $MgB_2$/Nb Wire +10% $Al_2O_3$ | 10% $Al_2O_3$ |
| 7 | $MgB_2$ Bulk Pure | Pure |
| 8 | $MgB_2$ Bulk + 8% Al | Al |
| 9 | $MgB_2$ Bulk + 10% SiC | SiC |

### 2.1.2 Mass and density calculation

To avoid a possible change in the superconducting properties by the removal of the Nb sheath, the DC magnetization measurements were carried out with the Nb sheath. As the mass of superconductor is the most important parameter for the analysis of the data, a thorough determination of mass and density of the $MgB_2$ core were extremely important.

Pieces of length 4.5 ± 0.2 mm were cut from each wire. Both ends were polished using silicon carbide paper in a polishing machine (ECOMET 3 from BUEHLER). The influence of water usage to avoid heat generation during the polishing process was shown to result in a degradation of the superconducting properties up to a maximum of 20%.

Pictures of both cross-sectional sides of each of these pieces were taken in an optical microscope (Polyvar from Reichert-Jung) using a magnification of 50. A typical image of the cross-section is shown in Fig 2.1. To take into account the slightly irregular shape of core and sheath, the area ratio $A_{core}/A_{total}$ (filling factor $f$) was determined by cutting out both areas from the photographs and by comparing the masses of the thus obtained two pieces of paper ( $m^p_{Nb}$ and $m^p_{core}$) with the total mass of paper ($m^p_{total}$)

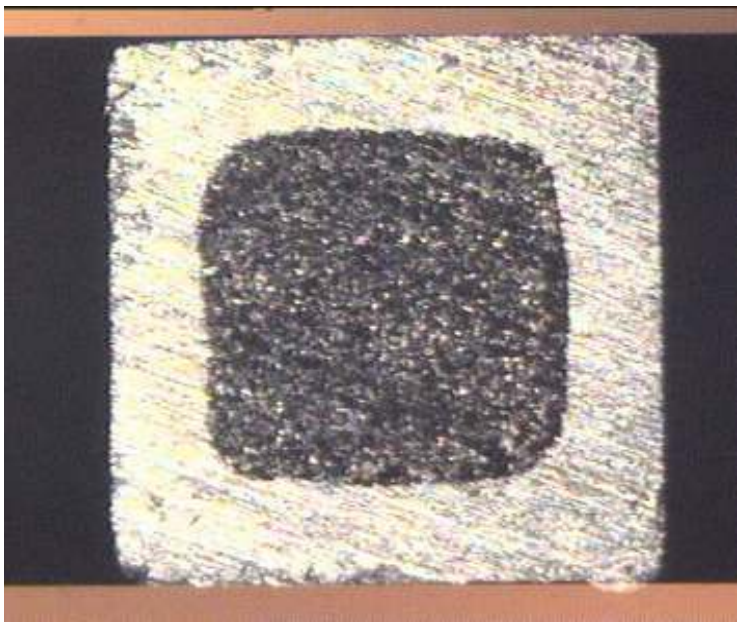

**Figure 2.1 Typical cross-section of $MgB_2$/Nb wire with 10% $B_4C$ addition.**

**Table 2.2 Dimensions of the core of $MgB_2$ Nb sheathed wire and bulk samples.**

| sample | $mass_{(total)}$ (mg) | length (mm) | $mass_{(core)}$ (mg) | area $_{(core)}$ $(mm)^2$ | density $_{(core)}$ $(g/cm^3)$ |
|---|---|---|---|---|---|
| 0% SiC | 33.2511 | 4.515 | 6.44 | 0.571 | 2.49 |
| 3% SiC | 31.8890 | 4.350 | 5.21 | 0.572 | 2.09 |
| 10% SiC | 32.2846 | 4.410 | 5.64 | 0.565 | 2.26 |
| 20% SiC | 33.6839 | 4.700 | 7.36 | 0.590 | 2.65 |
| 10% $B_4C$ | 33.9216 | 4.530 | 6.71 | 0.556 | 2.67 |
| 10% $Al_2O_3$ | 32.1245 | 4.470 | 6.56 | 0.614 | 2.39 |
| Pure | 17.1861 | 5.331 | 17.18 | 1.792 | 1.80 |
| Al | 25.2611 | 6.515 | 25.26 | 1.874 | 2.07 |
| SiC | 11.5910 | 2.516 | 11.59 | 2.277 | 2.02 |

$$\frac{\mathrm{A_{core}}}{\mathrm{A_{total}}} = \frac{m^p{}_{core}}{m^p{}_{total}} = f$$

The area of Nb can be calculated using the filling factor *f*

$$A_{Nb} = (1 - f)A_{total} \qquad 2.1$$

The mass of the core is determined

$$m_{core} = m_{total} - \rho_{Nb} A_{Nb} L \qquad 2.2$$

where *L* is the length of the wire.

The density of niobium used for the wire preparation, was calculated taking a long piece with a defined geometry (5 cm x 0.23 cm x 0.02 cm) . The calculated value ($\rho_{Nb}$, = 8.0067 g/cm$^3$) was very near to the theoretical value (8.00 g/cm$^2$). Masses and dimensions for all the samples are given in Table 2.2.

### 2.1.3 X-Ray Diffraction

To study the phase purity and to calculate lattice parameters, X-ray diffraction investigations were performed. The core mass was ground to powder and X-ray measurements were carried out by a 2Θ scan between 10 and 80 degrees with a Siemens X-ray diffractometer (D5000) using Cu$K_\alpha$ radiation. The corresponding X-ray tube voltage and current were 35 kV and 35 mA, respectively. The step size was 0.02 degree and the step time 10 s. The fitting of the measured X-ray pattern for evaluation of the cell parameters was performed by Powder Cell 2.4 [You03].

### 2.1.4 Scanning electron microscopy (SEM)

SEM investigations were carried out to study the microstructure of the samples. The samples were polished with fine silicon carbide paper using different polishing machines (Planopol 3 and Knoth-Ror from Struers). The SEM images of cross-sections both parallel and perpendicular to wire axis, were taken using XL30 ESEM Philips machine with a magnification of 1000 at 20 kV.

## 2.2 Magnetic measurements

All DC magnetic measurements were performed by a 9 T vibrating sample magnetometer (VSM) of Quantum Design Physical Property Measurement System (PPMS) with a vibrating frequency of 40 Hz and amplitude of 2 mm.

### 2.2.1 Transition temperature

To determine the transition temperature ($T_C$), the specimen were mounted in a standard brass sample holder and fixed with two quartz cylinders. After installing, the samples were cooled from room temperature to 1.9 K in zero magnetic field and then 100 Oe DC magnetic field was applied parallel to the wire axis. The magnetic measurements were recorded in the zero field cooled (ZFC) condition up to above $T_c$ with a temperature sweep rate of ~1 K/min. The temperature was then decreased under the same conditions to obtain the field cool (FC) curve. The onset temperature $T_c$ was determined from the ZFC curve to be the first point deviating from the zero moment line. The width of the transition temperature ($\Delta T_c$) was calculated using a 10 to 90% criterion.

### 2.2.2 Upper critical field

Upper critical fields ($H_{c2}$) were determined from $M(T)$ measurements performed at different fields. The used fields are equal to the upper critical fields for those temperatures, for which the diamagnetic signal vanishes (equal to $T_c$ for the given field).

### 2.2.3 Hysteresis and relaxation measurements

The samples were cooled to the measuring temperature from above $T_c$ in zero magnetic field. Magnetic hysteresis loops were then recorded with a constant sweep rate of 63 Oe/s between -2 and 9 T. These *M-H* curves were recorded for each sample in the temperature range between 4.2 and 30 K.

For the relaxation measurements, the field sweep was interrupted at 1 and 3 T both in increasing and decreasing fields and the time decay of magnetic moment was recorded for up to 30 minutes. Such relaxation measurements were also carried out at different fields in the range between 1 T and the irreversibility field for one temperature (10 K) in order to obtain the field dependence of the relaxations for all samples.

The obtained magnetization contains both a reversible and an irreversible part, and because only the irreversible part shows time dependence, the reversible part has to be subtracted from the measured total moment. This reversible magnetization is determined as the average of the increasing and the decreasing branch of the hysteresis loops assuming the irreversible magnetization at a given field is the same for increasing and decreasing field. This assumption is true only for a system with pure bulk pinning. In case of surface pinning the irreversible magnetization shows a difference for increasing and decreasing fields.

## 2.3 Analyses

### 2.3.1 Critical current density

The critical state model developed by C. P. Bean [Bea62,64] gives a relation between critical current density ($J_c$) and irreversible magnetization. $J_c$ was determined from the hysteresis loops using an extended Bean critical state model [Che89], which for a bar shape sample is given by

$$J_c(\mathrm{A/cm^2}) = \frac{20\Delta M}{a\left(1-\frac{a}{3b}\right)}$$

where $\Delta M$ (emu/g) is the width of the hysteresis loop, $a$ (cm) the width and $b$ (cm) the length of the bar shaped sample perpendicular to the applied field.

### 2.3.2 Pinning force

The pinning force is given by [Cam72]

$$\overrightarrow{F_p} = \overrightarrow{J_c} \times \vec{B}$$

If only one pinning mechanism is active in the whole temperature range, the field dependence of $F_p$ should scale for all temperatures, if $F_p$ is normalized to its maximum value and $B$ by $B_{c2}$. From the shape of the thus obtained curves information about pinning mechanisms are possible [Dew74].

### 2.3.3 Mean effective activation energy

As a first approximation, the magnetization obtained from relaxation measurements shows a logarithmic time dependence which can be analyzed within the Anderson flux creep theory [And62] which assumes the movement of flux lines to be triggered by thermal activation over barriers which have all the same height $U_0$.

With the assumption of a linear dependence of the effective barrier height (*U)* on the current density *J*, *U* is given by [And64]

$$U(J) = U_0 - JV_c BX = U_0\left(1 - \frac{J}{J_c}\right) \qquad 2.3$$

where *X* is the hopping distance and $V_c$ the volume of the jumping flux bundle. In this theory X and $V_c$ are assumed to be constant and independent of *T* and *J.* Using the flux diffusion equation [Beas69]

$$\frac{\partial B}{\partial t} = \nabla\left[B_a X \nu_0 exp\left(\frac{-U}{k_B T}\right)\right]$$

where $B_a$ is the local flux density, $\nu_0$ the attempt frequency and $k_B T$ the activation energy, the logarithmic time dependence of the current density can be derived as

$$M(t,T) = M_0\,(T)\left[1 - \left(\frac{k_B T}{U(T)}\right) ln\left(\frac{t}{\tau}\right)\right] \qquad 2.4$$

where $M_0(T)$ is the irreversible magnetization at t = 0 and $\tau$ the relaxation time.

To avoid divergence at $t = 0$, $ln(t/\tau)$ is replaced by $ln(1+t/\tau)$ leading to

$$M(t,T) = M_0\,(T)\left[1 - \left(\frac{k_B T}{U(T)}\right) ln\left(1 + \frac{t}{\tau}\right)\right] \qquad 2.5$$

As $M_0(T)$ cannot be directly determined in the experiment, $M_0(T)$ is replaced by $M(t_b,T)$; $t_b$ was chosen as 600 s and $\tau$ was assumed to be in the interval from $10^{-12}$ to $10^{-6}$s [Hag89].

With

$$M(t_b,T) = M_0\,(T)\left[1 - \left(\frac{k_B T}{U(T)}\right) ln\left(1 + \frac{t_b}{\tau}\right)\right] \qquad 2.6$$

an expression for the mean effective pinning energy

$$< U\ (T) > = k_B T \left( -\frac{1}{S} + ln\left(1 + \frac{t_b}{\tau}\right)\right) \qquad 2.7$$

is obtained, with the normalized creep rate

$$S = \frac{1}{M(t_b,T)}\left(\frac{dM}{dlnt}\right) \qquad 2.8$$

calculated from the creep rate (dM/dlnt) which is obtained directly as the slope in the relaxation measurements divided by the irreversible magnetization at time $t_b$ eq. (2.6).

### 2.3.4 Activation energy distribution

In the Anderson flux creep theory [AND62], it is assumed that all energy barriers between adjacent pinning regimes have the same value. While using this model for the analysis of experimental data, an unphysical increase in the activation energy with temperature was reported for high temperature superconductors [Tuo88].

Hagen et al [Hag89] have proposed a modification in the Anderson model which can explain this increase by a distribution of activation energies.

Introducing the distribution function, $m(U)$ to equation (2.5) gives

$$M(t_b,T) = M_0 \frac{b(T)}{a(T)} \int_{U_0(t,T)}^{\infty} m(U)\left[1 - \left(\frac{k_B T}{U(T)}\right) ln\left(1 + \frac{t_b}{\tau}\right)\right] dU \qquad 2.9$$

with the cut-off energy

$$U_0(t_b,T) = \frac{k_B\ T}{b(T)} ln\left(1 + \frac{t_b}{\tau}\right) \qquad 2.10$$

and $M_0 = M(t = 0, T = 0)$, $b(T)$ and $a(T)$ are temperature dependent functions given by

$$a(\Theta) = \left(\frac{1+\Theta^2}{1-\Theta^2}\right)^{\frac{m}{2}},\ b(\Theta) = (1-\Theta^2)^2 \left(\frac{1+\Theta^2}{1-\Theta^2}\right)^{\frac{n}{2}},\ \Theta\ = \frac{T}{T_c}.$$

Using $m$ = 0 and $n$ = 2 as obtained by Hagen and Griessen [Hag90] for a YBCO single crystal and taking into account that the distribution function has to be normalized to 1, an expression for the distribution function can be derived as

$$m\big(U_0(t_b,T)\big) = \frac{1}{M_0 k_B\left(\frac{4}{b(T)}-3\right)}\left[\frac{d}{dT}\left(\frac{dM}{dlnt}\right) - \frac{1}{T}\left(\frac{dM}{dlnt}\right)\right]. \qquad 2.11$$

With the only assumption concerning $b(T)$ ($m$ = 0, $n$ = 2) this function can directly be determined from the temperature dependence of the creep rate d$M$/dln$t$. $M_0$ is obtained from experimental curve of $M(t_b,T)$ versus $T$ by making an extrapolation to $T$ = 0 for different $t_b$ values.

### 2.3.5 Non-linear energy current relation

To avoid the short-coming of an unphysical linear $U(J)$ relation, as assumed in the Anderson theory and the Hagen and Griessen model, the $U(J)$ relation was directly determind from the relaxation curves following the scheme given by Maley et al [Mal90], who proposed a method without a prior selection of any model. Starting with the flux diffusion equation for a slab of thickness $d$

$$\frac{dB}{dt} = \frac{4\pi dM}{dt} = \frac{2B_a X \nu_0}{d}\, exp\left(\frac{-U(j,B)}{k_B T}\right)$$

and rearranging the terms one gets

$$\frac{U}{k_B} = -Tln\left[\frac{dM}{dt} - \ln\left(\frac{B_a X \nu_0}{2\pi d}\right)\right]$$

$$\frac{U}{k_B} = -Tln\left[\frac{dM}{dt}\right] + C \qquad 2.12$$

where $C = \ln\left(\frac{B_a X \nu_0}{2\pi d}\right)$ is in first approximation assumed to be a temperature independent quantity.

Equation (2.12) can be used to obtain the $U(J)$ relation by plotting $-Tln\left[\frac{dM}{dt}\right]$ over $M_{irr}$, which is according to Bean proportional to the critical current density $J_c$, and by choosing a value for $C$ for which all the points lie on one smooth line. This procedure works for a limited temperature region. To take into account a possible temperature dependence of the potential well, Tinkham et al [Tak88] have proposed a temperature dependent term

$g(T) = 1 - \left(\frac{T}{T_c}\right)^2$. Taking into account this term, equation (2.12) can be written as

$$\frac{U/k_B}{g(T)} = \frac{\left[-Tln\left[\frac{dM}{dt}\right]+C\right]}{1-\left(\frac{T}{T_c}\right)^2} \qquad 2.13$$

Relation (2.13) can be used to determine $(U/k_B)/g(T)$ from experimental data and its dependence on $J_c$ is found by plotting the obtained value as a function of corresponding $M_{irr}$(~ $J_c$).

# Chapter 3: Results

## 3.1 X-Ray diffraction

The X-ray images obtained for core material of the $MgB_2$/Nb wires are shown in Fig. 3.1. For 0% SiC, beside the peaks of pure $MgB_2$ some small peaks at 2Θ = 42.8° and 62.26°, which can be identified as being due to traces of MgO (denoted as Z) can be seen. However, the samples with SiC addition show additional peaks at 2Θ = 24.2° and 40.0° whose intensities increase with SiC concentration. These peaks (denoted as Y) are belonging to the secondary phase $Mg_2Si$. The appearance of these peaks is an indication that SiC has dissociated and that C is incorporated into the matrix. No traces of MgO are present in the samples with SiC inclusions. A quantitative analyses of the amount of $Mg_2Si$ in terms of vol% as well as the determination of the lattice parameters were carried out. The results are given in Table 3.1. The *a* parameter decreases slightly with substitution. No systematic change is found in the value of parameter *c.*

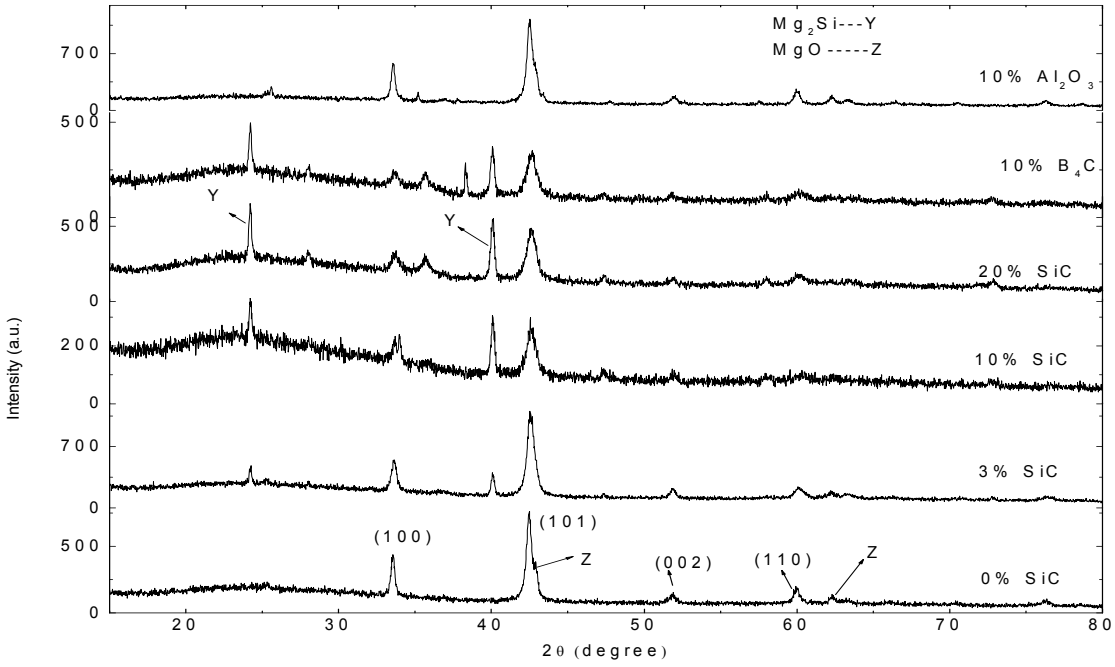


**Figure 3.2 X-ray images of $MgB_2$/Nb wires with and without additives.**

**Table 3.1 Lattice parameters and vol% of $MgB_2$ and $Mg_2Si$ obtained from X-ray analysis of $MgB_2$/Nb wires.**

| sample | *a* (Å) | *c* (Å) | $MgB_2$ Vol% | $Mg_2Si$ Vol% |
|---|---|---|---|---|
| 0% SiC | 3.082 | 3.518 | 100 | - |
| 3% SiC | 3.073 | 3.515 | 96 | 4 |
| 10% SiC | 3.080 | 3.537 | 71 | 29 |
| 20% SiC | 3.080 | 3.525 | 64 | 36 |
| 10% $B_4C$ | 3.065 | 3.509 | 67 ± 3 | 13 |
| 10% $Al_2O_3$ | 3.082 | 3.512 | 100 | - |

## 3.2 Scanning electron microscopy

SEM images of $MgB_2$/Nb wires and bulk samples are shown in Figs 3.2 and 3.3, respectively. Mean grain sizes obtained from the SEM images are given in Table 3.2. The wires have grain sizes between 9 and 11 µm while the bulk samples have slightly larger grain size (in the range of 12 to 15 µm).

**Table 3.2 Mean grain size of $MgB_2$/Nb wires and bulk samples obtained from the SEM images.**

| Sample | 0 % SiC | 3 % SiC | 10 % SiC | 20 % SiC | $B_4C$ | $Al_2O_3$ | Pure | Al | SiC |
|---|---|---|---|---|---|---|---|---|---|
| mean grain Size (µm) | 10 ± 3 | 11 ± 2 | 9 ± 3 | 11 ± 4 | 9 ± 3 | 11 ± 2 | 15 ± 3 | 12 ± 4 | 14 ± 3 |

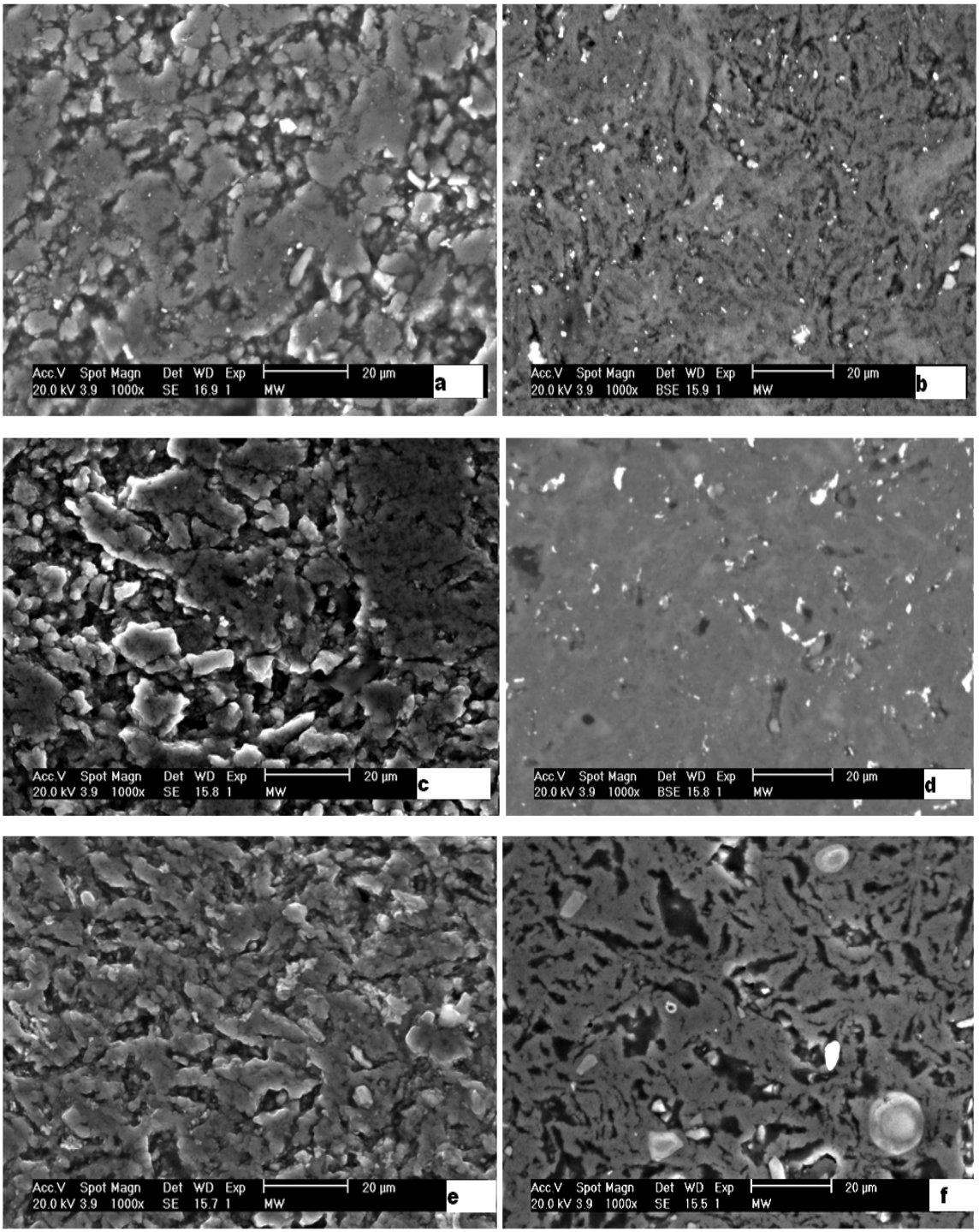


**Figure 3.2 SEM images of $MgB_2$/Nb wires with (a) 0% SiC (b) 3 % SiC (c) 10 % SiC (d) 20 % SiC (e) 10 % $B_4C$ and (f) 10 % $Al_2O_3$ additions.**

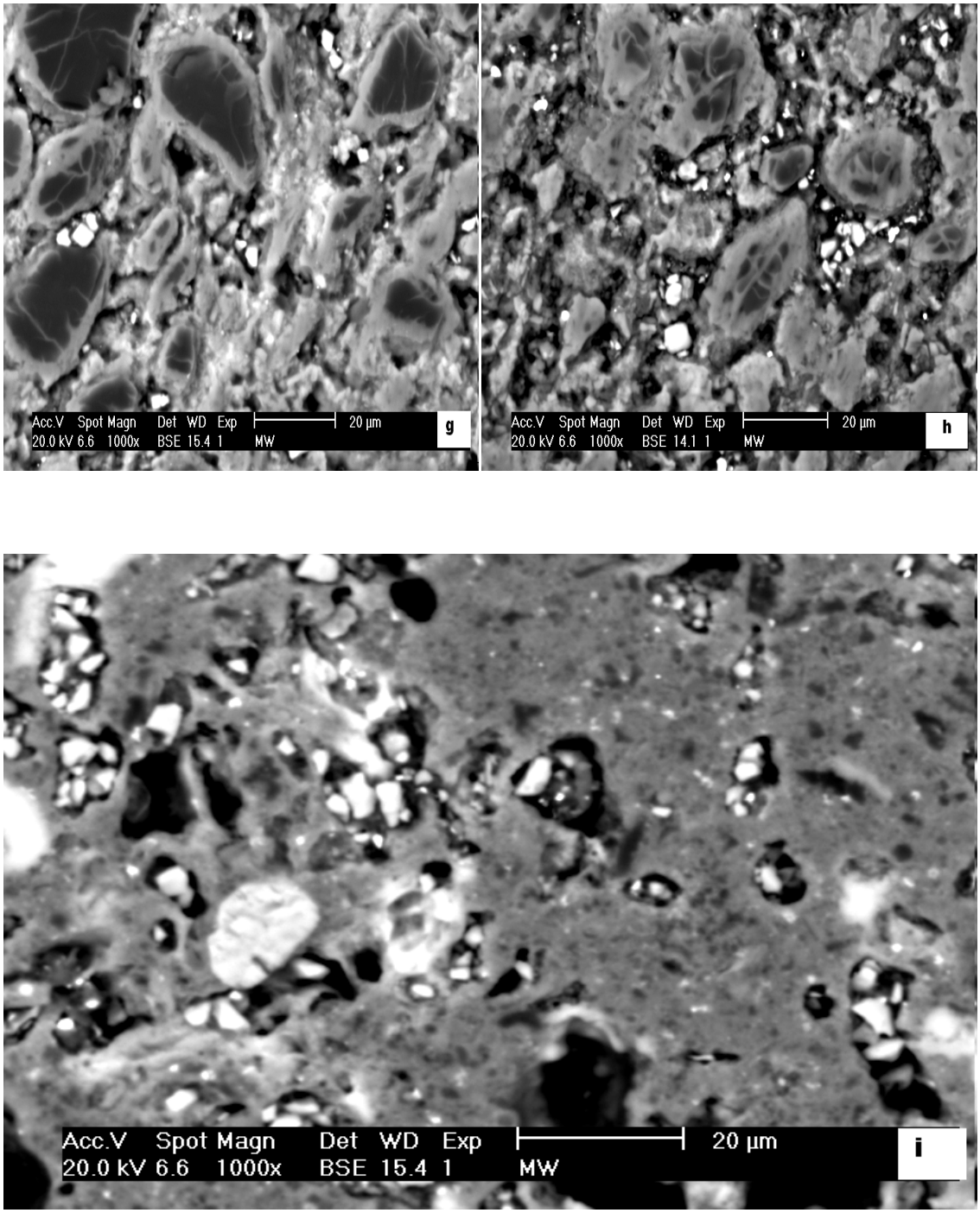


**Figure 3.3 SEM images of $MgB_2$ bulk samples (g) Pure (h) 8 % Al addition and (i) 10 % SiC addition.**

## 3.3 Transition Temperature

Fig. 3.4 shows temperature dependence of magnetic moment for $MgB_2$/Nb wires with different SiC concentrations. The obtained transition temperature ($T_c$ ) is highest for the wire with 0% SiC additive while for other concentrations, $T_c$ shifts to lower values with increasing concentration. In case of 3% SiC addition, indication of a small amount of secondary phase is present visible in the inset as a second kink, at approximately the $T_c$ of 0% sample. The difference in $T_c$ between 10% and 20% SiC is smaller (~1 K) than the difference between the 3% and 10% samples (~6.4 K). The width of the transition $\Delta T_c$ increases with concentration up to 10% with a slightly sharper transition for the 20% SiC compound. The $T_c$ and $\Delta T_c$ values for all samples are given in Table 3.3.

For the wires with different additives but constant concentration (10 wt%), it can be noted that $Al_2O_3$ addition shows the highest $T_c$ onset followed by $B_4C$ while SiC has the smallest $T_c$ in this series (Fig. 3.5a). A similar tendency is found in case of the transition width (Table 3.3).

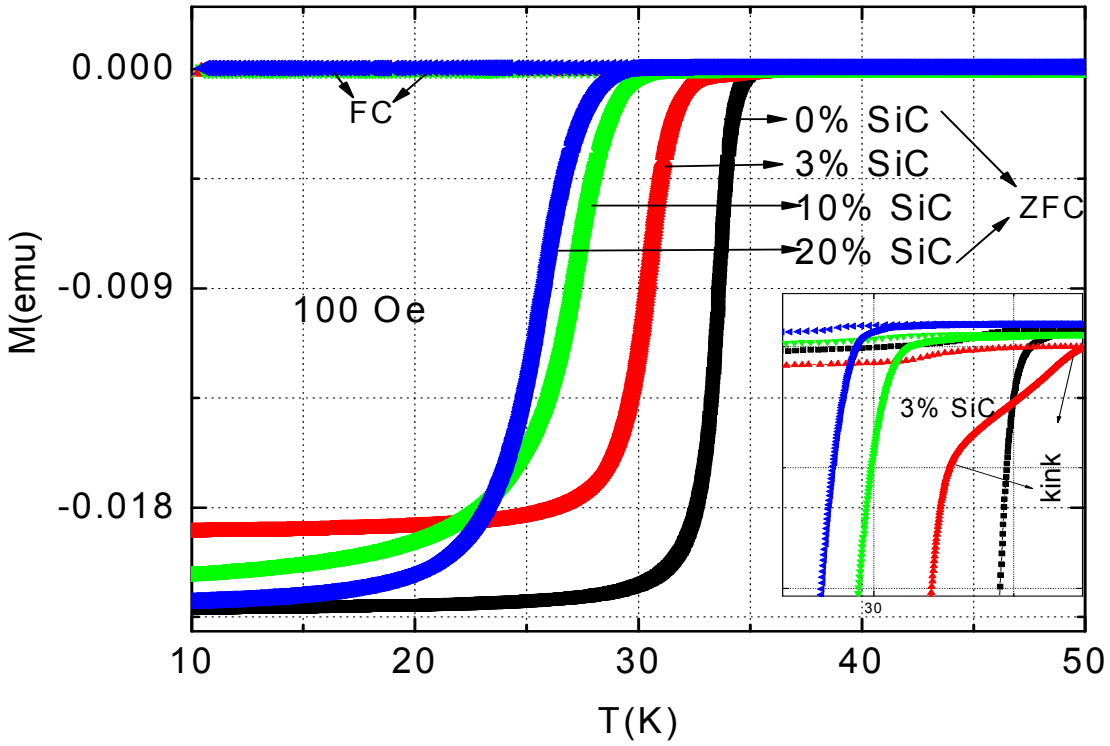


**Figure 3.4 Zero field cooled and field cooled curves of magnetic moment in 100 Oe magnetic field for wires with different SiC concentrations.**

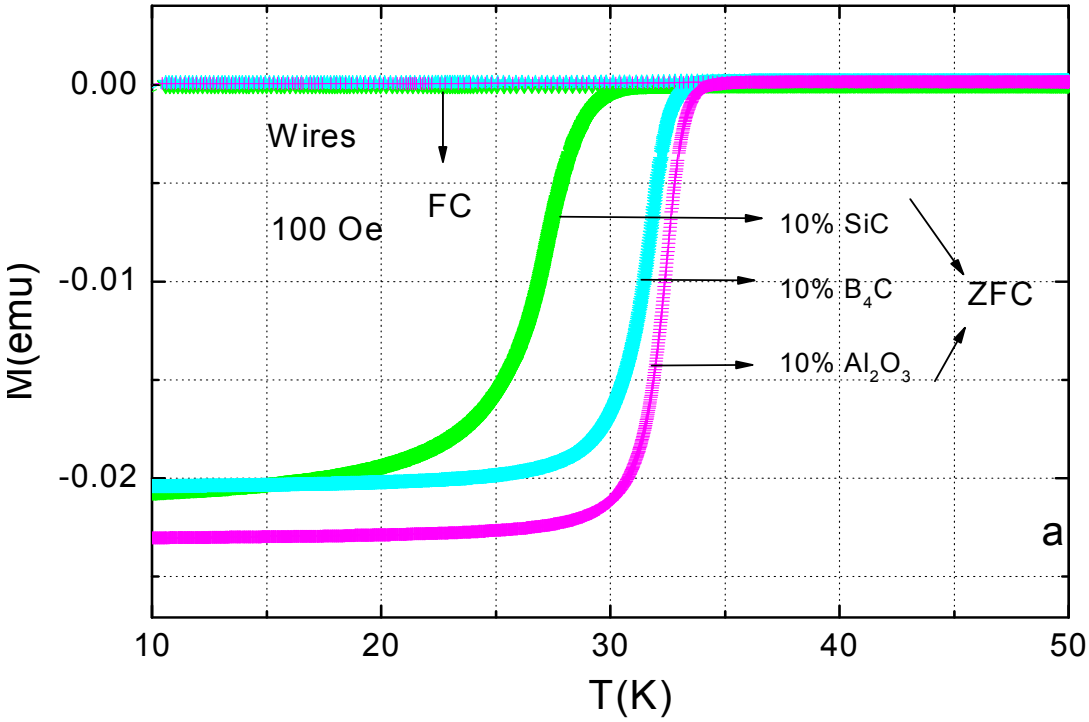


**Figure 3.5a Magnetic moment versus temperature for wires with different additives and same concentration.**

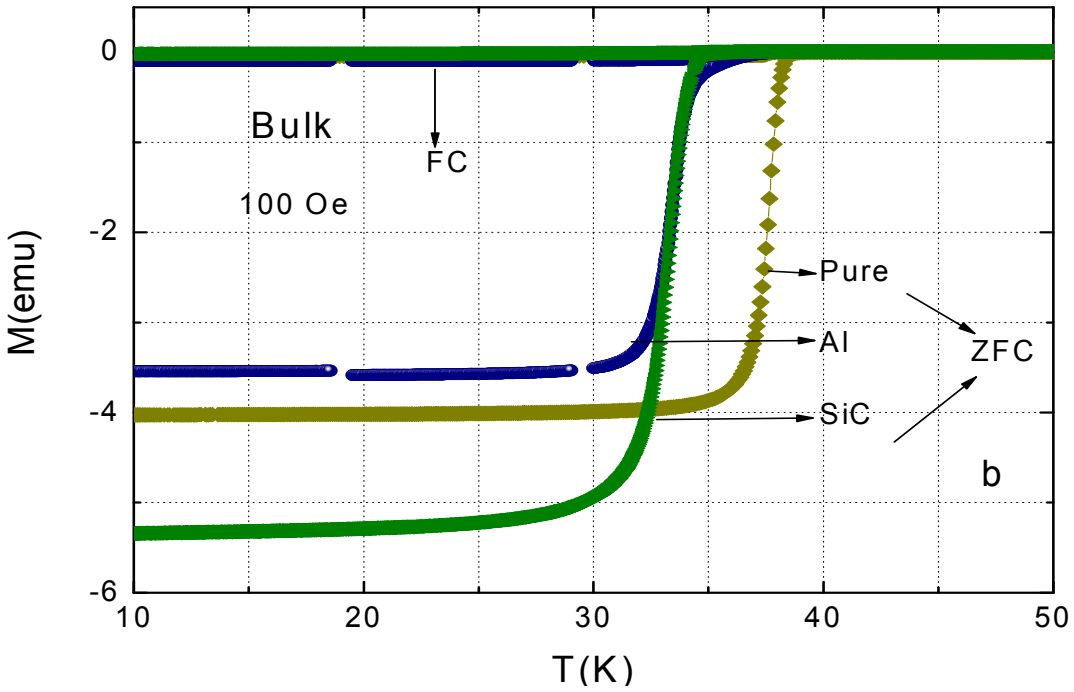


**Figure 3.5b Magnetic moment versus temperature for bulk samples with and without additives.**

For bulk samples, $M(T)$ curves are shown in Fig. 3.5b. The reduction in $T_c$ and the increase in $\Delta T_c$ of the SiC substituted sample is stronger than for the Al substituted one. The values are given in Table 3.3.

A comparison of wires with bulk samples having similar content of additives shows that for 10% SiC in case of wires $T_c$ is smaller than in case of bulk samples. The reverse tendency is seen for the $\Delta T_c$ values. For both wires and bulk samples $T_c$ is highest and $\Delta T_c$ lowest for pure samples. Al and $Al_2O_3$ additions seem to have the least influence on both $T_c$ and $\Delta T_c$, while SiC additions in both wires and bulk samples depress $T_c$ and broaden the width of transition temperature strongly. In terms of critical temperature, the overall performance of bulk is better than that of wires.

**Table 3.3 Superconducting transition temperature ($T_c$) and transition width for measured samples**

| Sample | $T_c$ (K) | $\Delta T_c$ (K) |
|---|---|---|
| 0% SiC | 37.5 | 2.3 |
| 3% SiC | 37.3 | 3.5 |
| 10% SiC | 31.0 | 6.0 |
| 20% SiC | 30.0 | 5.1 |
| 10% $B_4C$ | 35.0 | 3.5 |
| 10% $Al_2O_3$ | 36.0 | 2.6 |
| Pure | 38.5 | 0.9 |
| Al | 37.0 | 2.1 |
| SiC | 35.0 | 2.9 |

## 3.4 Magnetic hysteresis loops

In Figures 3.6 to 3.14 hysteresis loops obtained from DC magnetic measurements for temperatures between 4.2 and 30 K for the investigated samples are shown. The maximum applied magnetic field was 9 T. Magnetic flux jumps are present at low temperatures and low fields. In case of all wires and bulk with SiC addition, these jumps are observed at T ≤ 8 K while for pure and Al samples the jumps appear below 3 K Such jumps are visible at lowest temperatures in Figs. 3.10, 3.11, and 3.14.

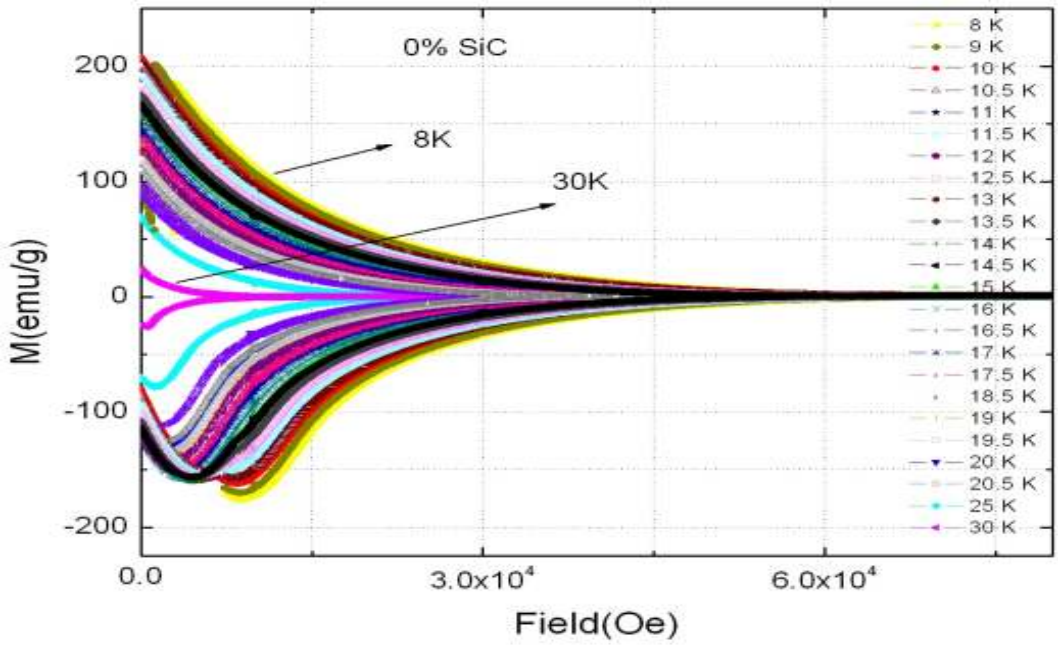


**Figure 3.6 Magnetic hysteresis loops for $MgB_2$/Nb wire with 0% SiC addition measured at different temperatures.**

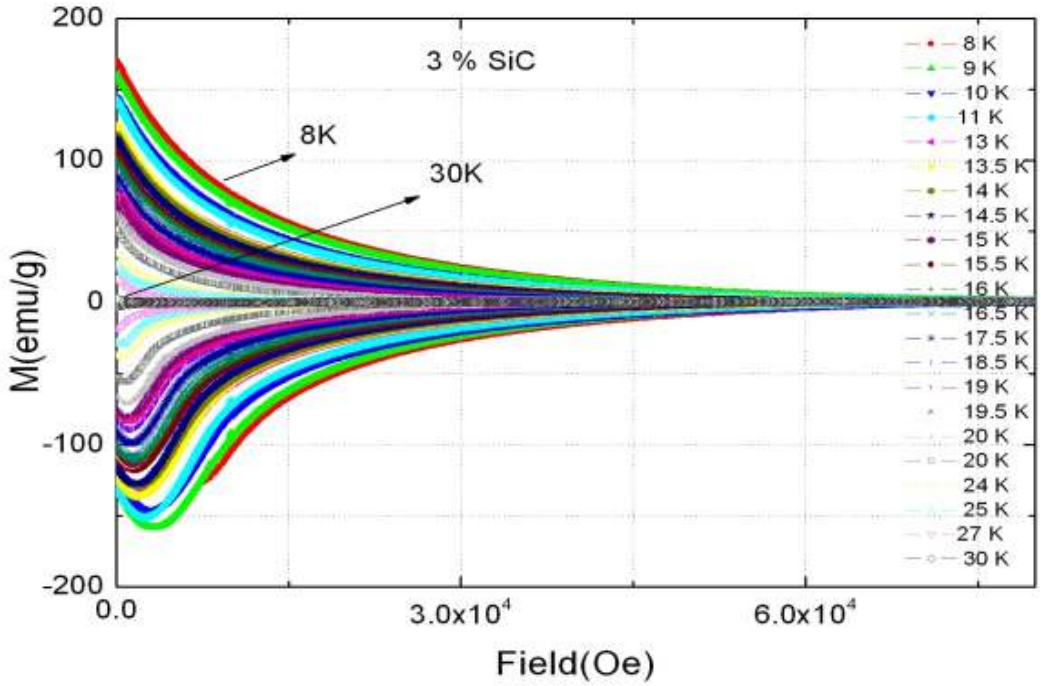


**Figure 3.7 Magnetic hysteresis loops for $MgB_2$/Nb wire with 3% SiC addition measured at different temperatures.**

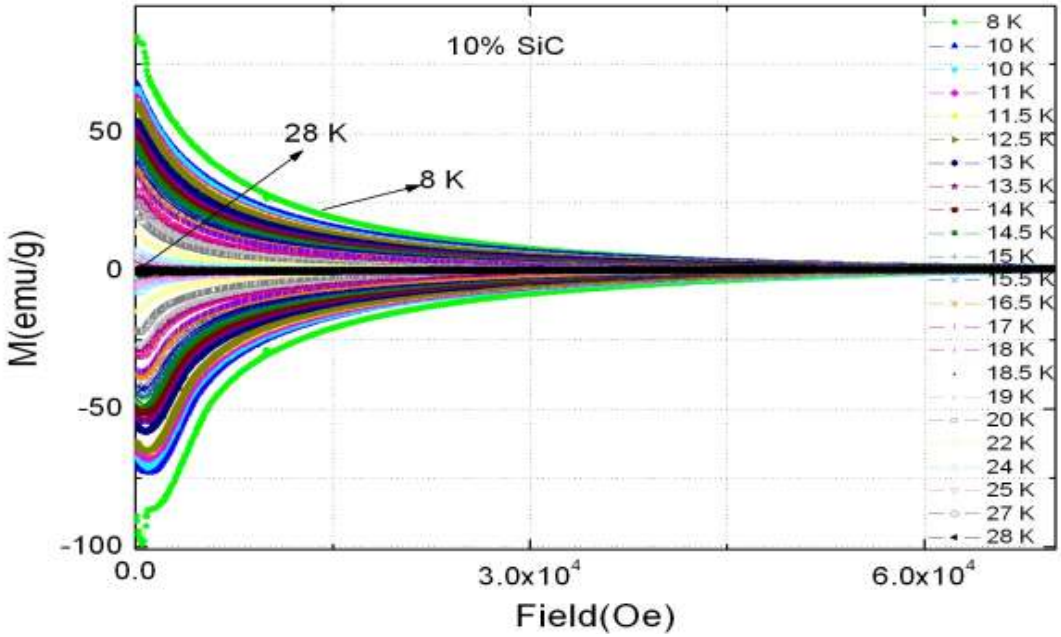


**Figure 3.8 Magnetic hysteresis loops for $MgB_2$/Nb wire with 10% SiC addition measured at different temperatures.**

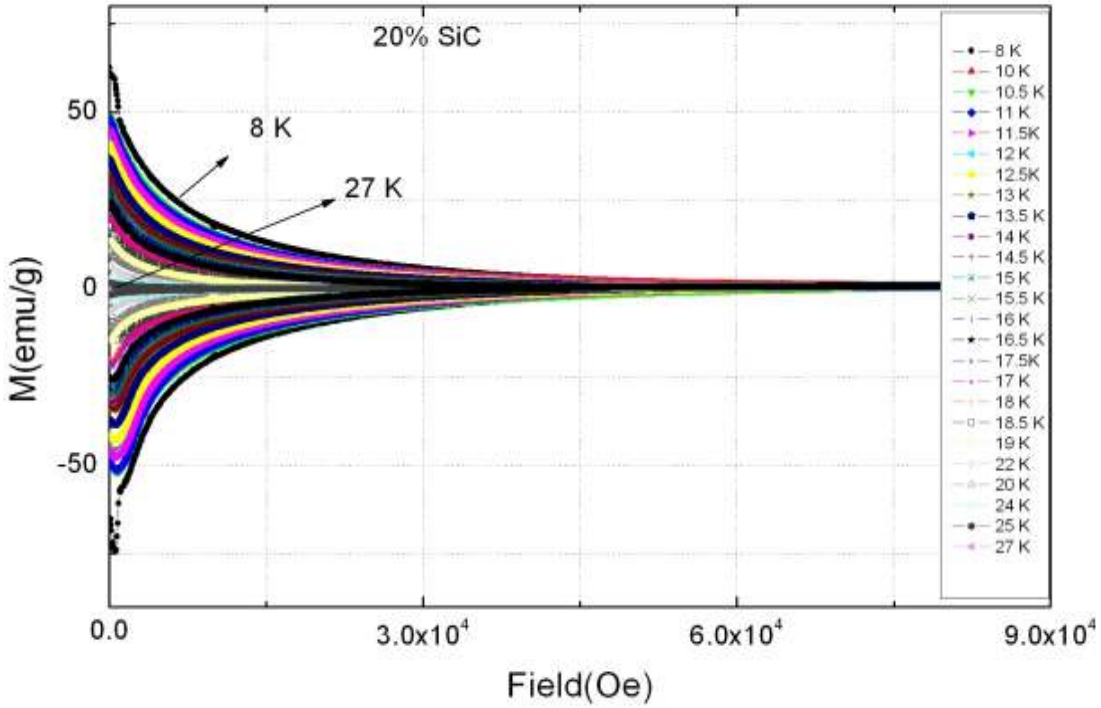


**Figure 3.9 Magnetic hysteresis loops for $MgB_2$/Nb wire with 20% SiC addition measured at different temperatures.**

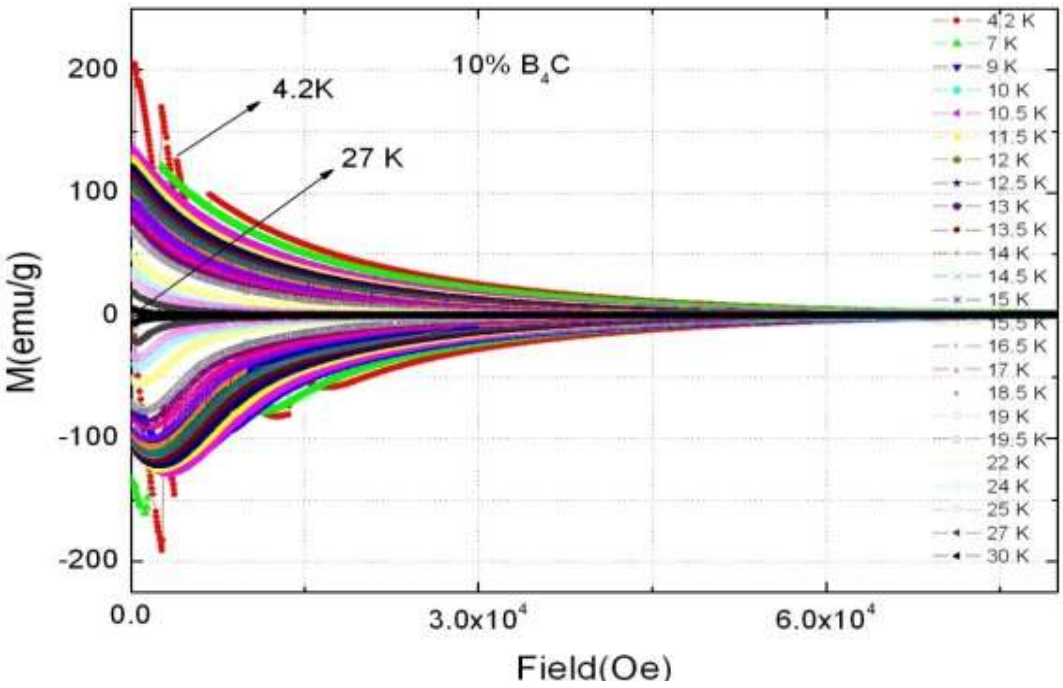


**Figure 3.10 Magnetic Hysteresis loops for $MgB_2$/Nb wire with 10% $B_4C$ addition measured at different temperatures.**

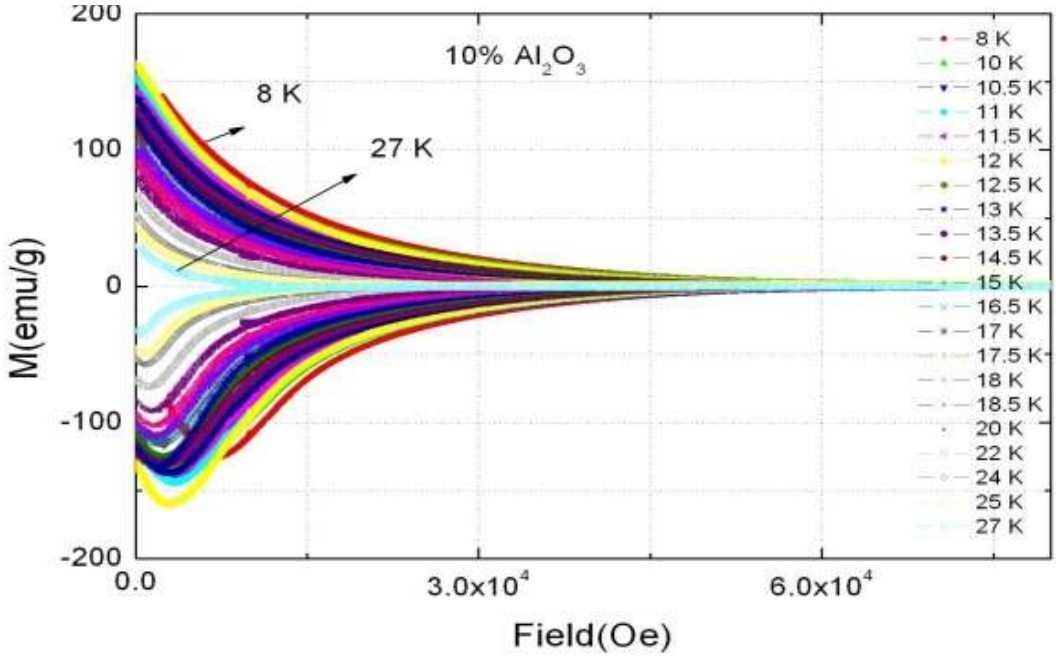


**Figure 3.11 Magnetic hysteresis loops for $MgB_2$/Nb wire with 10% $Al_2O_3$ addition measured at different temperatures.**

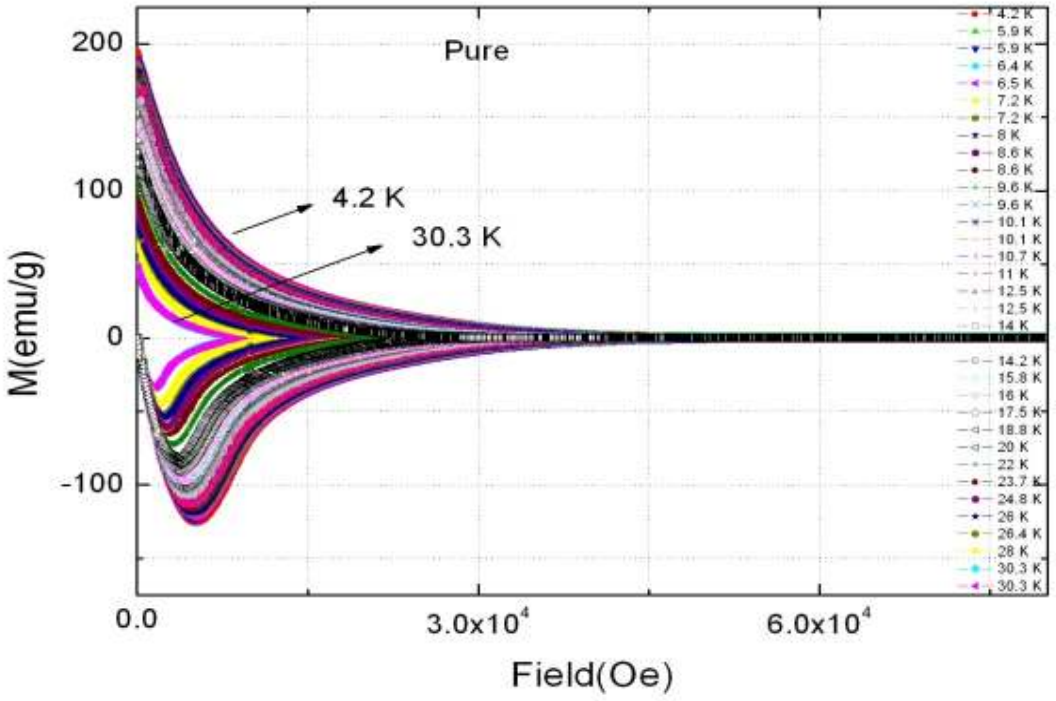


**Figure 3.12 Hysteresis loops in case of pure $MgB_2$ bulk sample measured at different temperatures.**

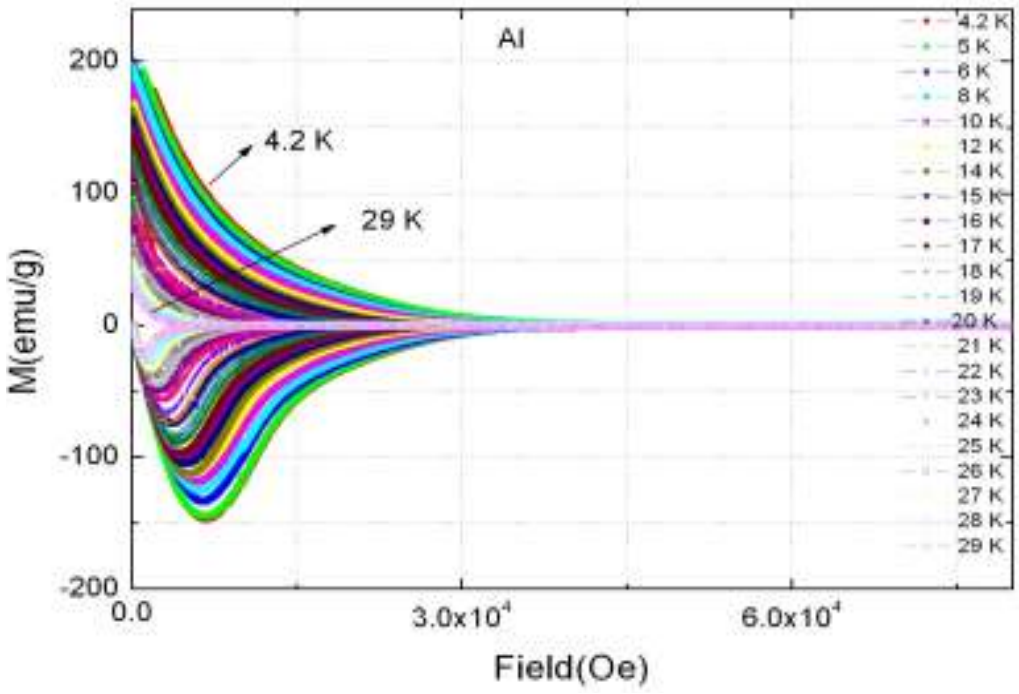


**Figure 3.13 Hysteresis loops of $MgB_2$ bulk sample with 8% Al addition measured at different temperatures.**

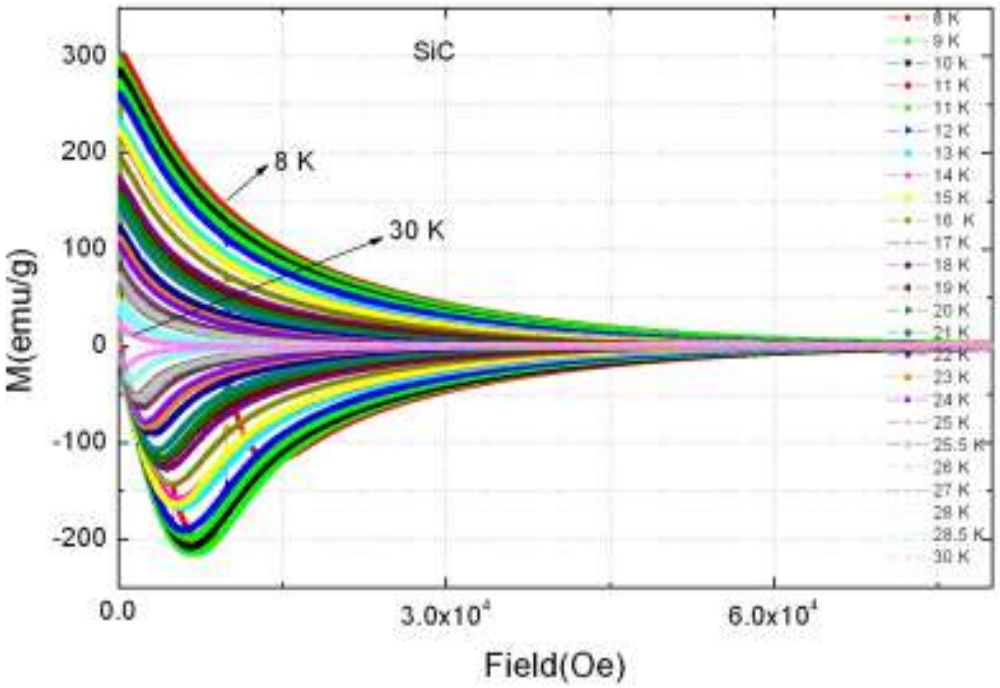


**Figure 3.14 Hysteresis loops of $MgB_2$ bulk sample with SiC addition measured at different temperatures.**

## 3.5 Critical current density

Critical current density was determined from the width of the hysteresis loops using Bean's critical state model (Ch. 2.3.1). The results are shown in Figs. 3.15 to 3.23 for all samples.

Due to the flux jumps which are present at low fields and temperatures, for the analysis of $J_c$ only measurements above the region of flux jumps were considered. The field and temperature dependence of $J_c$ are described in more detail in Chs. 3.5.1 and 3.5.2.

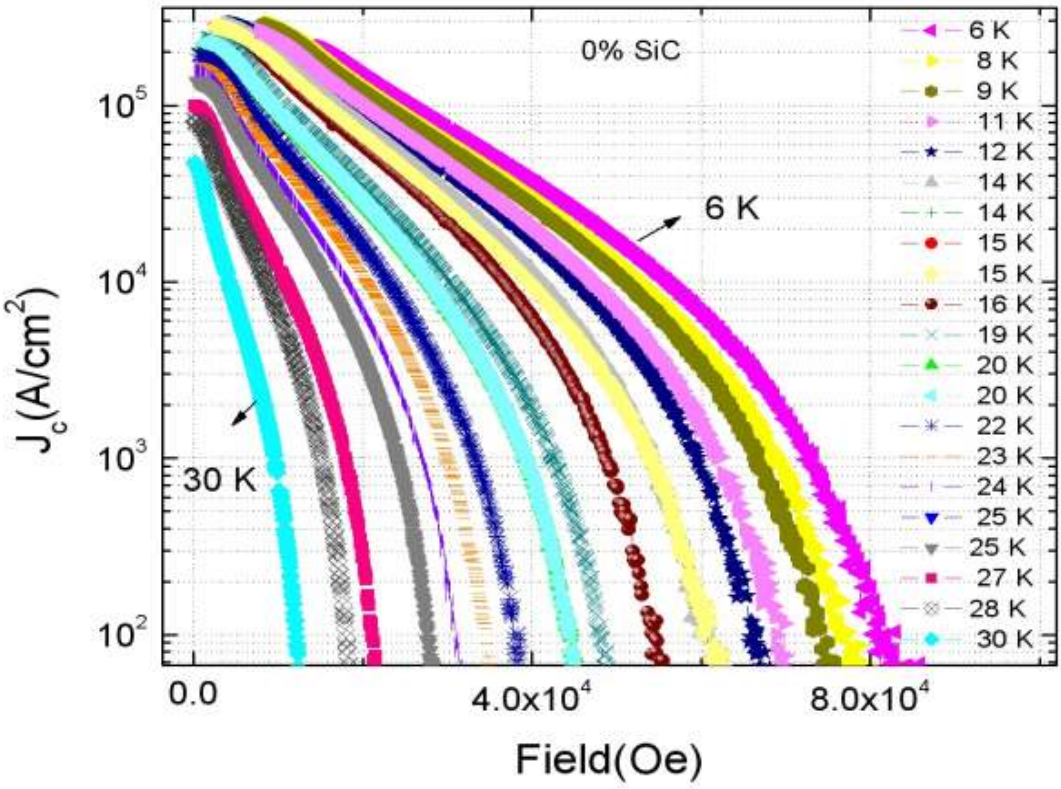


**Figure 3.15 Critical current density versus field for $MgB_2$/Nb wire with 0% SiC concentration at different temperatures.**

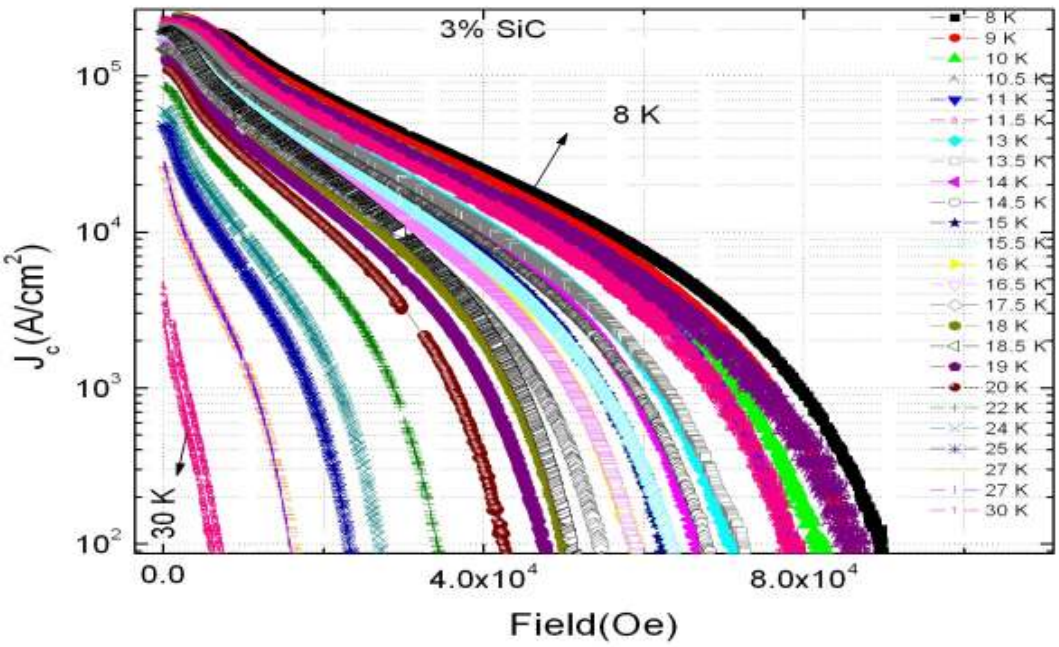


**Figure 3.16 Critical current density versus field for $MgB_2$/Nb wire with 3% SiC concentration at different temperatures.**

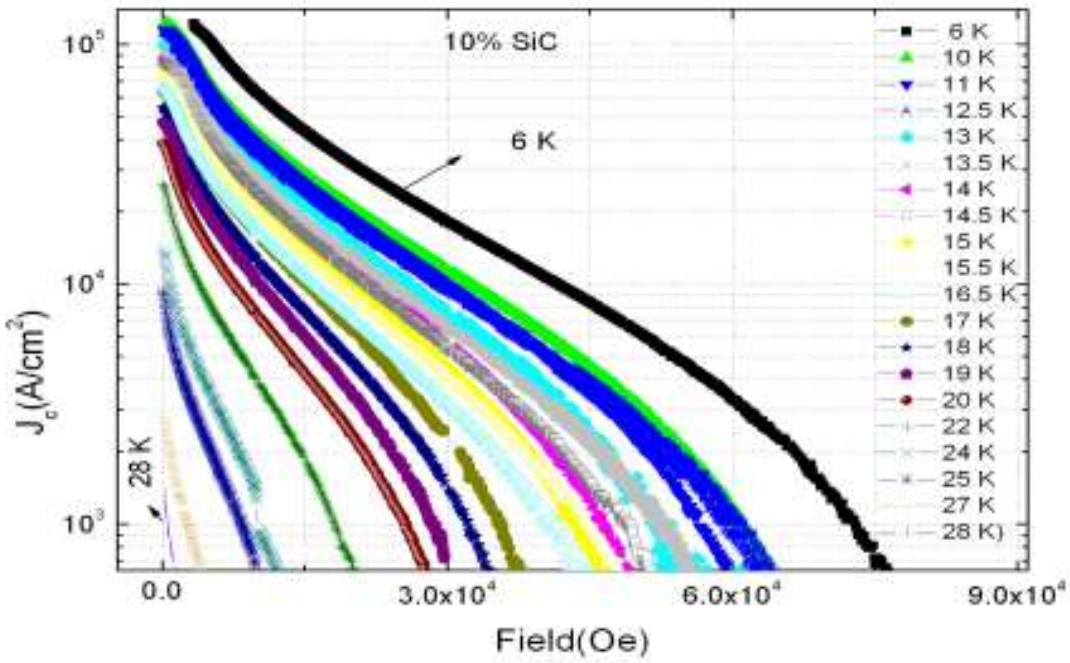


**Figure 3.17 Critical current density versus field for $MgB_2$/Nb wire with 10% SiC concentration at different temperatures.**

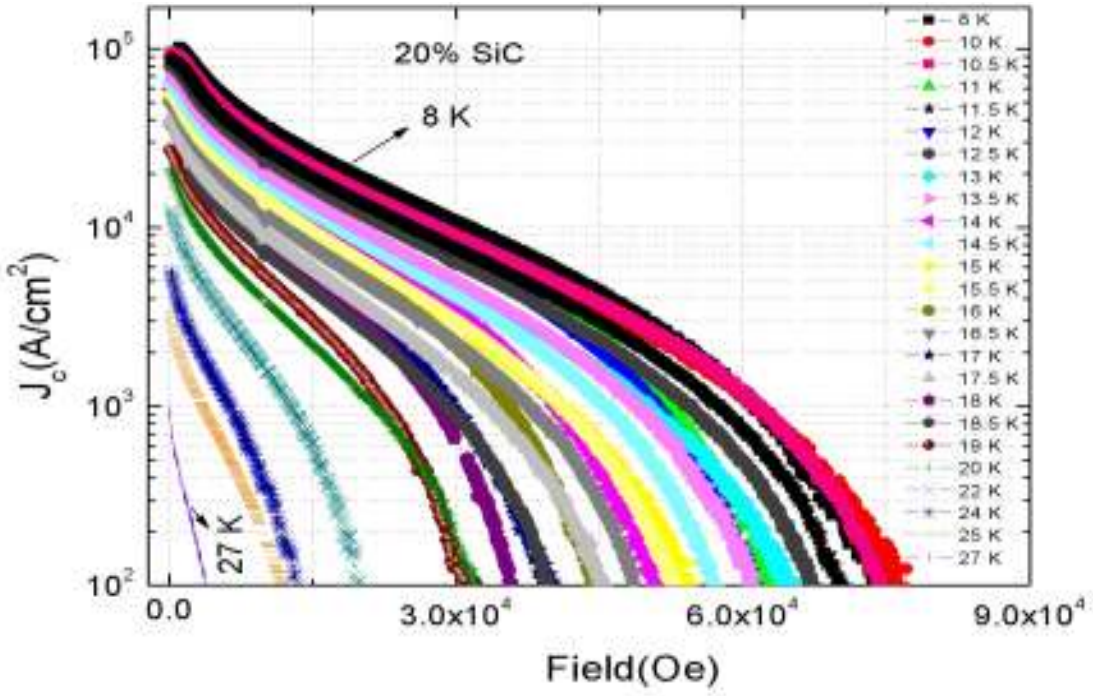


**Figure 3.18 Critical current density versus field for $MgB_2$/Nb wire with 20% SiC concentration at various temperatures.**

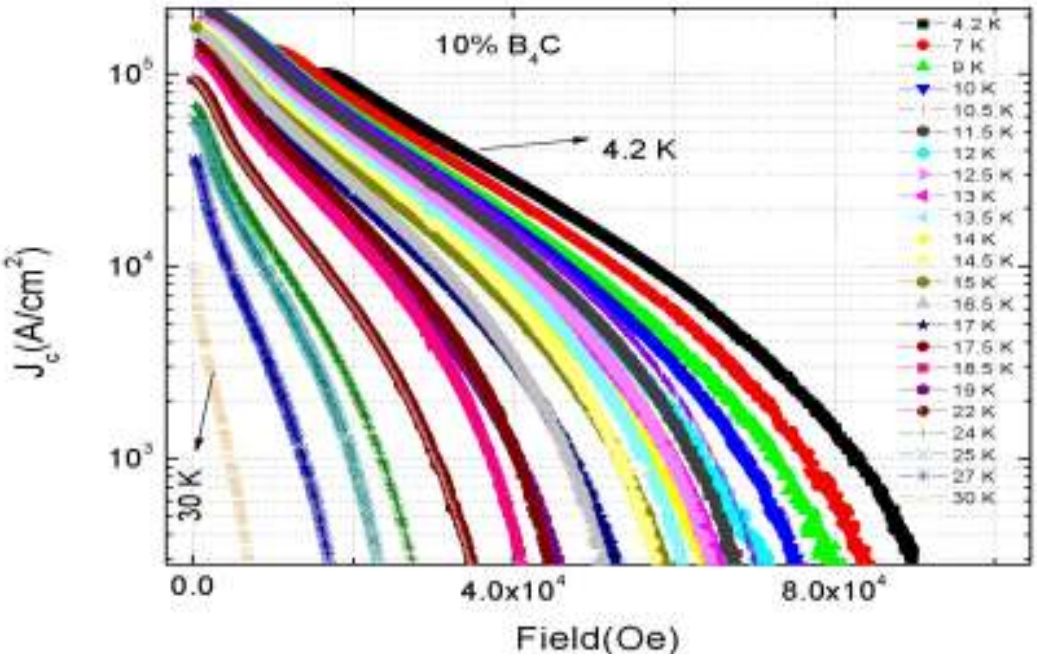


**Figure 3.19 Critical current density versus field for $MgB_2$/Nb wire with 10% concentration of $B_4C$ at different temperatures.**

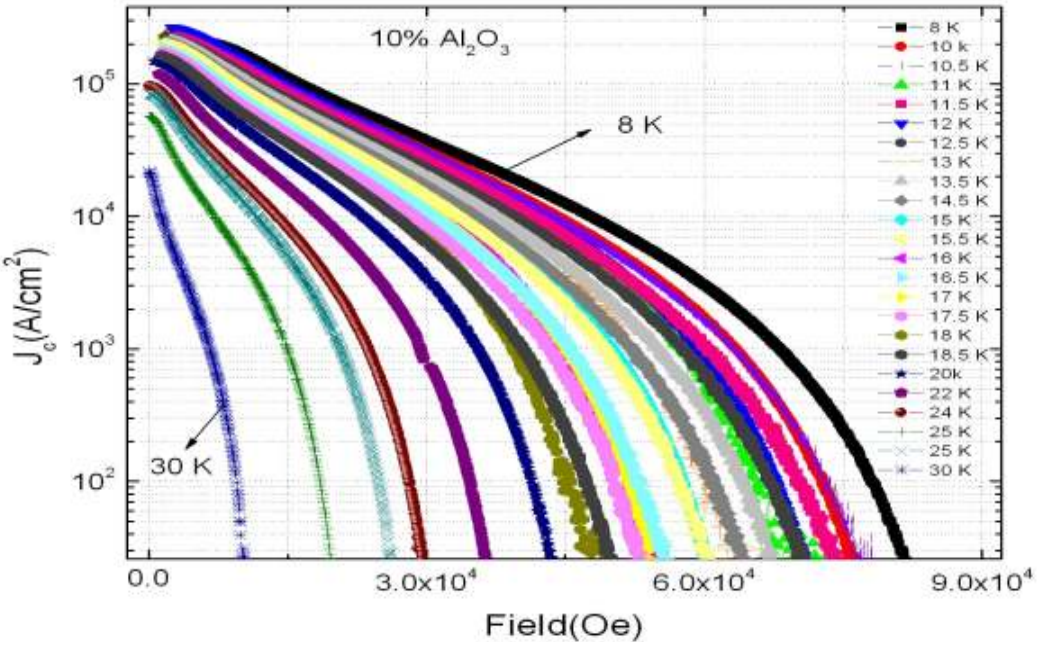


**Figure 3.20 Critical current density versus field for $MgB_2$/Nb wire with 10% concentration of $Al_2O_3$ at various temperatures.**

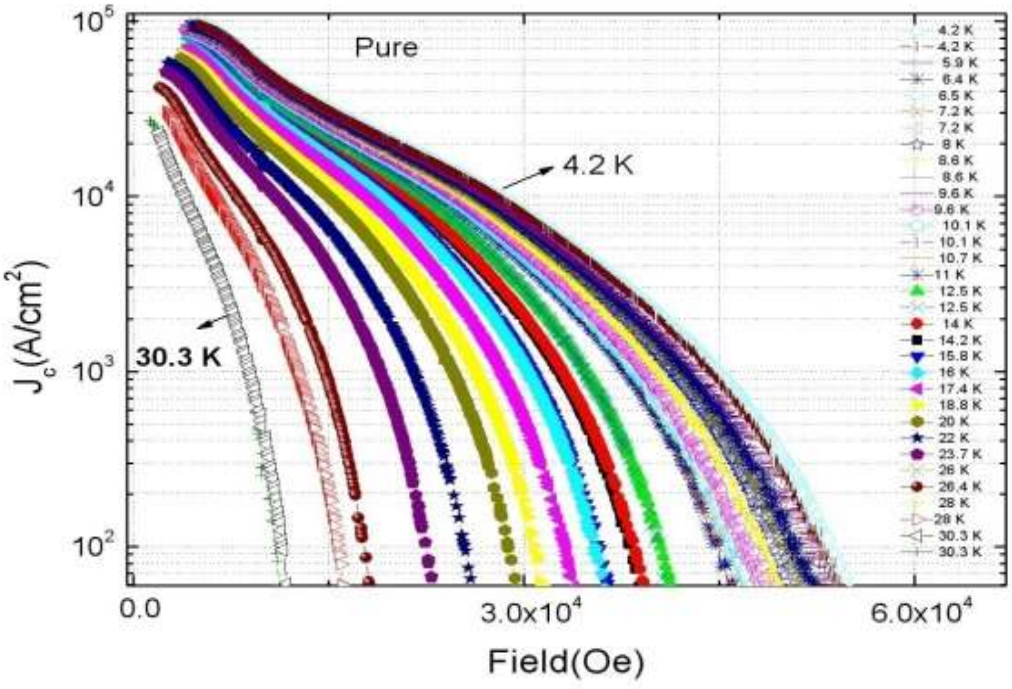


**Figure 3.21 Critical current density versus field for pure $MgB_2$ bulk sample at different temperatures.**

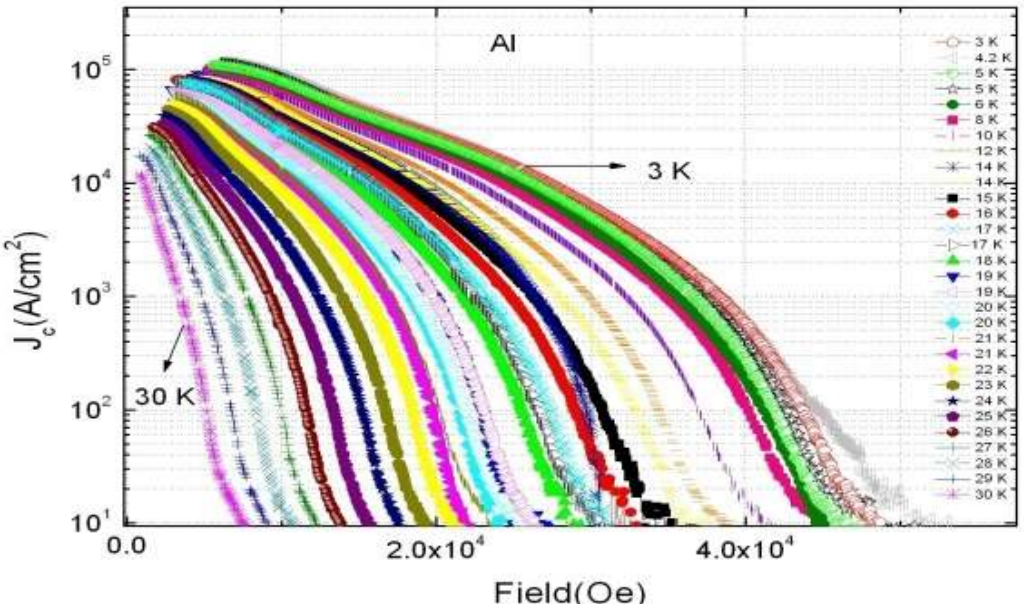


**Figure 3.22 Critical current density versus field for $MgB_2$ bulk samples with Al addition at different temperatures.**

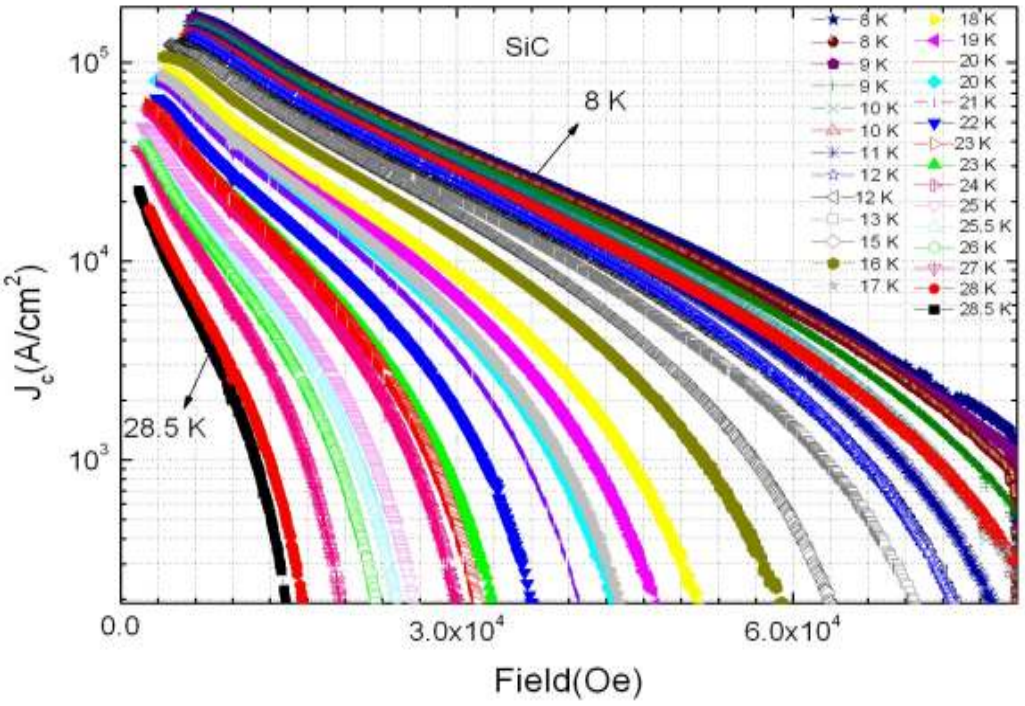


**Figure 3.23 Critical current density versus field for $MgB_2$ bulk samples with 10% SiC addition at different temperatures.**

### 3.5.1 Field dependence of critical current density

For discussion of the field dependence of $J_c$, the results for two typical temperatures, namely 10 K, representative for the low temperature region, and 25 K, representative for the high temperature range, are shown in Figs. 3.24 - 3.26 for all samples. In case of the SiC substituted wires (Fig. 3.24a), at 10 K the wire with 0% SiC shows highest $J_c$ below 5 T. At higher fields $J_c$ for 3% SiC addition is highest. A similar crossover is seen between 10% and 20% concentrations at about 6 T. Below this field the 10% and above this field the 20% substituted sample has higher $J_c$. All these crossovers are not visible at 25 K. The wire with 0% SiC has the highest $J_c$ at 25 K for the whole observed field range

In Fig.3.24b the same data are presented in normalized form, where $J_c$ is normalized to its first value. It is clearly seen that the SiC additions improves the field dependence of the current density, although the absolute value of $J_c$ in the low field range is reduced. The crossover between 10% and 20% vanishes. The crossover between 0% and 3% is shifted to the lower field value of 4 T. Although at low fields and temperatures the 0% sample has the highest $J_c$ values, because of the appearance of a plateau in $J_c$ which extends up to ~1 T, in higher fields this sample shows the steepest decrease of $J_c$ with field. The slope for the three SiC added samples is approximately the same.

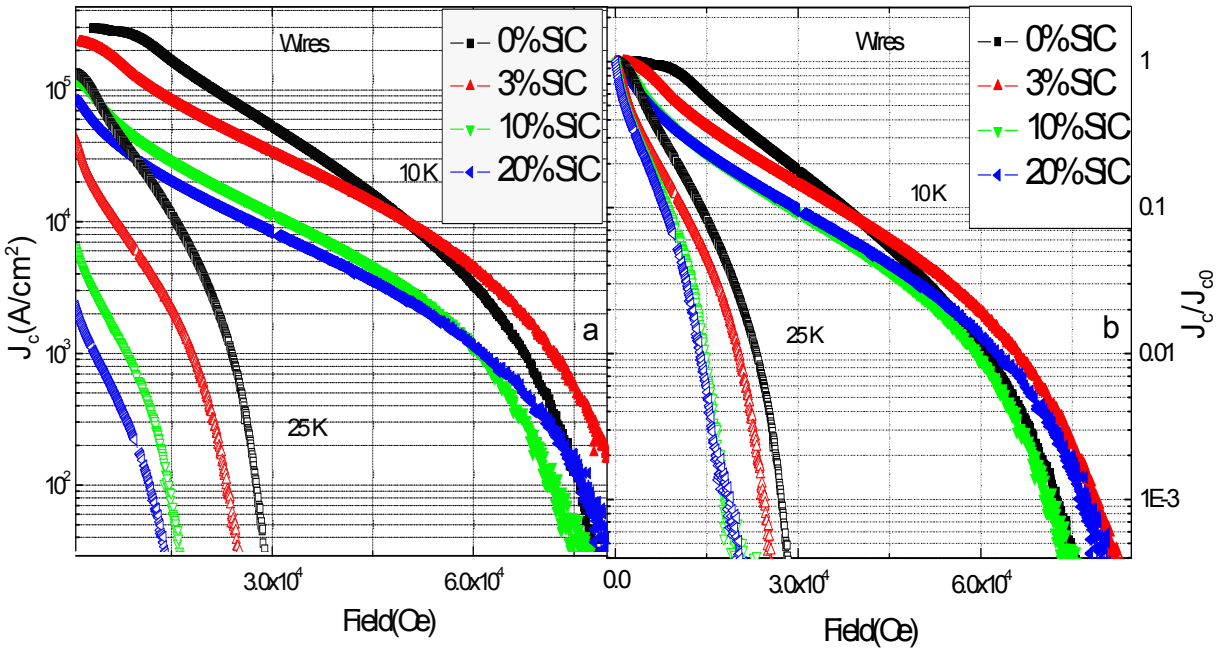


**Figure 3.24 Field dependence of $J_c$ (a) and normalized $J_c$ (b) for different concentrations of SiC in $MgB_2$/Nb wires at 10 K (full symbols) and 25 K (open symbols).**

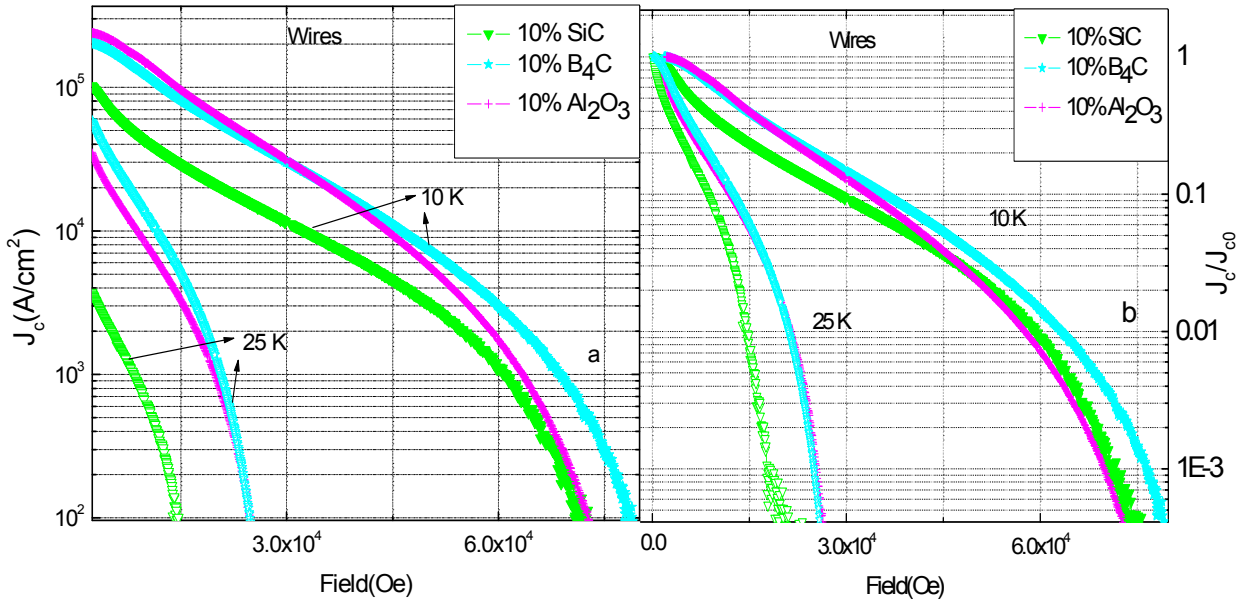


**Figure 3.25 Field dependence of $J_c$ (a) and normalized $J_c$ (b) versus field for $MgB_2$/Nb wires with same concentration of different additives at 10 K (full symbols) and 25 K (open symbols).**

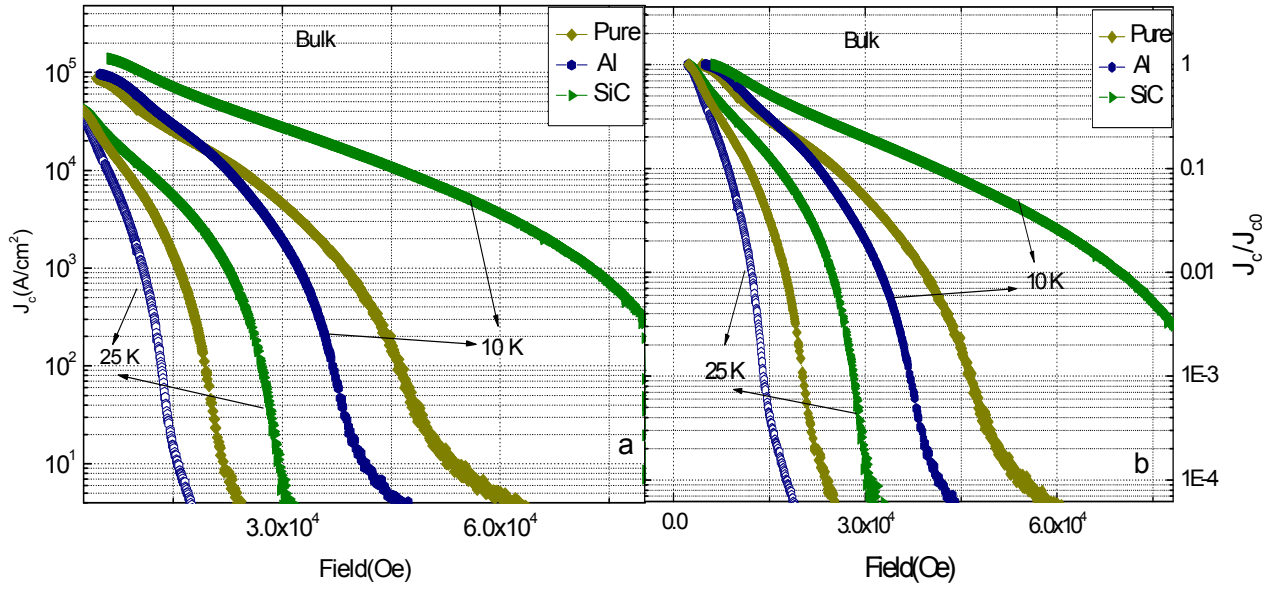


**Figure 3.26 Field dependence of $J_c$ (a) and normalized $J_c$ (b) versus field for $MgB_2$ bulk samples with and without different additives at 10 K (full symbols) and 25 K (open symbols).**

In case of the wires with constant concentration (10%) but different type of additives, it is seen that $Al_2O_3$ shows a higher $J_c$ at 10 K and below 3.3 T while for higher fields $J_c$ is larger in case of $B_4C$ (Fig 3.25a).

After normalization (Fig. 3.25b) the crossover at 10 K between the $Al_2O_3$ and the $B_4C$ curve shifts to 1.6 T. An additional crossover appears between the $Al_2O_3$ and the SiC sample. The latter has a higher normalized $J_c$ value above 4.8 T. At 25 K no crossover is visible. Both $B_4C$ and $Al_2O_3$ are very similar in their field dependence. The sample with SiC is worst.

The SiC addition in this series gives the smallest $J_c$ for all fields and temperatures investigated. From the point of flatness of the field dependence, the sample with 10% $B_4C$ inclusions is the best.

In case of the bulk samples $J_c$ is highest in the whole temperature and field range for the sample with SiC addition (Fig 3.26a). In contrast to this, substitution with Al makes the field dependence of $J_c$ worse. Only below 1.9 T at 10 K critical current density is a little bit higher than in the pure compound, but at higher fields $J_c$ drops faster with field. As can be seen in the normalized representation both pure and Al substituted sample show similar field dependence with a step-like decrease in medium fields (Fig 3.26b). For the pure sample this step appears between 4 and 6 T, for the Al substituted compound it is observed between 3 and 4 T.

### 3.5.2 Temperature dependence of critical current density

The critical current density versus temperature curves for three typical fields are shown in Figs. 3.27-3.29.

In case of wires with different SiC concentrations, the sample with 0% SiC shows higher $J_c$ than the other concentrations at low temperatures and 1 T but changes more rapidly with temperature compared to the other samples. The wire with 3% SiC concentration has better performance in terms of temperature at high field. The wires with 10% and 20% SiC addition show similar temperature dependence.

In wires with same concentration of different additives, the sample with $Al_2O_3$ addition has highest $J_c$ at 1 T. However the sample with $B_4C$ has the highest $J_c$ at high field. The wire with SiC addition has the smallest $J_c$ for all fields and temperatures.

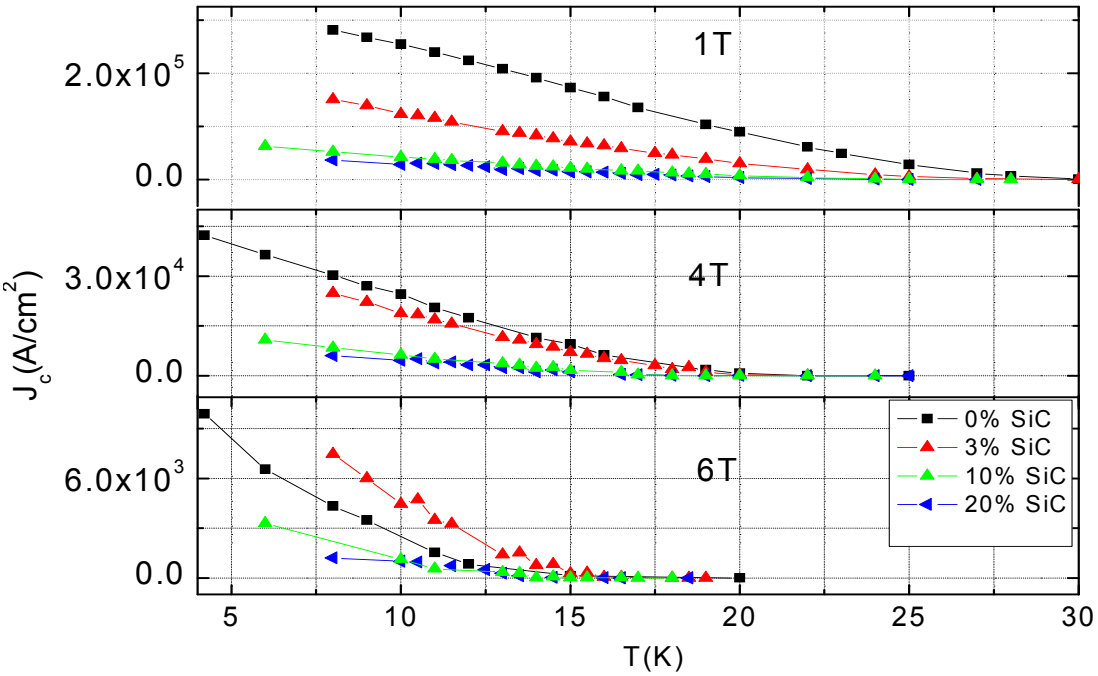


**Figure 3.27 Current density as a function of temperature at 1, 4 and 6 T for wires with different concentrations of SiC.**

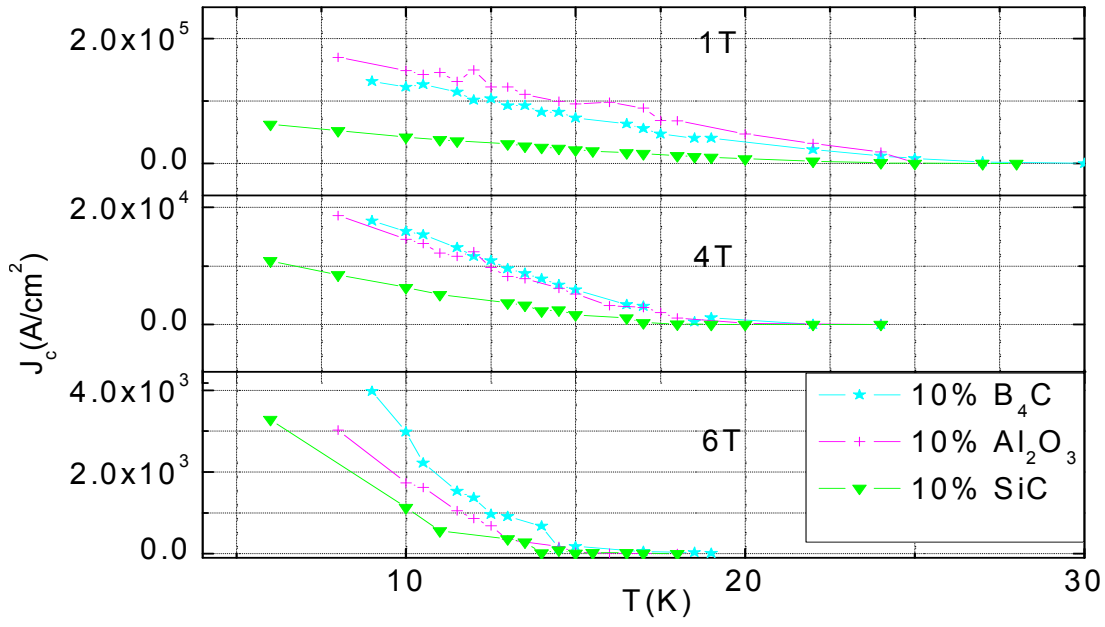


**Figure 3.28 Current density as a function of temperature at 1, 4 and 6 T for $MgB_2$/Nb wires with same concentrations of different additives.**

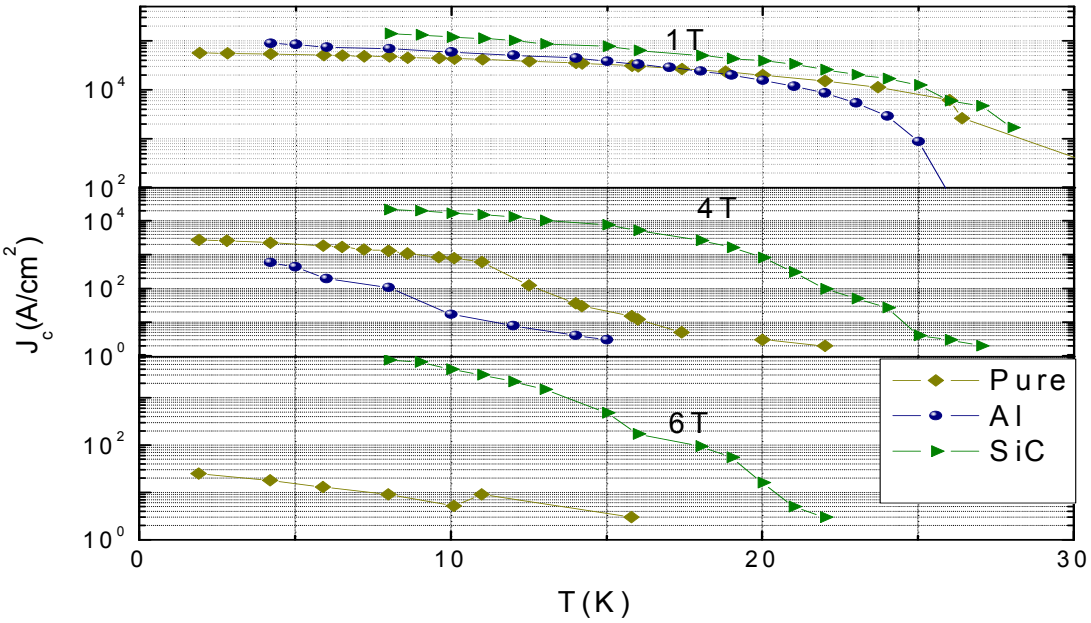


**Figure 3.29 Temperature dependence of current density at 1, 4 and 6 T for $MgB_2$ bulk with and without additives.**

In the bulk samples, it can be seen that the sample with SiC addition has highest $J_c$ value for all fields and temperatures. However, the $J_c$ for this sample becomes similar to other samples in this series at high temperature due to its strong temperature dependence. The sample with Al addition shows higher $J_c$ than pure sample at low temperature and low field.

## 3.6 Irreversibility field

The irreversibility field ($B_{irr}$) as a function of temperature determined from the $J_c$-$B$ curves using a 100 A/cm$^2$ criterion, is shown in Fig 3.30a and 3.30b for measured samples. The wire with 3% SiC addition shows higher values of $B_{irr}$ up to 20 K above which 0% SiC has the highest $B_{irr}$ in this series (Fig.3.30a). The 0% SiC becomes worse than all other samples below 10 K. Wires with 10 and 20% SiC additions have similar $B_{irr}$ below 17 K where they show a crossover and 10% SiC gives higher values at higher temperatures. The temperature dependence of $B_{irr}$ is flatest for the 0% SiC sample in this series especially at low temperature.

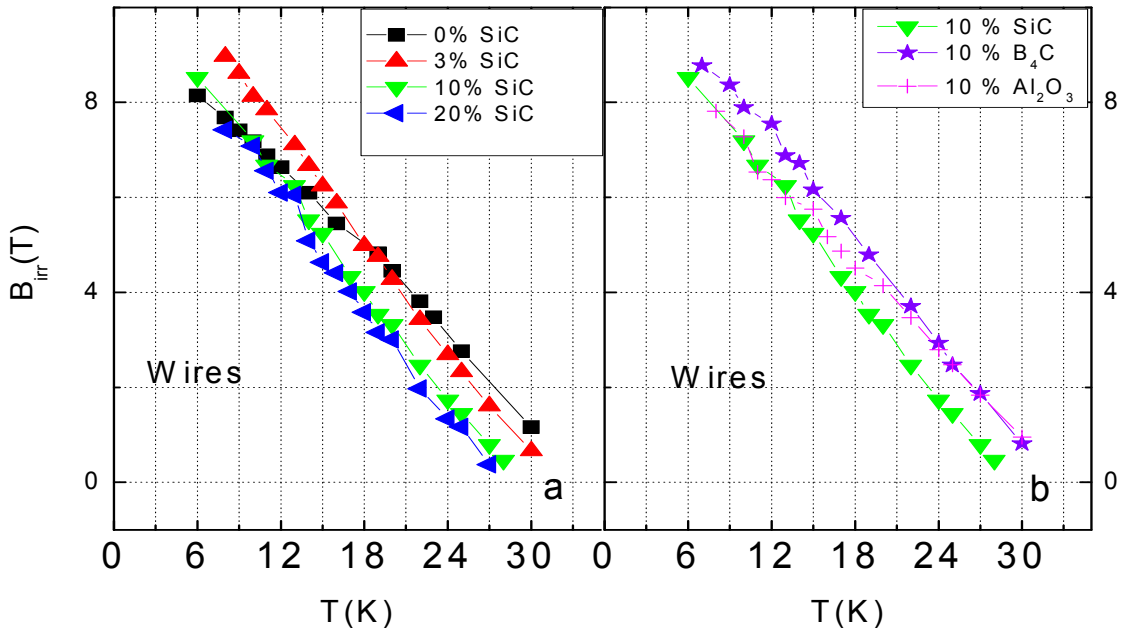


**Figure 3.30 $B_{Irr}$ versus temperature determined from $J_c$-$B$ curves with 100 A/cm$^2$ criterion for wires with (a) SiC additions and (b) same concentration of different additives.**

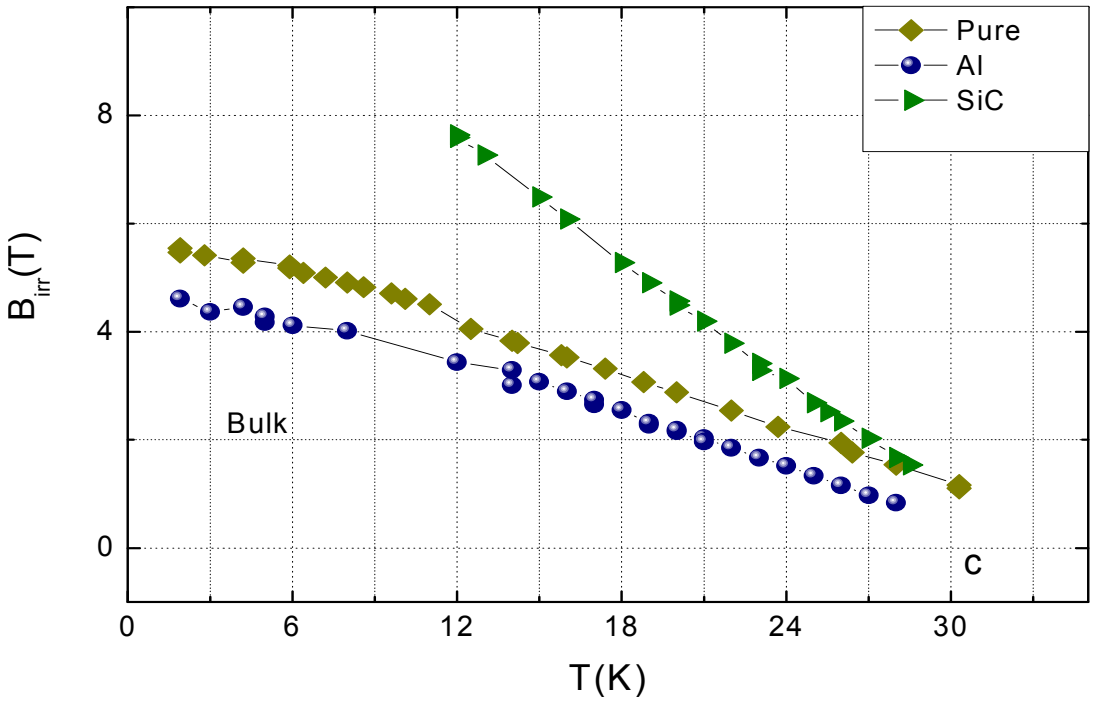


**Figure 3.30c $B_{Irr}$ versus temperature determined from $J_c$-$B$ curves with 100 A/cm$^2$ criterion for bulk samples with and without additives.**

In case of the wires with the same concentration but different contents (Fig. 3.30b), the sample with 10% $B_4C$ has highest $B_{irr}$ in the whole temperature range, while SiC addition shows the lowest. The temperature dependence of $B_{irr}$ is more flat for the sample with $Al_2O_3$ than for the samples with $B_4C$ and SiC addition. Both of which show a very similar temperature dependence.

In case of bulk samples (Fig.3.30c), the compound with SiC has the highest irreversibility field but a very sharp decrease with temperature giving similar value of $B_{irr}$ as for the other samples at about 28 K. Al addition shows the smallest $B_{irr}$. At low temperature, for 0% SiC inclusions the wire has higher $B_{irr}$ than the bulk sample e.g. at 10 K, the value of $B_{irr}$ is 7.5 T and 4.5 T for wire and bulk, respectively. At 30 K the values become very similar (≈1 T). The SiC addition in bulk increases $B_{irr}$ stronger than in case of wires.

## 3.7 Upper critical field

Upper critical fields ($H_{c2}$) for all samples are given in Figs. 3.31 for wires (a), (b) and bulk samples (c). The Nb sheathed wire with 3% SiC addition shows highest $H_{c2}$ up to 23 K. For higher temperatures, the 0% and 3% SiC have approximately the same $H_{c2.}$ Below 20 K the critical field for 10% SiC is nearly the same as that of the 0% SiC sample and for higher temperatures $H_{c2}$ decreases stronger with temperature than for the other samples. Above 15 K the wire with 20% SiC has the lowest $H_{c2}$ in this group.

For the wires with same concentration but different type of addition (Fig. 3.31b), $H_{c2}$ for the $B_4C$ substituted sample is highest. $H_{c2}$ for the sample with $Al_2O_3$ is lowest below 23 K, but becomes as high as for the $B_4C$ substituted compound above 25 K. SiC and $B_4C$ have similar $H_{c2}$ up to 15 K beyond which SiC decreases more rapid with temperature.

For the bulk samples, the pure one has the highest $H_{c2}$ for the whole range of temperature (Fig. 3.31c). $H_{c2}$ for the Al sample has a smaller value at low temperature, becoming better than SiC at high temperature with a crossover at about 20 K.

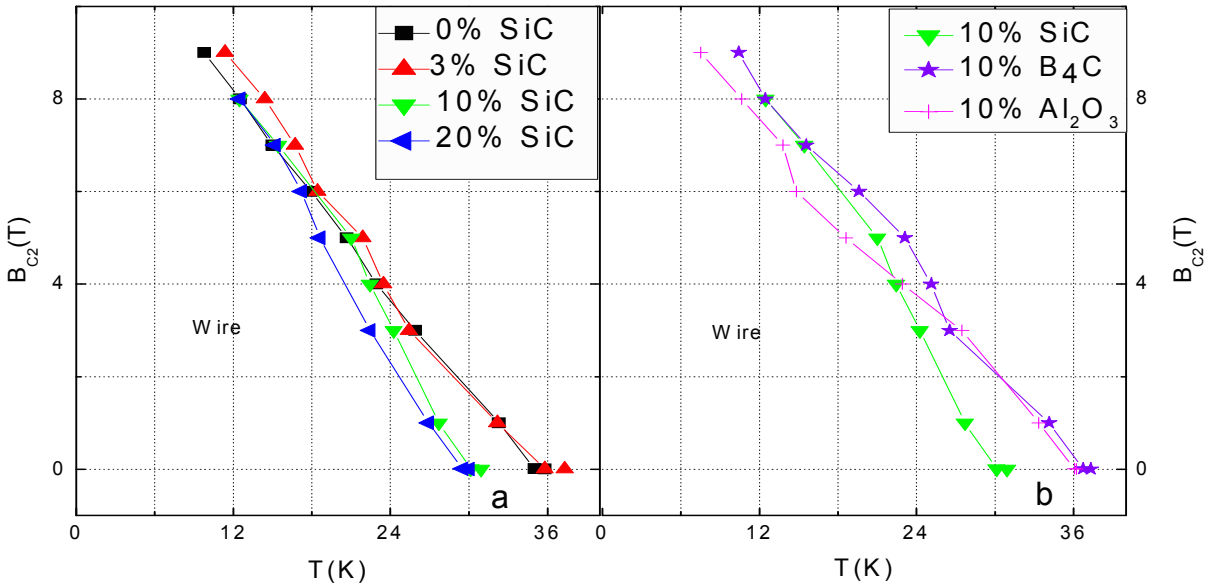


**Figure 3.31 $B_{c2}$ as a function of temperature calculated from the field dependence of the onset $T_c$ for wires with (a) different SiC concentrations and (b) same concentration of different additives.**

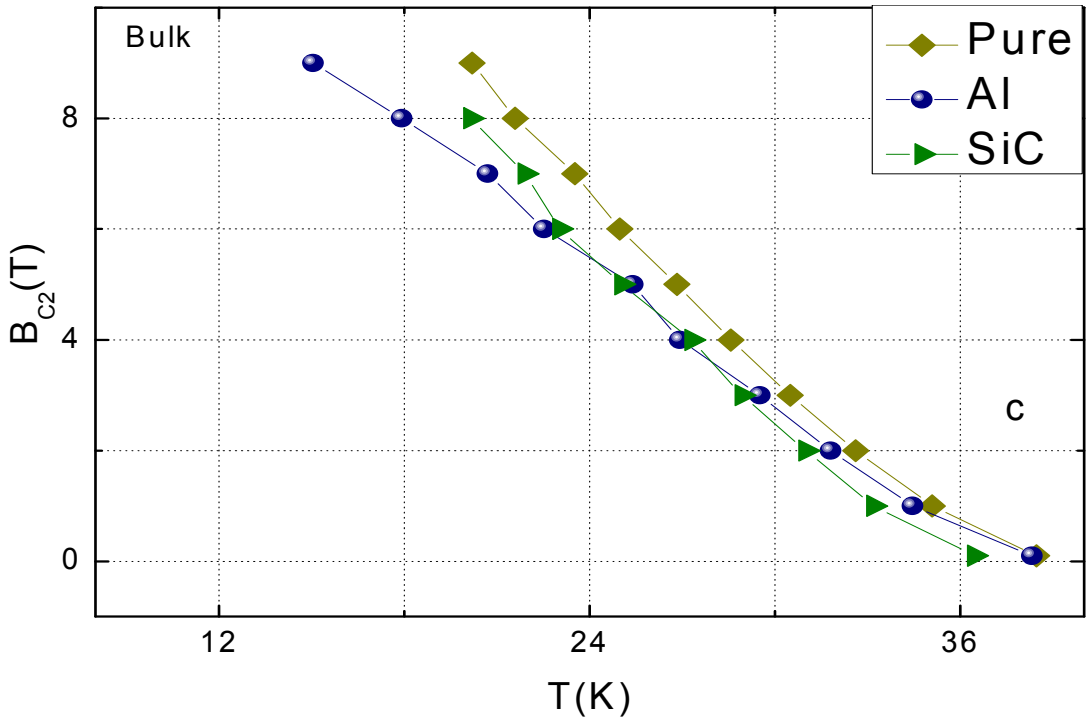


**Figure 3.31c $B_{c2}$ as a function of temperature calculated from the field dependence of the onset $T_c$ for bulk samples with and without additions.**

The pure bulk sample shows higher $H_{c2}$ values than the wire with 0% SiC. At 20 K the difference between $H_{c2}$ values in case of pure bulk and 0% SiC wire is approximately 4 T. This difference is reduced to ~1.5 T at 30 K.

A comparison of the influence of 10% SiC addition in bulk and wire gives similar large differences.

## 3.8 Pinning force

The pinning force ($F_p$) was determined from $J_c$-$B$ curves for the measured temperatures and was normalized to its maximum value. Similarly the corresponding field was normalized to $B_{irr}$ for each temperature. The results for normalized $F_p$ versus normalized field are shown in Figs. 3.32 to 3.40 for all samples.

The maxima for all samples are near or below 0.2. The degree of scaling, defined by the spread in field and pinning force at $B/B_{irr}$ = 0.5 and $F_p/F_{p,max}$ = 0.5, is best for the Al containing samples, both for the bulk and for the wire with 10% $Al_2O_3$ addition. Generally, wires show more spread than bulk samples. With increasing concentration of the additives, scaling gets worse. The largest spread is found for the wire with 10% SiC substitution. For the samples with $B_4C$ and $Al_2O_3$ scaling is much better than for the 10% SiC wire. A small deviation from the expected shape of the curve, visible as a small hump around $B/B_{irr}$ = 0.5, appears in the bulk samples without and with Al substitution.

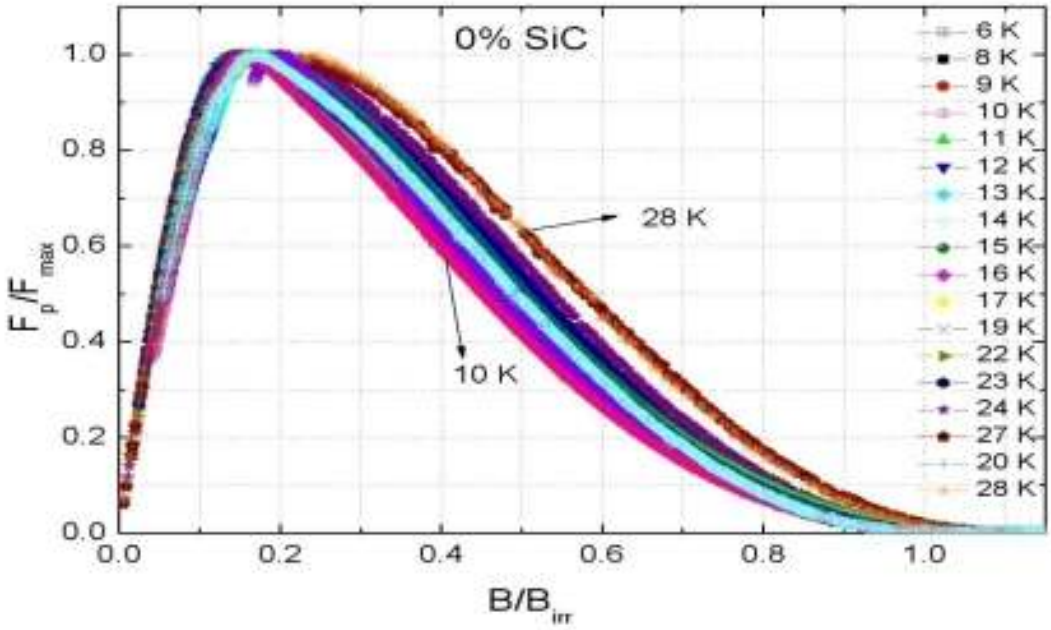


**Figure 3.32 Normalized pinning force as a function of normalized magnetic field for $MgB_2$/Nb wire with 0% SiC addition at different temperatures.**

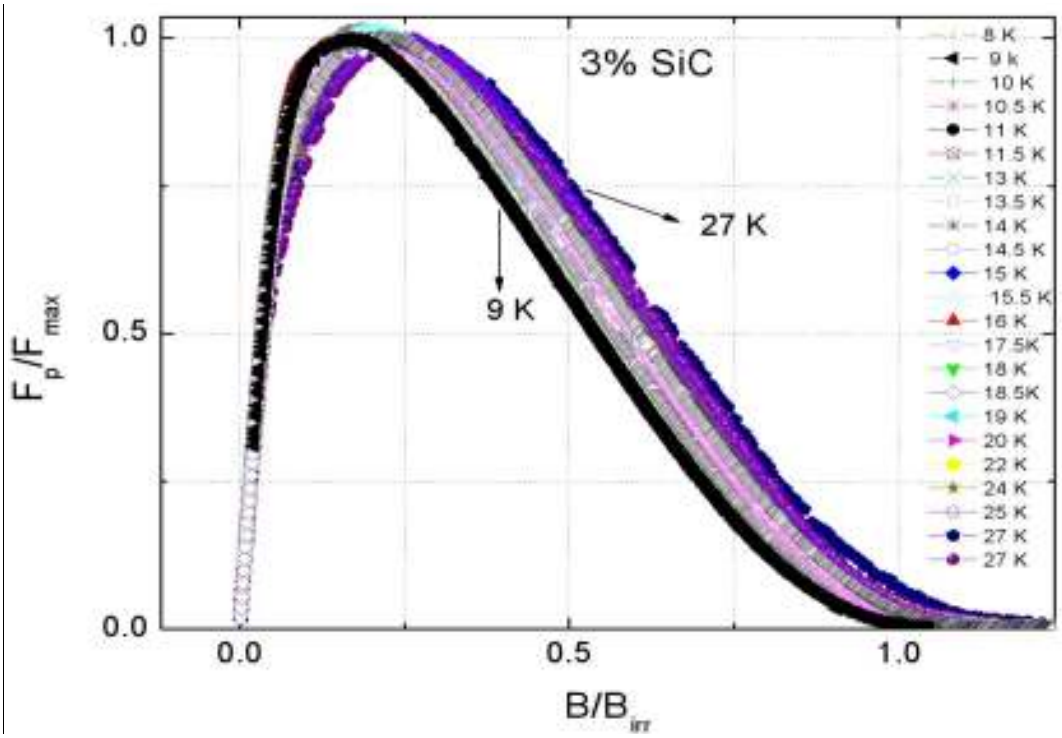


**Figure 3.33 Normalized pinning force as a function of normalized magnetic field for $MgB_2$/Nb wire with 3% SiC addition at different temperatures.**

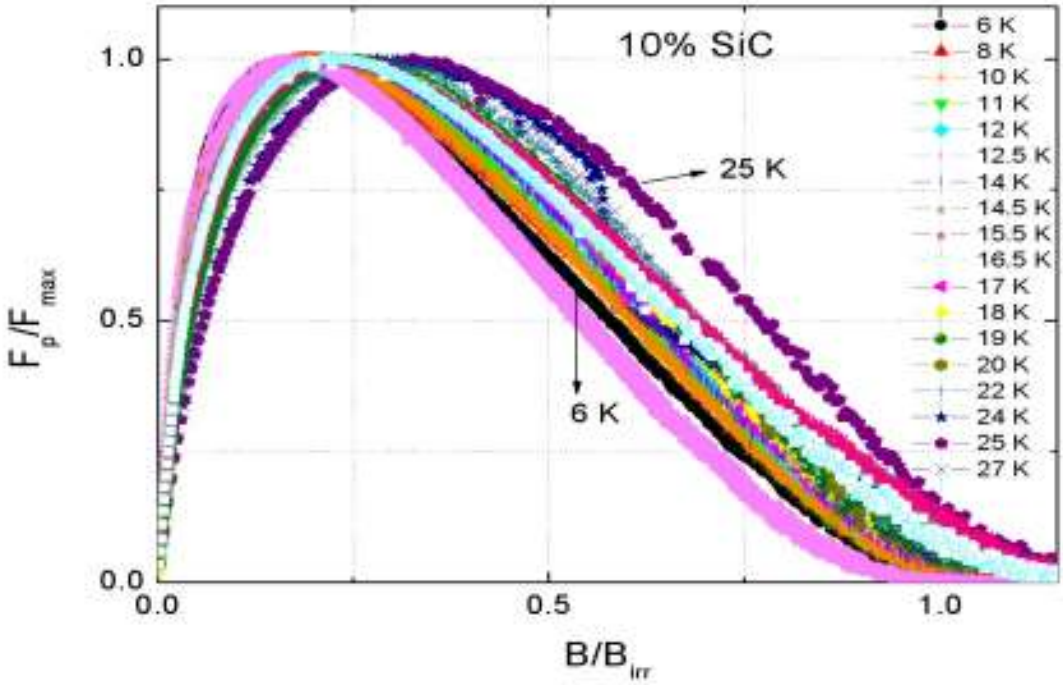


**Figure 3.34 Normalized pinning force as a function of normalized magnetic field for $MgB_2$/Nb wire with 10% SiC addition at different temperatures.**

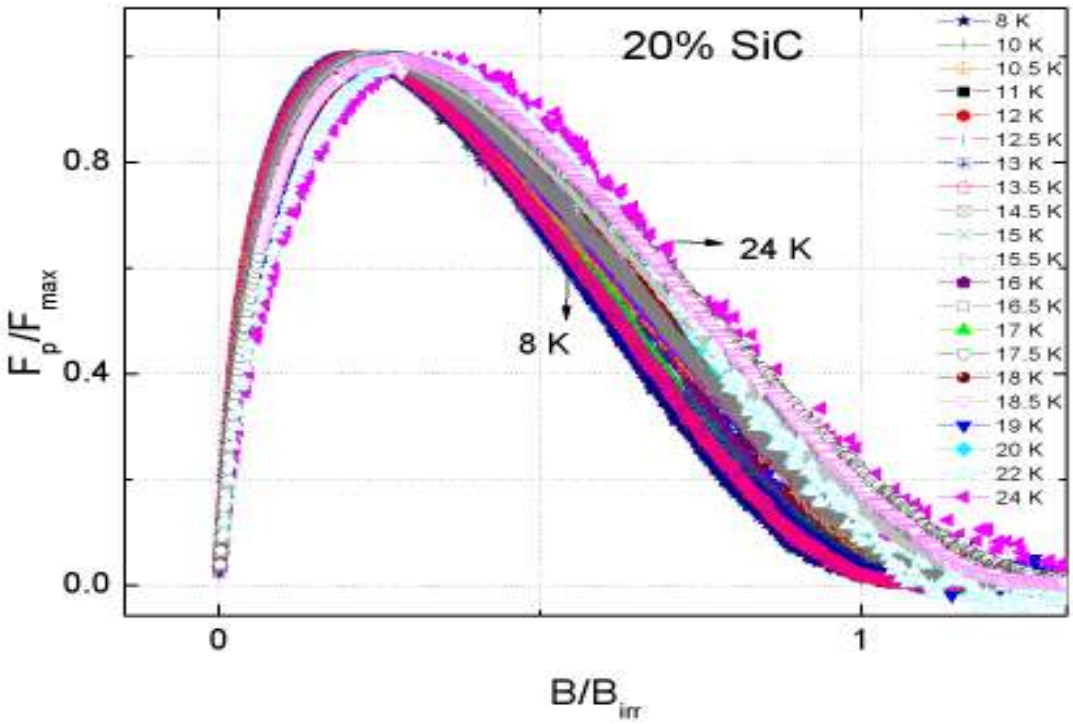


**Figure 3.35 Normalized pinning force as a function of normalized magnetic field for $MgB_2$/Nb wire with 20% SiC addition at different temperatures.**

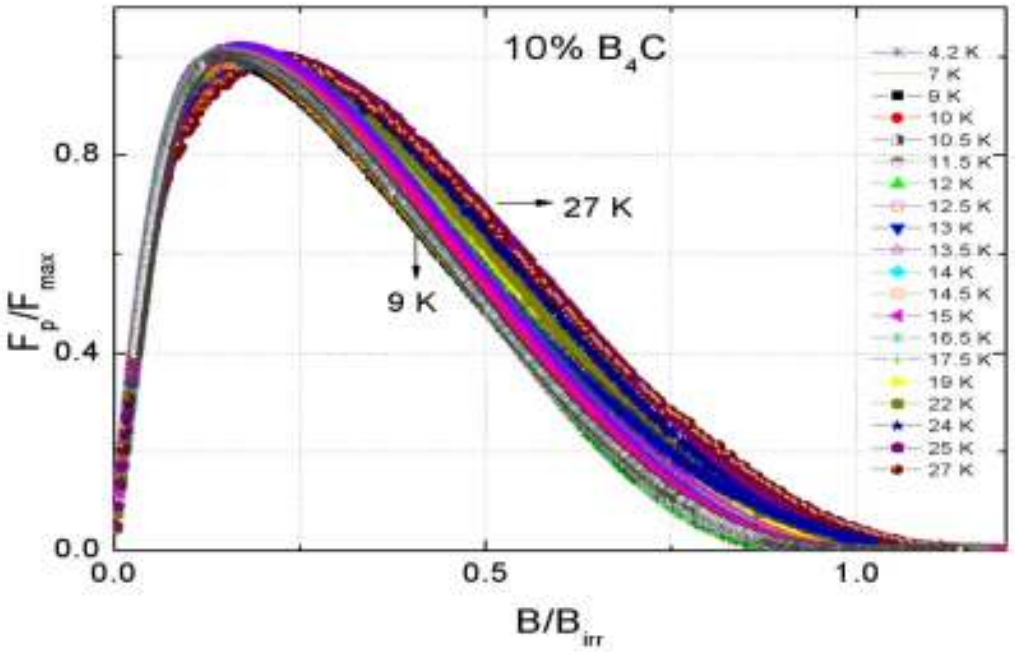


**Figure 3.36 Normalized pinning force as a function of normalized magnetic field for $MgB_2$/Nb wire with 10% $B_4C$ addition at different temperatures.**

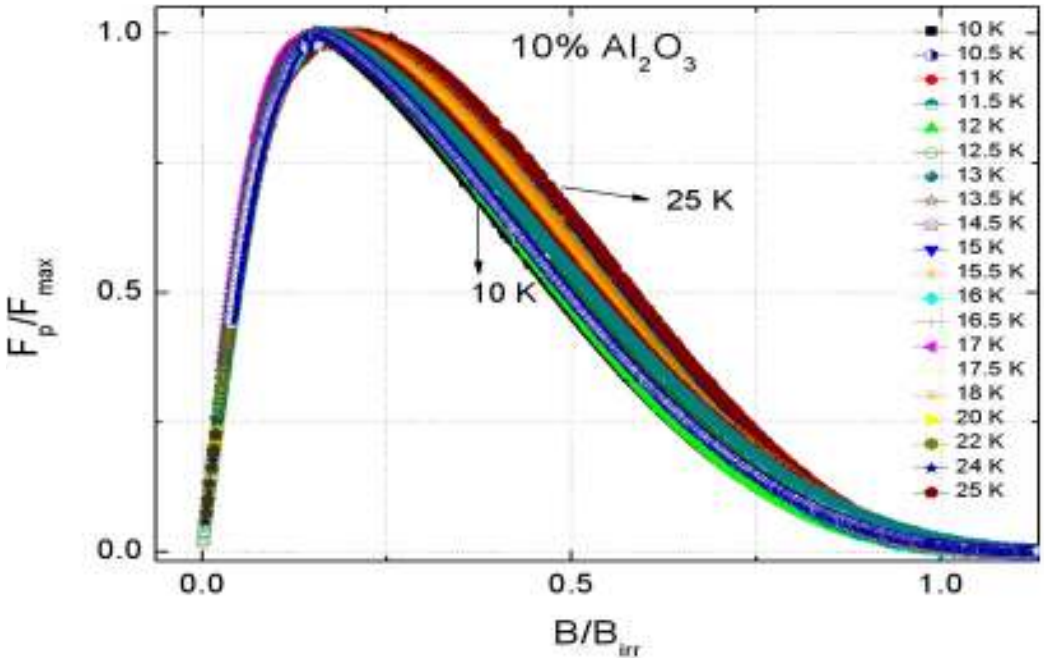


**Figure 3.37 Normalized pinning force as a function of normalized magnetic field for $MgB_2$/Nb wire with 10% $Al_2O_3$ addition at different temperatures.**

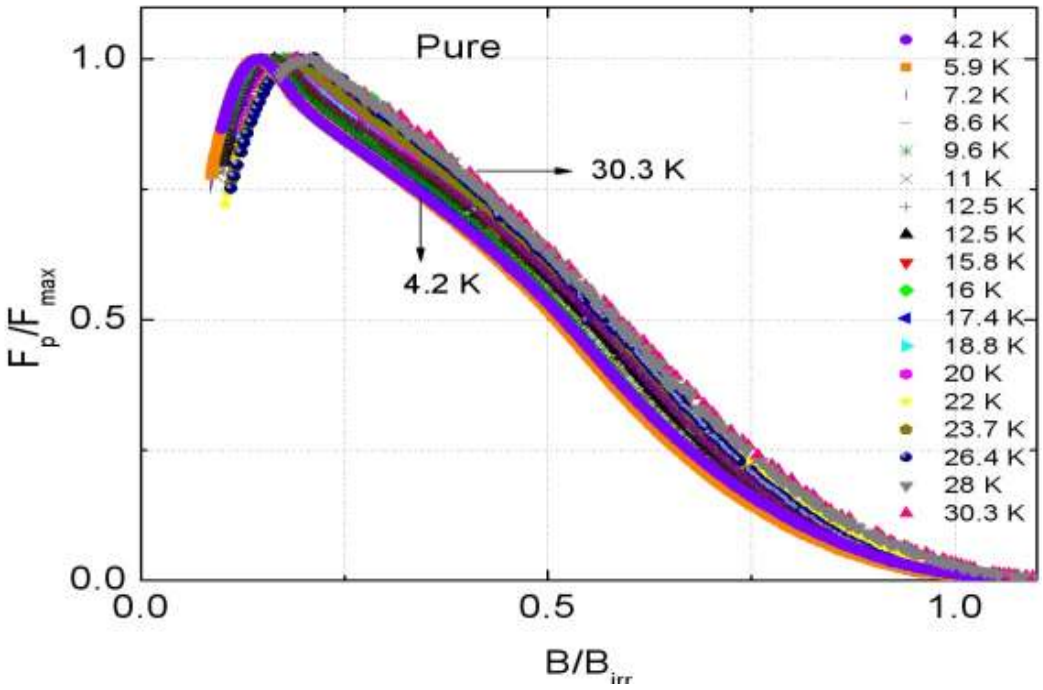


**Figure 3.38 Normalized pinning force as a function of normalized magnetic field for pure bulk samples addition at different temperatures.**

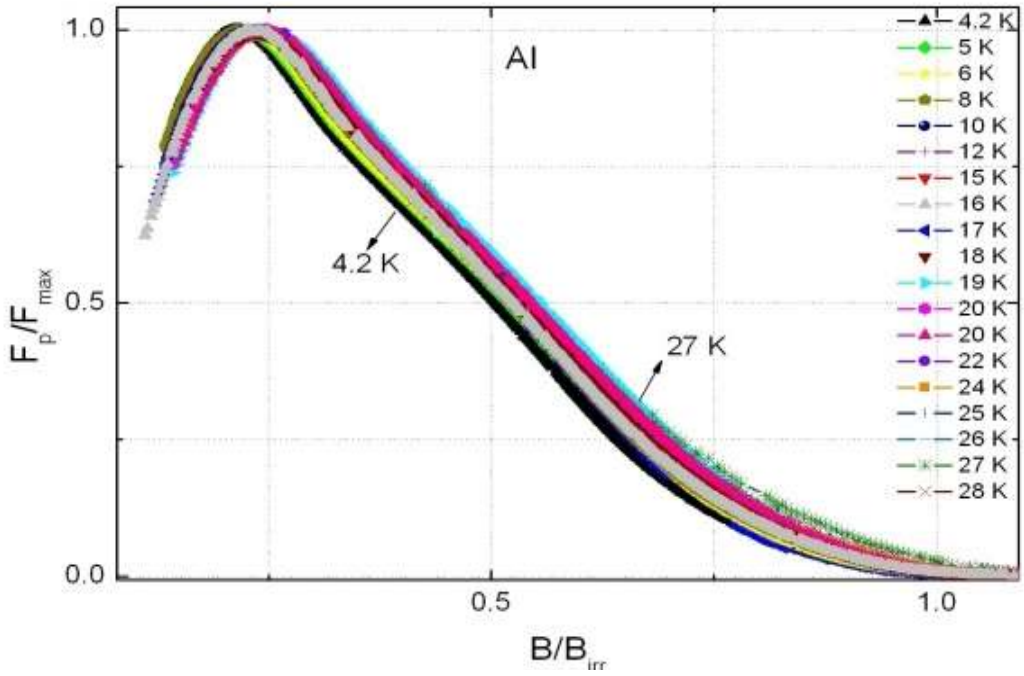


**Figure 3.39 Normalized pinning force as a function of normalized magnetic field for bulk samples with Al addition at different temperatures.**

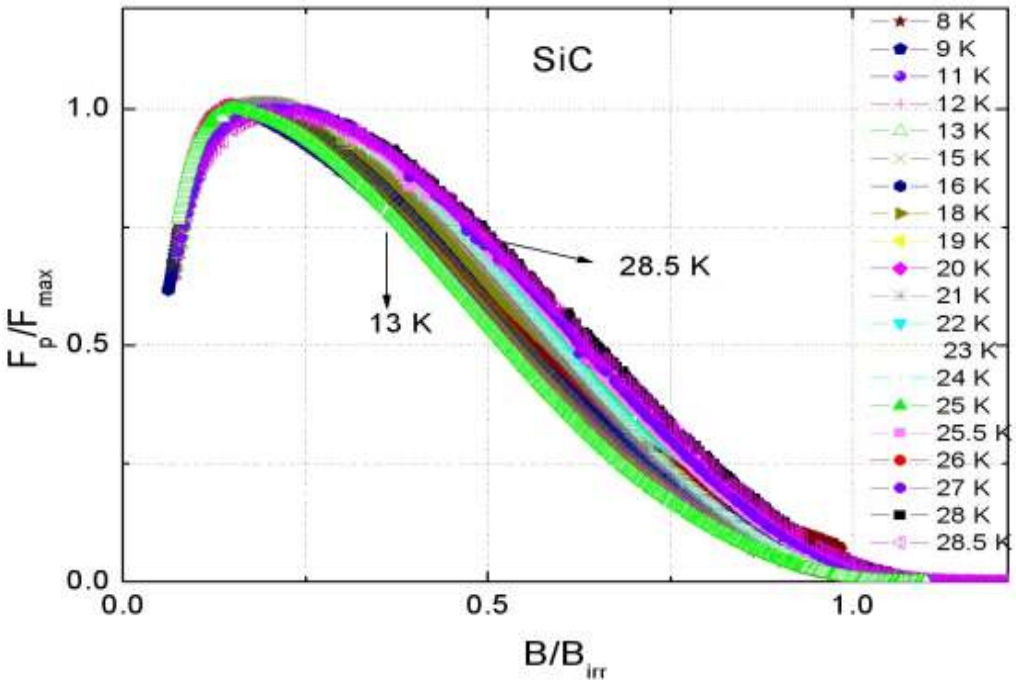


**Figure 3.40 Normalized pinning force as a function of normalized magnetic field for bulk samples with SiC addition at different temperatures.**

## 3.9 Magnetic relaxation measurements

Relaxation curves were obtained from magnetic measurements for all samples between 8 and 30 K at 1 and 3 T in increasing field. Typical normalized relaxation curves are shown in Figs. 3.41, 3.42a and 3.42b for one temperature at 1 and 3 T for all measured samples. The wires with different SiC concentrations show an increasing normalized relaxation with increasing SiC concentration at both 1 and 3 T. In the wires with constant concentration of different additives, 10 % SiC has the strongest relaxation rate at both fields, whereas relaxations for $Al_2O_3$ and $B_4C$ substituted wires are nearly the same. In bulk samples the sample with Al addition shows smallest relaxation at 1 T but highest one at 3 T. The bulk sample with SiC inclusions has the weakest time dependence at 1 T but highest at 3 T.

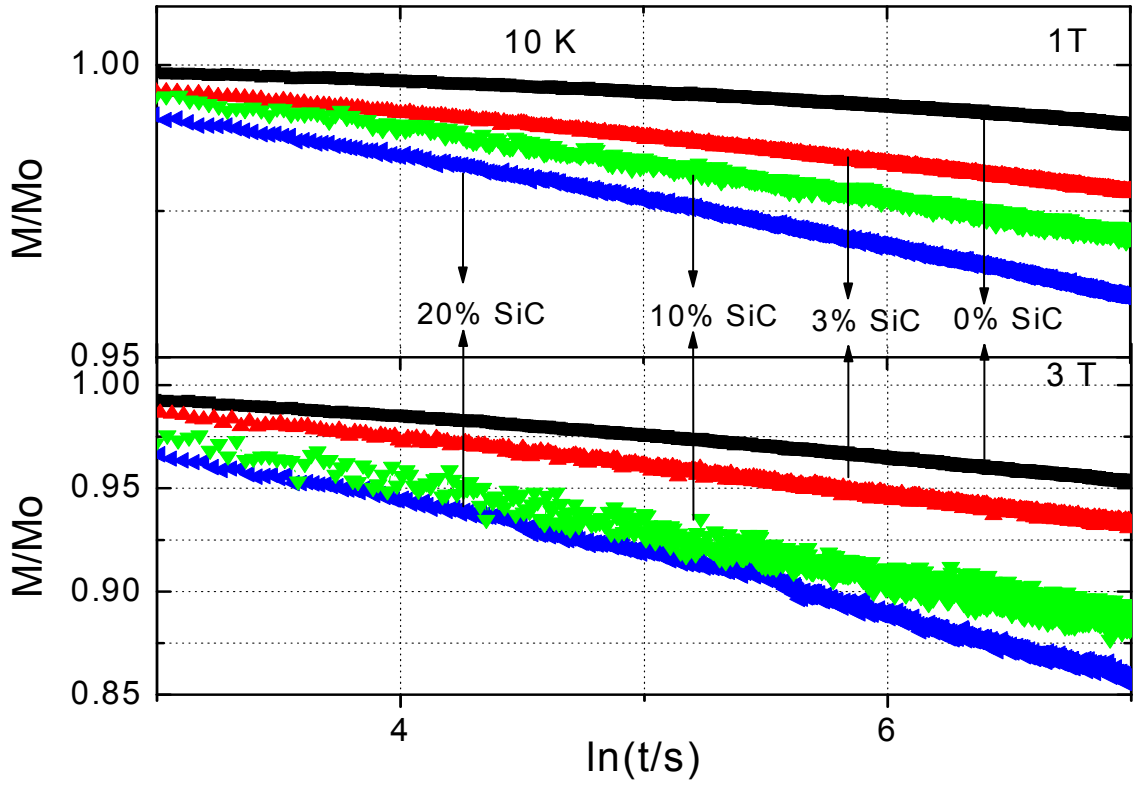


**Figure 3.41 Time dependence of normalized magnetic moment versus logarithmic time for $MgB_2$ wires with different SiC concentrations for 10 K at two fields.**

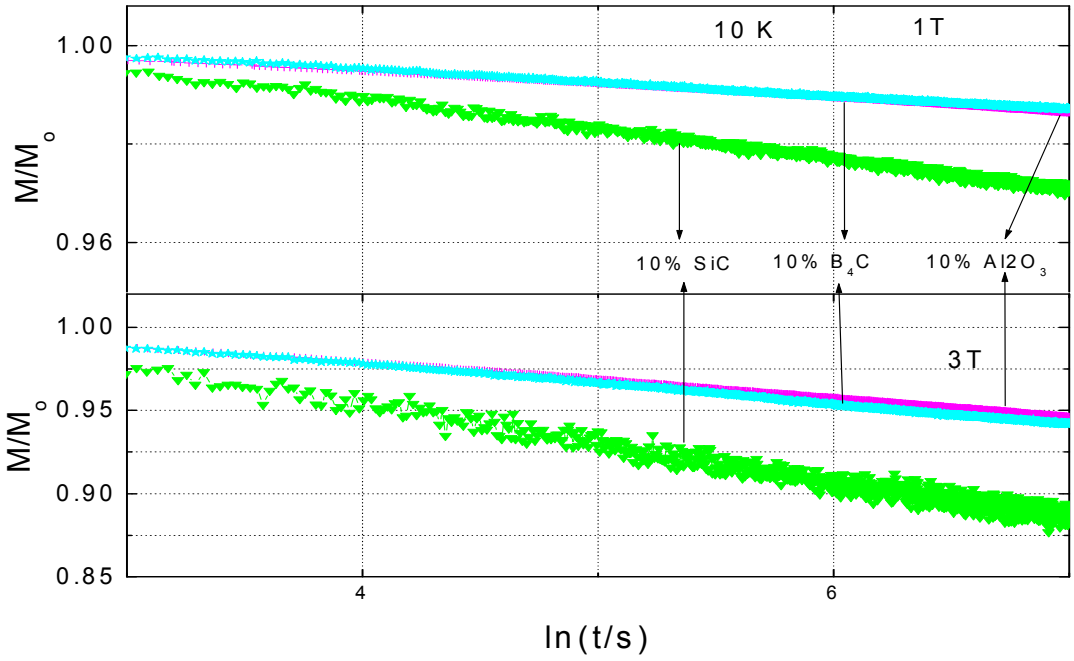


**Figure 3.42a Time dependence of normalized magnetic moment for $MgB_2$ wires with same concentration of different additives for 10 K at two fields.**

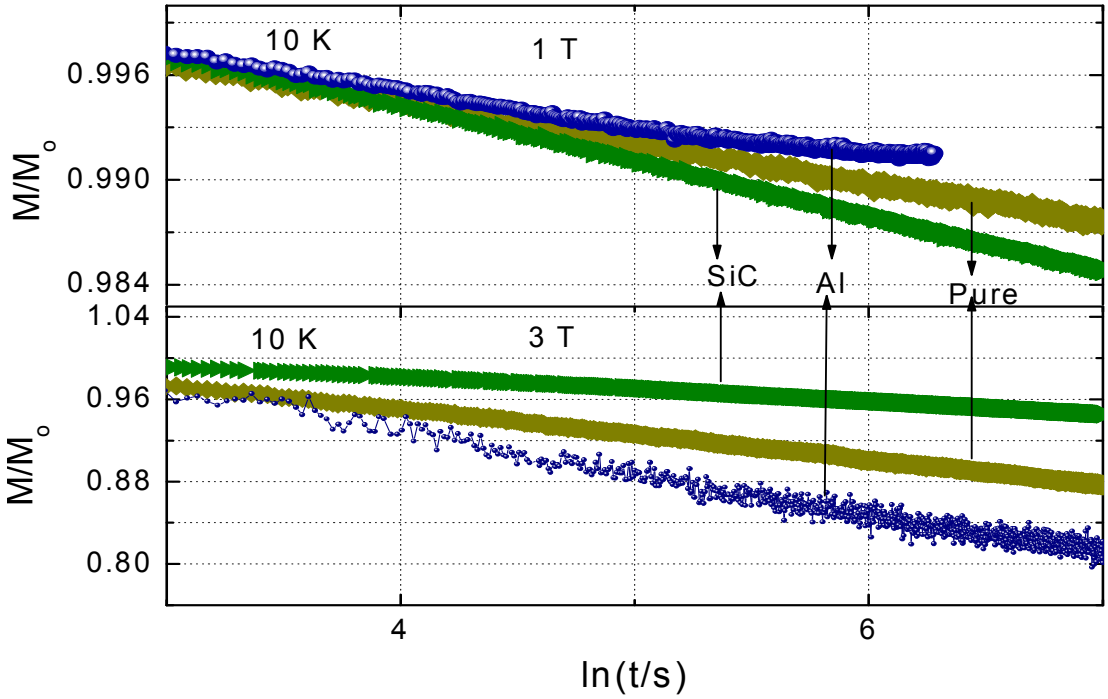


**Figure 3.42b Time dependence of normalized magnetic moment for bulk samples for 10 K at two fields.**

## 3.10 Mean effective activation energy

Figs. 3.43 to 3.45 show the temperature dependence of the creep rate obtained from the relaxation curves. In each case the creep rate increases with temperature up to a maximum and then decreases with further increasing temperature. The maximum shifts to lower temperatures at the higher field. In case of wires with SiC additions the creep rate decreases systematically with increasing concentration of SiC for both fields. The wire with 0% SiC has the maximum at about 15 K for 1 T which shifts to 10 K at 3 T. All other concentrations show the maxima at about 10 K both at 1 and 3 T.

In the wires with constant concentration of different additives, the wires with $B_4C$ and $Al_2O_3$ additions show similar creep rates for both fields and in the whole temperature range while sample with SiC addition has the smallest creep rate in this group for both fields

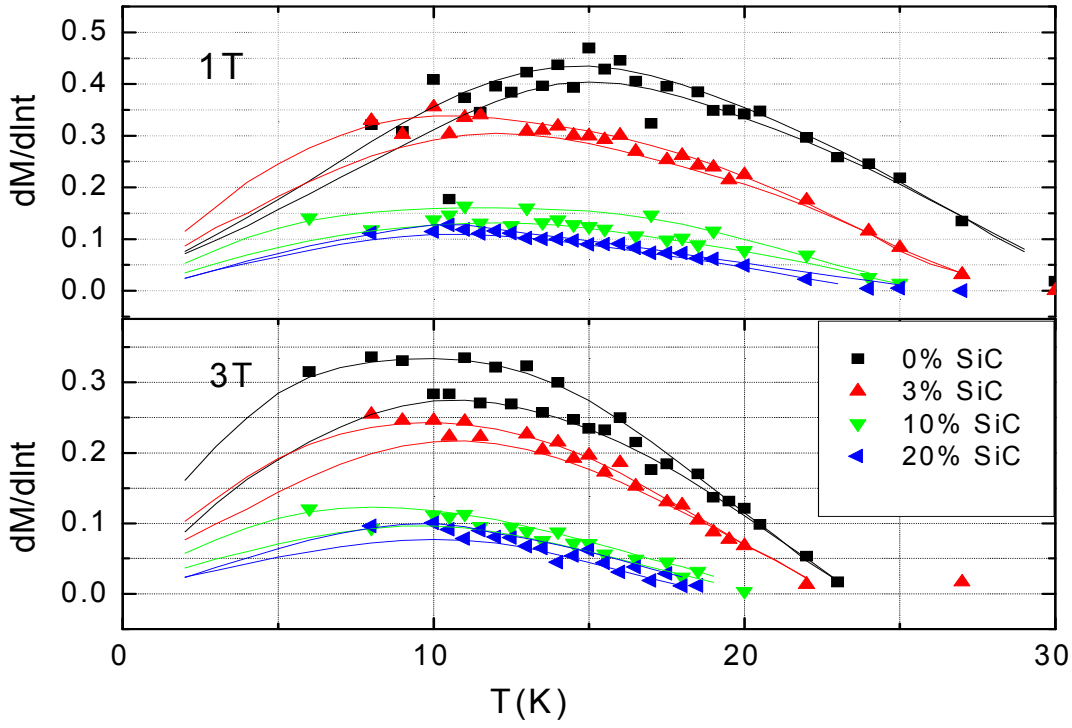


**Figure 3.43 Temperature dependence of the creep rate for $MgB_2$/Nb wires with different SiC concentrations at two fields. For each sample the lines represent the two curves which were used in the analysis of the activation energy distribution.**

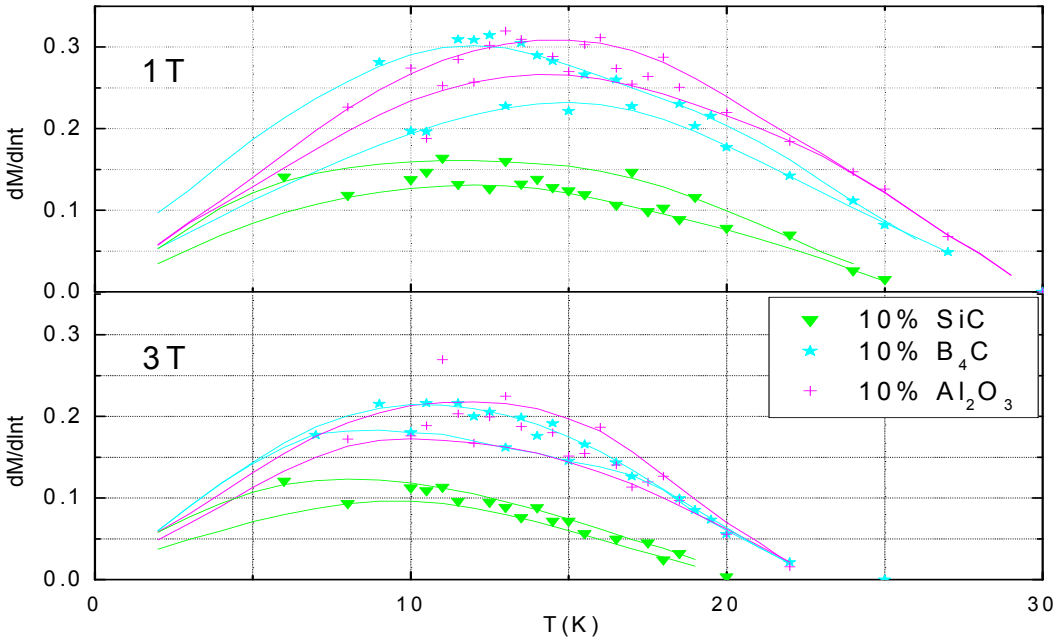


**Figure 3.44 Temperature dependence of the creep rate for $MgB_2$/Nb wires with constant concentration of different additives at two fields. For each sample the lines represent the two curves which were used in the analysis of the activation energy distribution.**

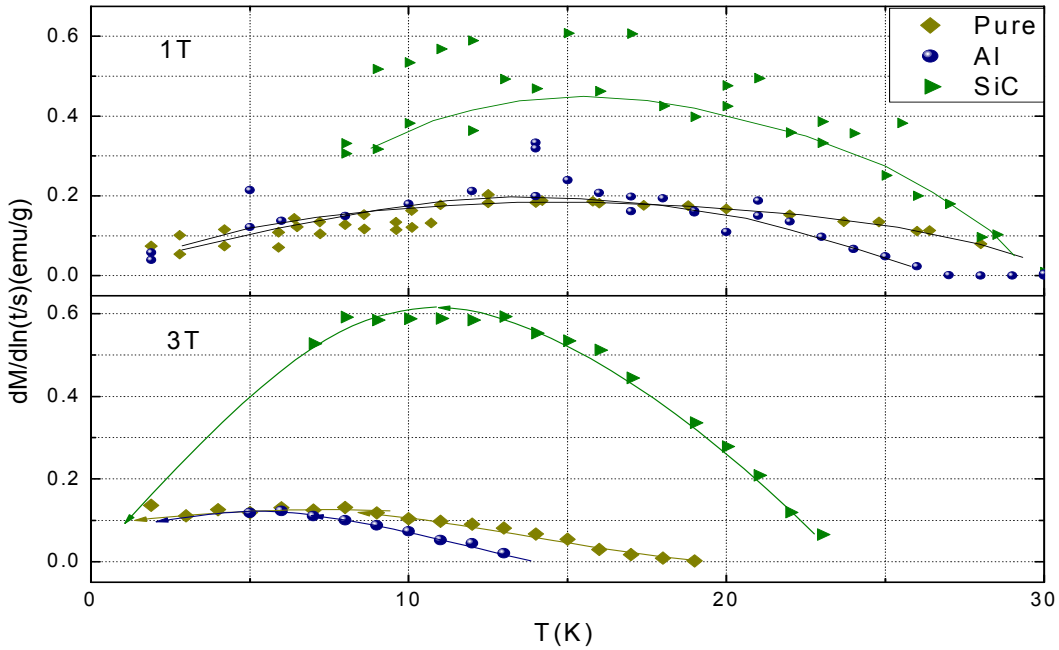


**Figure 3.45 Temperature dependence of the creep rate for $MgB_2$ bulk samples with and without particle additions at two fields.**

In bulk samples the SiC addition gives a higher creep rate value at 3 T than all other samples and the difference between 1 T and 3 T is not as pronounced as for all other samples especially at low temperature. Pure and Al substituted samples have similar temperature dependence of the creep rate.

Normalizing the creep rate according to equation (2.8) and making use of Anderson flux creep theory, the mean effective activation energies were determined by equation (2.7), assuming the relaxation time to be in the range between $10^{-12}$s and $10^{-6}$s. The thus obtained mean effective activation energies were averaged to <*U*>. The results are shown in Figs. 3.46 to 3.48 for all samples.

For all measured samples the mean effective activation energy shows a maximum at rather low temperatures. Within measuring accuracy no difference between <*U*> obtained from relaxations measured in increasing or decreasing field is found. Only for the wire with 0% SiC a systematic deviation below 15 K seems to be present (Fig.3.46).

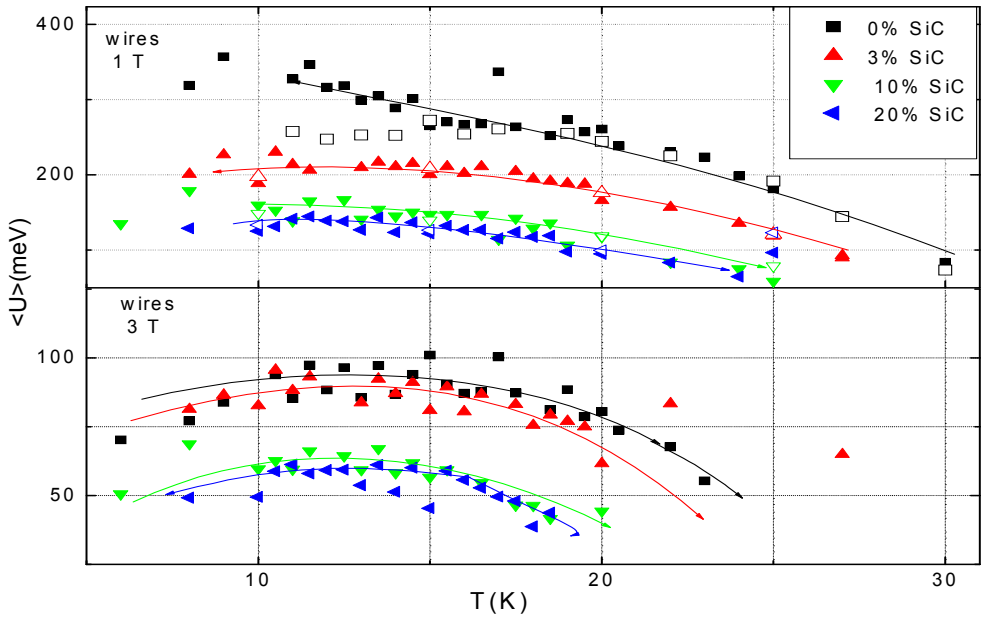


**Figure 3.46 Temperature dependence of mean effective activation energy of $MgB_2$/Nb wires with different concentrations of SiC at two fields. Full (open) symbols represent activation energies taken in increasing (decreasing) field.**

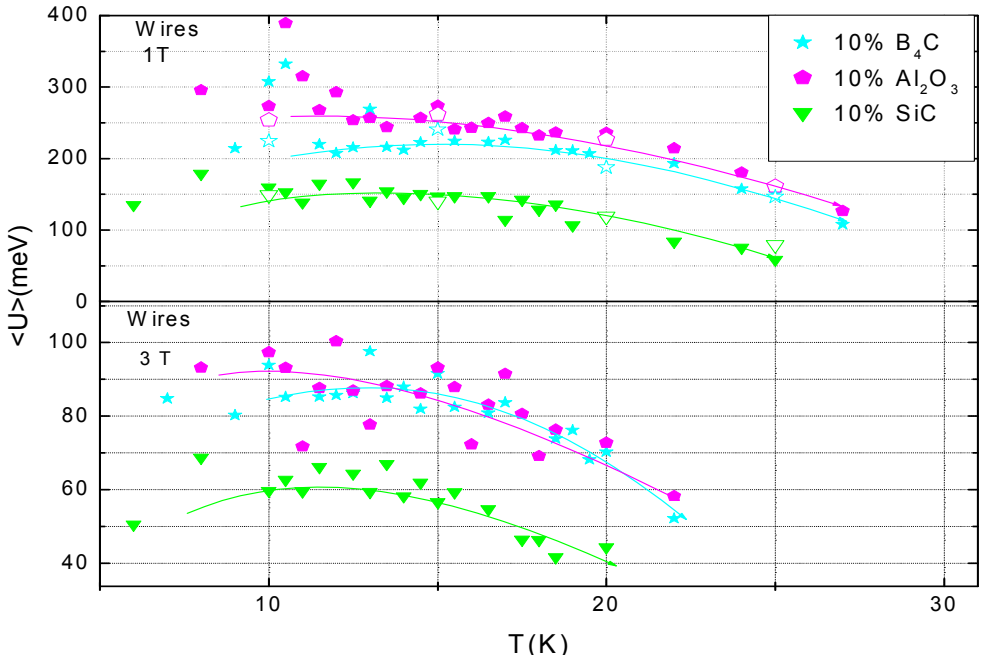


**Figure 3.47 Temperature dependence of mean effective activation energy of $MgB_2$/Nb wires with different particles addition having same concentration for two fields. Full (open) symbols represent activation energies taken in increasing (decreasing) field.**

The wire with 0% SiC has highest activation energy at 1 T, whereas at 3 T <*U*> is nearly the same for 0% and 3% SiC substituted samples. For the other SiC concentrations the activation energy decreases with increasing concentration as shown in Fig. 3.46. Although slightly higher, the mean effective activation energy for the 10% SiC substituted sample is nearly the same as for the 20% SiC substituted one for both fields.

In case of the wires with same concentration but different additives (Fig. 3.47) it turns out that both the $B_4C$ and $Al_2O_3$ substituted samples have higher mean effective activation energies than the SiC substituted compound for both 1 and 3 T. Within measuring accuracy no difference between the first two samples could be found.

It can be seen from Fig. 3.48 that the activation energies of bulk samples at 1 T are the same for increasing (solid symbols) and decreasing field (open symbols). Whereas the increase of <*U*> at low temperatures and 1 T is only weakly indicated in case of the wires, it is clearly seen in the bulk compounds. The highest mean effective activation energy is found for the pure sample at 1 T. At 3 T for temperatures below 16 K, <*U*> is highest for the sample with SiC inclusions.

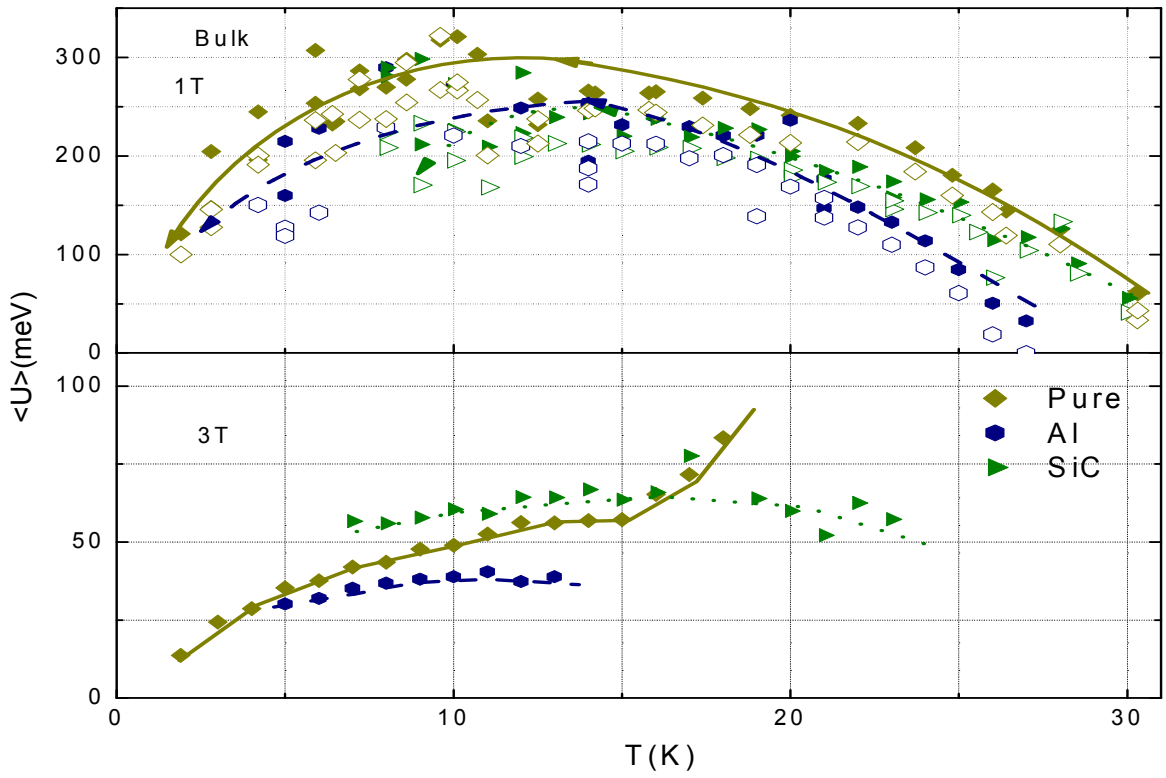


**Figure 3.48 Temperature dependence of the mean effective activation energy for bulk $MgB_2$ samples in two fields. Full (open) symbols represent activation energies taken in increasing (decreasing) field.**

## 3.11 Field dependence of mean effective activation energy

In order to study the field dependence of the mean effective activation energy, relaxation measurements were carried out at 10 K at different fields in the range 1 to 7 T for all samples. The results are given in Fig. 3.49.

In $MgB_2$/Nb wires highest <*U*> is observed for 0% SiC addition below 4.5 T. At higher fields 3% SiC shows highest <*U*>. The wire with 20% SiC concentration has the lowest value of <*U*> below 6 T. For the field above 6.5 T, sample with 0% SiC shows lowest activation energy.

For wires with same concentration of different additives, the samples with $Al_2O_3$ and $B_4C$ additions show more or less similar activation energies in the whole field range while the sample with SiC addition has smallest <*U*> in whole field range. At higher fields, all three samples give similar <*U*>.

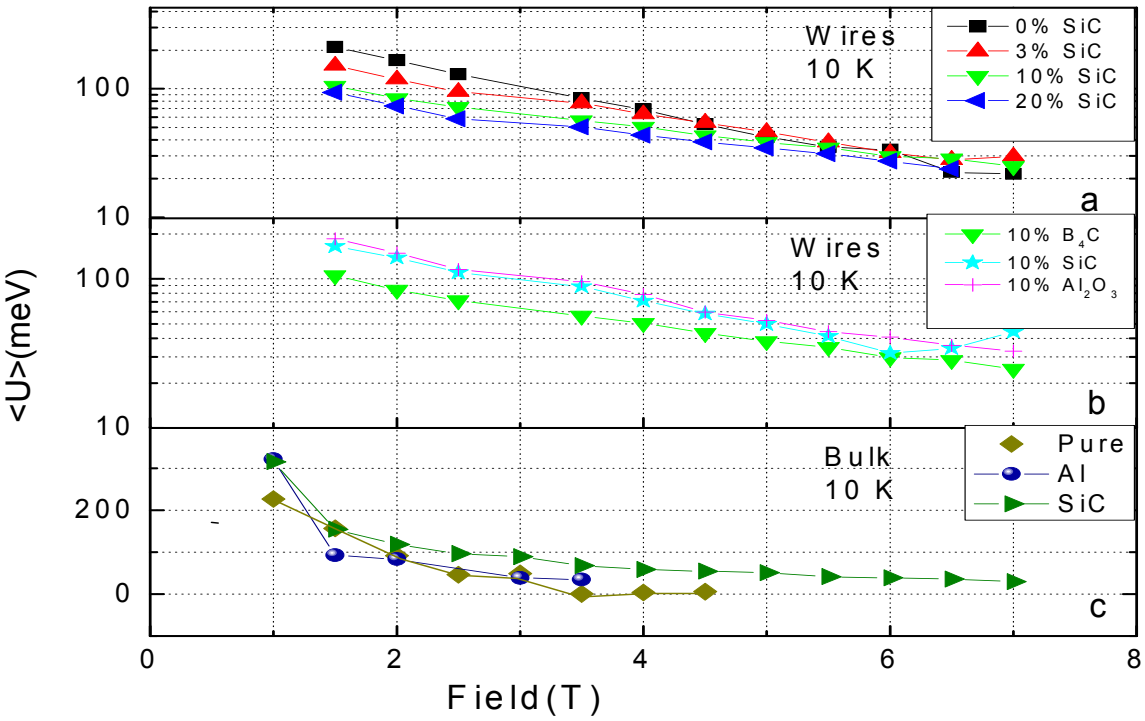


**Figure 3.49 Field dependence of mean effective activation energy at 10 K for wires (a), (b) and bulk samples (c).**

In case of bulk samples the irreversibility fields are 4.5 T for pure and 3.5 T for Al substituted sample, thus the relaxation measurements were carried out below these fields. The sample with SiC addition has the highest activation energy in the whole field range.

## 3.12 Activation energy distributions

Activation energy distributions were determined according to the model proposed by Hagen et al. [Hag90] (s. ch. 2.3.3). Expression (2.11) was used to determine the distribution function for the samples under study. A value of $10^{-12}$ s was used for the relaxation time. Due to the large scatter in the data of the creep rates for the wires (Figs. 3.43 and 3.44), two lines, representing an upper and lower limit of the temperature dependence of d*M*/dln*t*, were drawn through the data points. Both were used to determine the distribution functions. The two results define the error bars given in the figures. Only for the bulk samples a single line in each case was analyzed.

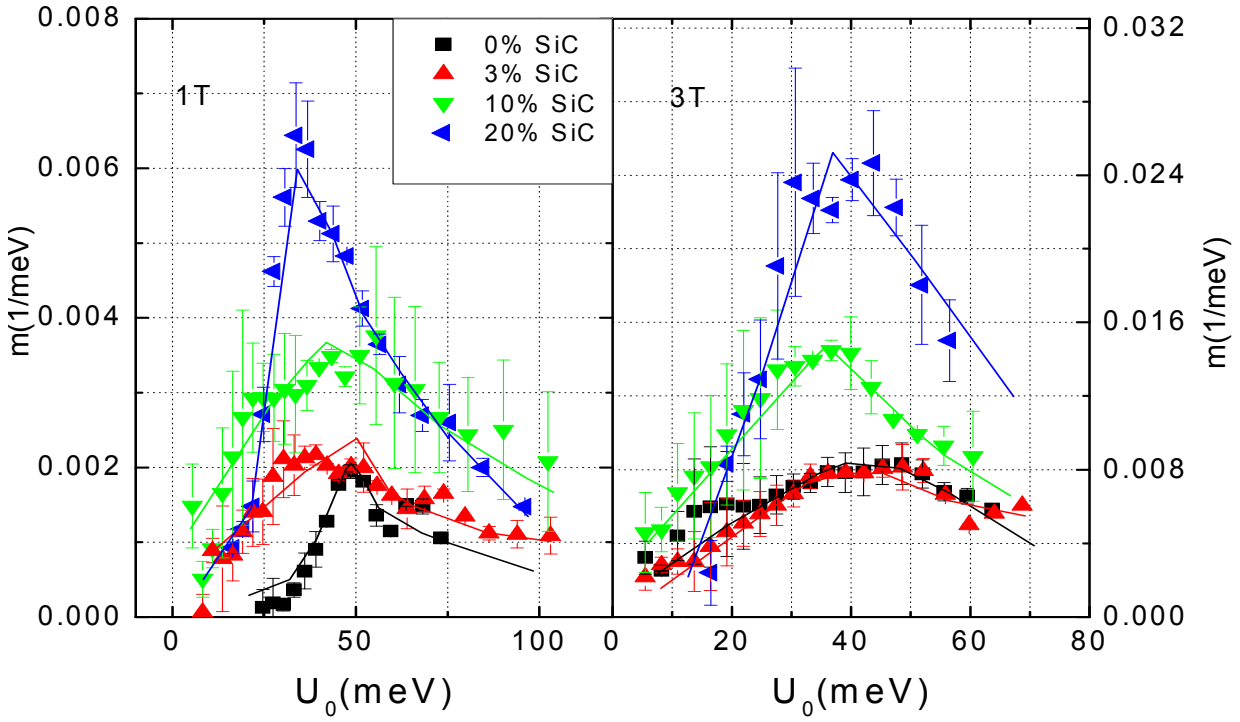


**Figure 3.50 Activation energy distributions for $MgB_2$/Nb wires with different SiC concentration at 1 T and 3 T.**

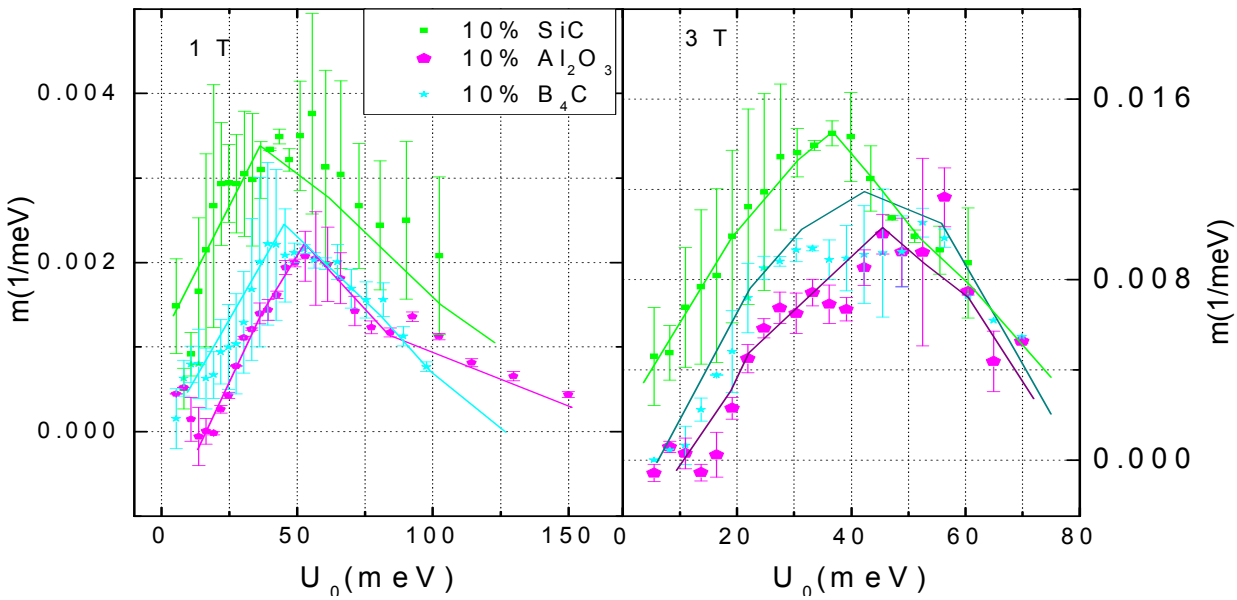


**Figure 3.51 Activation energy distributions for $MgB_2$/Nb wires with same concentration of different additives at 1 T and 3 T.**

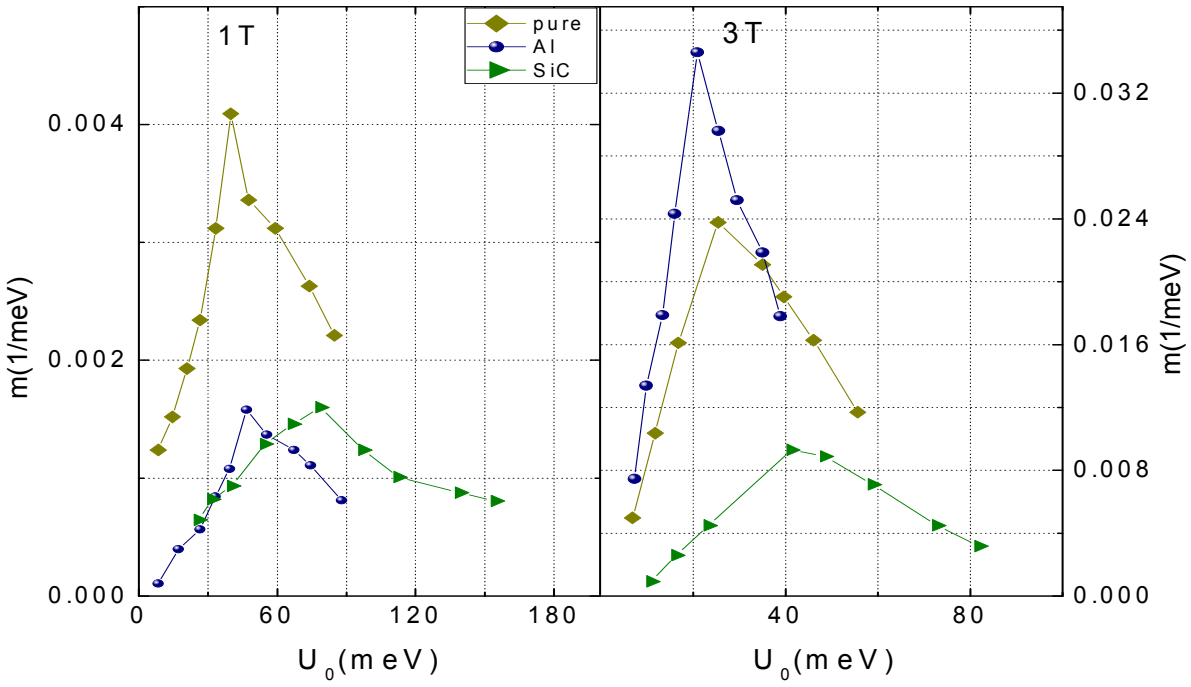


**Figure 3.52 Activation energy distributions for $MgB_2$ bulk samples with and without additives at 1 T and 3 T.**

The results are shown in Figs. 3.50 to 3.52. It can be seen that for all samples the distribution functions show a peak which is at higher energy at 1 T than at 3 T.

In case of wires with different SiC concentrations, the peaks shift to lower energy with increasing SiC concentration at 1 T. However at 3 T, it is noted that this shift is not very much pronounced. Samples with 0% and 3% SiC additions show very similar distribution function at 3 T.

For wires with the same concentration and different substitutions the peaks can be seen to be at lowest energy for SiC addition followed by wire with $B_4C$ addition while sample with $Al_2O_3$ has the peak at highest energy in this group.

For bulk samples (Fig. 3.52), one can observe that SiC addition shows the maximum in distribution at highest energy both at 1 and 3 T, while the maximum at the lowest energy is shown by the pure sample at 1 T and the sample with Al at 3 T.

## 3.13 Energy – current relation

In order to study the dependence of activation energy on critical current density, Maley's method was followed (s. ch. 2.3.5). Relation (2.13) was used to obtain the activation energy *U* from the relaxation data for all measured samples choosing a value of *C* for which most of the data points lie on a smooth curve. The results are shown in double logarithmic representation in Figs. 3.53 to 3.55 and the used *C* values are given in Table 3.4.

As expected the obtained *U*(*J*) curves are strongly non-linear for all samples. In wires with different SiC concentrations at 1T the activation energy is for all $M_{irr}$ values systematically decreasing with increasing SiC content. At 3 T the samples with 0% and 3% SiC show a crossover at about -44 emu/g. A similar crossover is seen between the curves for the samples with 10% and 20% SiC substitution at ~-7 emu/g.

In case of the wires with same concentration of different additives, the wire with $Al_2O_3$ addition has the highest activation energy at 1 T, while the sample with $B_4C$ substitution shows the highest activation energy at 3 T. No crossover is present for theses samples.

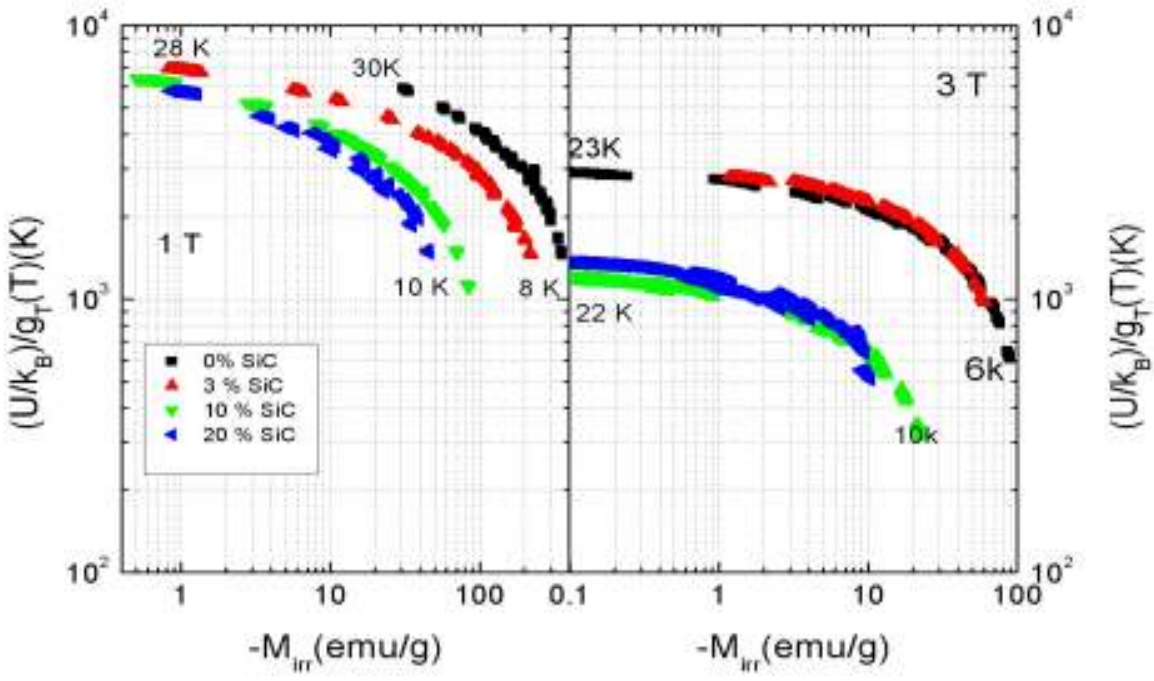


**Figure 3.53 Energy – current relation determined after Maley et al. [Mal90] at 1 and 3 T for $MgB_2$/Nb wires with different SiC substitution.**

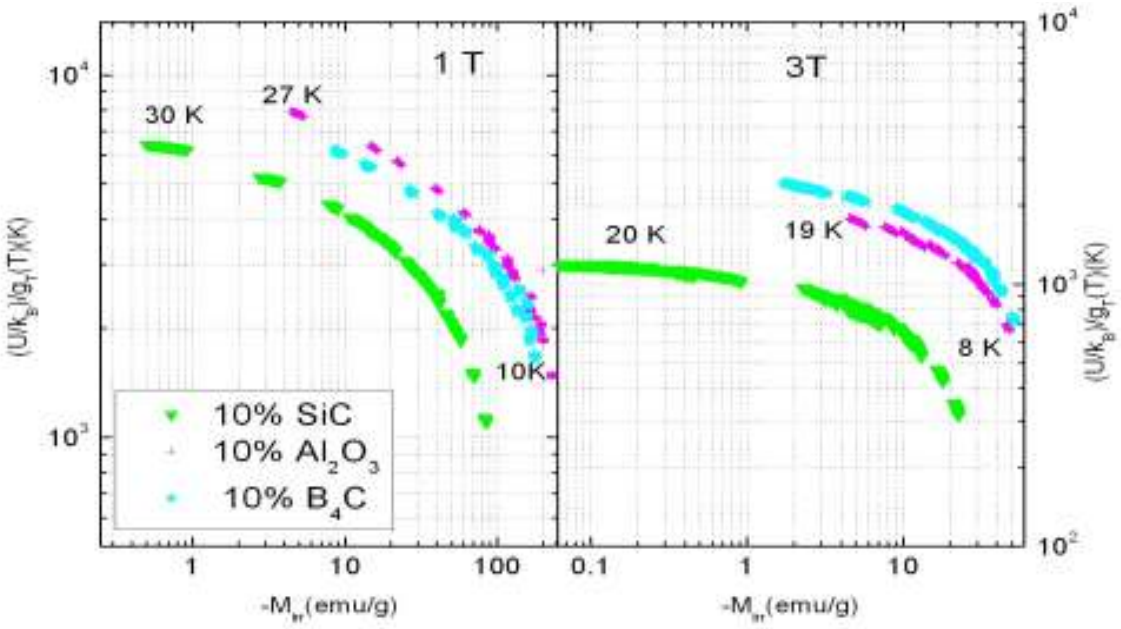


**Figure 3.54 Energy – current relation determined after Maley et al [Mal90] at 1 and 3 T for $MgB_2$/Nb wires with same concentration of different additives.**

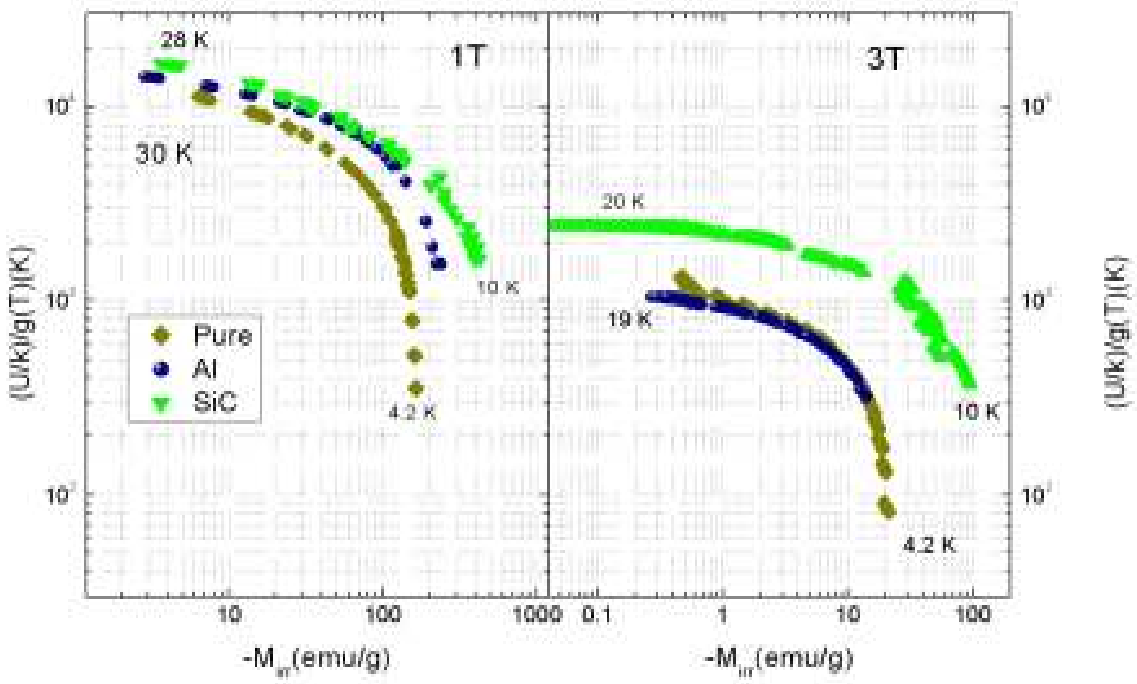


**Figure 3.55 Energy – current relation determined after Maley et al [Mal90] at 1 and 3 T for $MgB_2$ bulk samples with and without substitutions.**

**Table 3.4 Used *C*-values in the determination of the energy – current relation for all samples.**

| sample | *C* 1 T | *C* 3 T |
|---|---|---|
| 0% SiC | 180 | 100 |
| 3% SiC | 180 | 120 |
| 10% SiC | 180 | 50 |
| 20% SiC | 180 | 60 |
| 10% $B_4C$ | 180 | 80 |
| 10% $Al_2O_3$ | 180 | 80 |
| Pure | 180 | 40 |
| Al | 300 | 60 |
| SiC | 190 | 50 |

For the bulk samples, the SiC substituted one has the highest activation energy both at 1 T and 3 T. The lowest value of *U* is found for the pure sample at 1 T and for the sample with Al addition at 3 T.

The used *C* values (Table 3.4) show no systematic change. The *C* values are chosen to bring most of the relaxation data on one common curve. As can be seen (e.g. the data for the pure bulk sample at 3 T in Fig.3.55) there are deviations both at high and low temperatures, indicating that the chosen temperature function $g(T)$ cannot account for the full temperature range.

# Chapter 4 Discussion

## 4.1 Critical current density

The determination of critical current density from magnetic measurements using the critical state model [Bea62] needs a prior selection regarding the typical dimension of current flow, which is either the dimension of the whole sample if the system is non-granular or the dimension of the individual grains if the system behaves granular. Unlike high temperature superconductors $MgB_2$ was stated to have no weak link problem [Lar01] and therefore $MgB_2$ samples are usually assumed to be non granular. However, as some authors have reported this assumption might be a too simple one [Duo01, Nee05, Hor04].

Dou et al [Dou01] performed magnetic measurements on polycrystalline $MgB_2$ and have explained the observed step like decrease of $J_c$, which did not appear in direct transport measurements of the field dependence of the current density, in high fields by a change from non-granular to granular behaviour. In using the sample dimension at low fields and the grain dimension at high fields for the determination of $J_c$, they got the same smooth $J_c(B)$ dependence as found by the transport measurements.

A similar strong decrease of $J_c$ at high fields was found also for the $MgB_2$/Nb wires under study. From the SEM images of these wires the average grain size was approximated to be around 10 µm (Tab. 3.2). Using this value for determination of $J_c$ by the critical state model at the highest field, $J_c$ would be increased by a factor of approximately 70 leading to a value near to the one obtained in transport measurements (Fig. 4.1). This supports an increasing influence of granular behavior at high fields.

Horvat et al [Hor04] have investigated several $MgB_2$ bulk samples by magnetic measurements and explained their results by a model where the superconducting currents flow on three different length scales defining three different regions for $J_c$ separated by two transitions at $B_t$ and $B_i$. According to their investigations, in the region below $B_t$, the current flows around so-called cells, defined by a group of grains surrounded by voids, (≈10 µm range), between $B_t$

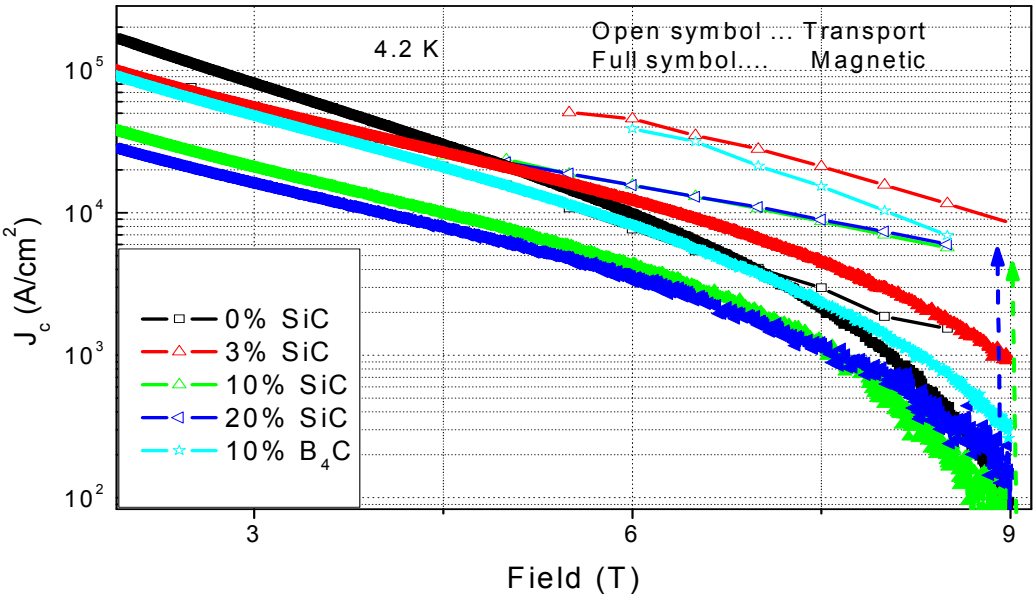


**Figure 4.1 Comparison of transport (open symbols) and magnetic (full symbols) measurements on $MgB_2$/Nb wires. For the 10 and 20 % SiC addition $J_c$ at the highest field is corrected (arrows) according to a granular behavior of the samples leading to a smooth $J_c(B)$ curve (dashed lines).**

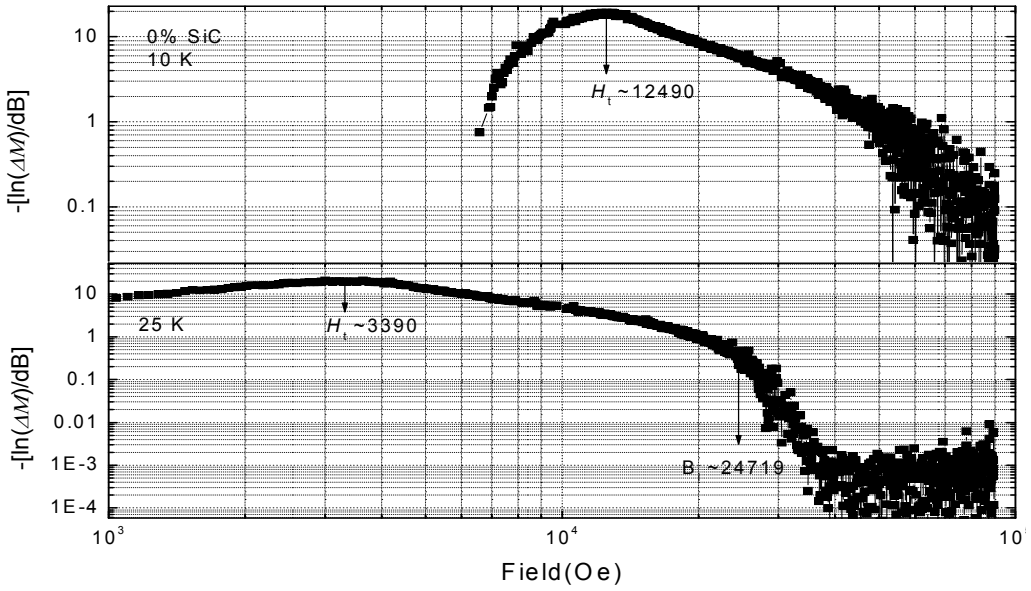


**Figure 4.2 Determination of $B_t$ and $B_i$ from the slope of (-ln($J_c$)-$B$) with field for $MgB_2$/Nb wire with 0% SiC at two temperatures according to Horvat et al. [Hor04]. Table 4.1 The field ($B_t$) determined from [-dln($J_c$)/d$B$] versus field curves and $B_{sb}$ determined from $J_c(B)$ curves for two temperatures.**

**Table 4.1 The field ($B_t$) determined from [-dln($J_c$)/d$B$] versus field curves and $B_{sb}$ determined from $J_c(B)$ curves for two temperatures.**

| Sample | $B_t$(G) 10 K | $B_t$(G) 25 K | $B_{sb}$(G) 10 K | $B_{sb}$(G) 25 K | $B_{lb}$(G) 10 K | $B_{lb}$(G) 25 K |
|---|---|---|---|---|---|---|
| 0% SiC | 12490 | 3390 | 8557 | 2042 | 27531 | 4532 |
| 3% SiC | 7130 | 1260 | 7054 | 887 | 16721 | 1732 |
| 10% SiC | 3160 | 237 | 1783 | 200 | 1783 | 200 |
| 20% SiC | 2010 | - | 1747 | 198 | 6946 | 1121 |
| 10% $B_4C$ | 8059 | 1929 | 2552 | 320 | 17832 | 2843 |
| 10% $Al_2O_3$ | 7235 | 1981 | 2985 | 385 | 21127 | 3621 |
| Pure | 7040 | 3721 | 5497 | 4430 | 10332 | 4591 |
| Al | 4590 | 3740 | 5638 | 9350 | 27598 | 12018 |
| SiC | 9681 | 3263 | 8557 | 2042 | 21824 | 7876 |

and $B_i$ currents flow around the whole sample (≈ mm range), while above $B_i$ the current flows in subgranular cells, which could be identified by transmission electron microscopy (≈1 µm range).

Assuming that the field dependence of the width of the hysteresis loops follows in each range a stretched exponential $\Delta M \sim \Sigma_i \alpha_i \exp[-(H/H_{0i})^{n_i}]$ with different parameters ($\alpha_i$, $H_{0i}$, $n_i$) for each region, Horvat et al [Hor01] have shown that $H_t$ and $H_i$ can best be determined in a plot showing the field dependence of the gradient $-d[\ln(\Delta M)]/dH$ in a log-log representation (Fig. 4.2).

The second transition field, $B_i$ could not be obtained in most of the cases due to large scatter in the data at high fields. One typical plot of such analysis is shown for one of the samples (0% SiC) for two different temperatures in Fig. 4.2. Results for $B_t$ are given in Table 4.1. The value of $B_t$ now gives a lower limit for the use of the $J_c$ values, which were determined by using the sample dimensions as characteristic length scale.

### 4.1.1 Field dependence of critical current density

To get information about possible pinning mechanism in the investigated samples, several models explaining the $J_c(B)$ behavior in type 2 superconductors, are used. The classical model of strong pinning is based on the direct summation of individual pinning forces $f_p$ to get the macroscopic pinning force $F_p$ [Cam72] i.e.

$$F_p = n_p f_p = J_c B \qquad 4.1$$

where $n_p$ is the density of pinning centers. In its simplest version this model gives a $J_c(B) \propto B^{-1}$ dependence.

If the flux line lattice is taken into account, the field dependence of $J_c$ is given by

$$J_c(B) \propto B^{-0.5}$$

In case of randomly distributed weak pinning centers, collective pinning theory [Lar79] can be used. According to this theory different regions of pinning can appear, depending on field and temperature. There is also a strong influence of dimensionality [2D or 3D] of pinning on the $J_c$ behavior. In case of 2D pinning at low temperatures and fields $J_c$ should be independent of field, because of single vortex creep. At higher temperatures and fields a region of collective pinning is present leading to a $J_c(B) \propto B^{-1}$ dependence. With increasing field a change from 2D to 3D pinning behavior is possible.

For 3D pinning a change from single vortex (sv) pinning to small flux bundle (sfb) pinning and large flux bundle (lfb) pinning should appear with increasing temperature and field [Bla94]. In case of sv pinning again a field independent $J_c$ should be found, whereas in the range of sfb pinning a streched exponential law with exponent 3/2 is proposed to appear

$$J_c\,(B) = J_c\,(0)\exp\left[-\left(\frac{B}{B_0}\right)^{\frac{3}{2}}\right] \qquad 4.2$$

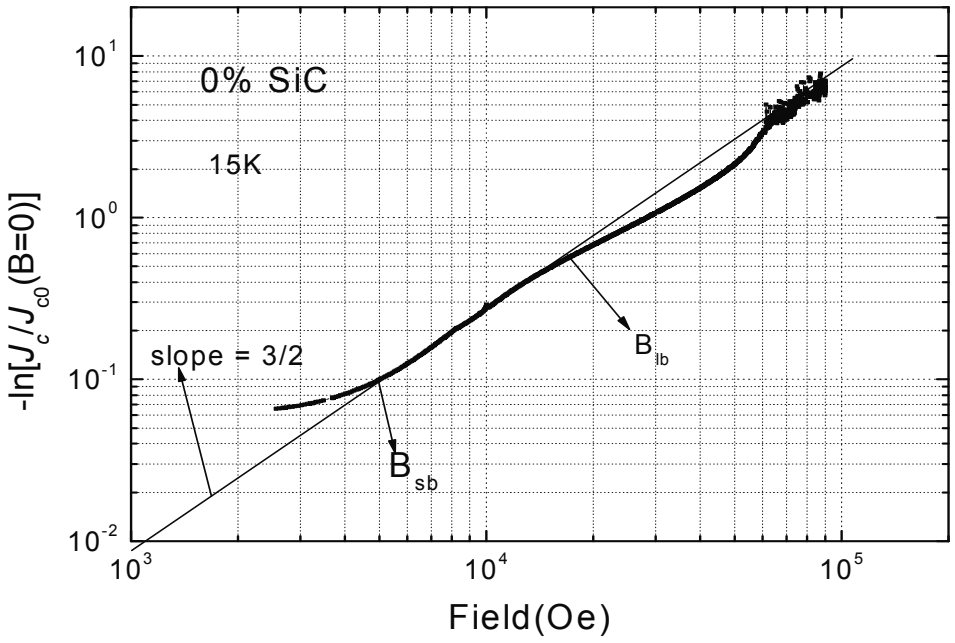


**Figure 4.3 Example for the determination of $B_{sb}$ and $B_{lb}$ from a double logarithmic plot of -ln[$J_c/J_{c0}$] versus field for $MgB_2$/Nb wire with 0% SiC at 15 K.**

Finally, for lfb pinning a power law $J_c(B) \propto B^{-3}$ is expected. The change from sv pinning to sfb pinning takes place at the field $B_{sb}$ and the change from sfb pinning to lfb pinning is defined by $B_{lb}$.

The two crossover fields $B_{sb}$ and $B_{lb}$ can be determined as those field, where $J_c(B)$ deviates from the behavior expected in the sfb pinning regime given by equation (4.2). This is best seen in a log-log representation of $-\ln(J_c/J_{c0})$ versus field as shown in Fig. 4.3. The obtained $B_{sb}$ and $B_{lb}$ values are given in Table 4.1.

In Figs. 4.4 to 4.12 the regions are marked in which some of the just mentioned relations for $J_c(B)$ are found in the experimental data for all samples.

The comparison of these figures shows that a possible $B^{-1}$ dependence is, if present, always found only at very low fields (maximum up to 2 T). Also its range is very narrow. It appears for nearly all samples in the same field and temperature range where also the stretched exponential with exponent 3/2 is found. The latter regime, limited by the fields $B_{sb}$ and $B_{lb}$ is for all samples, except the wires with 10 and 20% SiC additions, much larger than the range for $B^{-1}$. Therefore an interpretation in terms of 3D pinning seems to be the most plausible one.

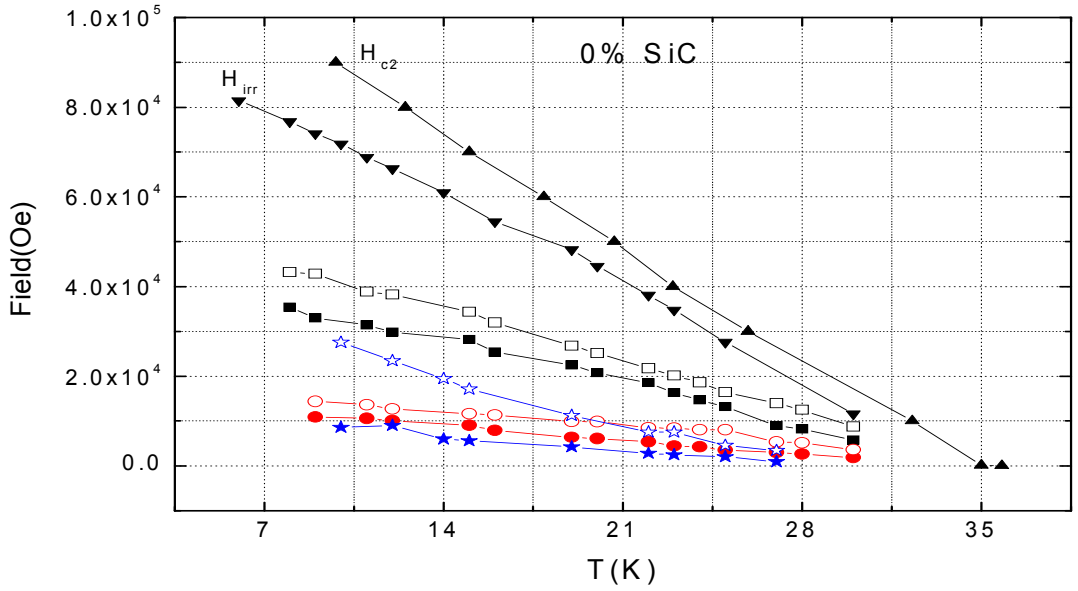


**Figure 4.4** $H_{irr}$ and $H_{c2}$ together with regimes of findings of different $J_c(B)$ relations for $MgB_2$/Nb wire with 0% SiC addition. Upper (○) and lower (●) limit for $J_c \sim B^{-1}$range, upper (□) and lower (■) limit for $J_c \sim B^{-3}$ range and $B_{sb}$ (★) and $B_{lb}$ (☆).

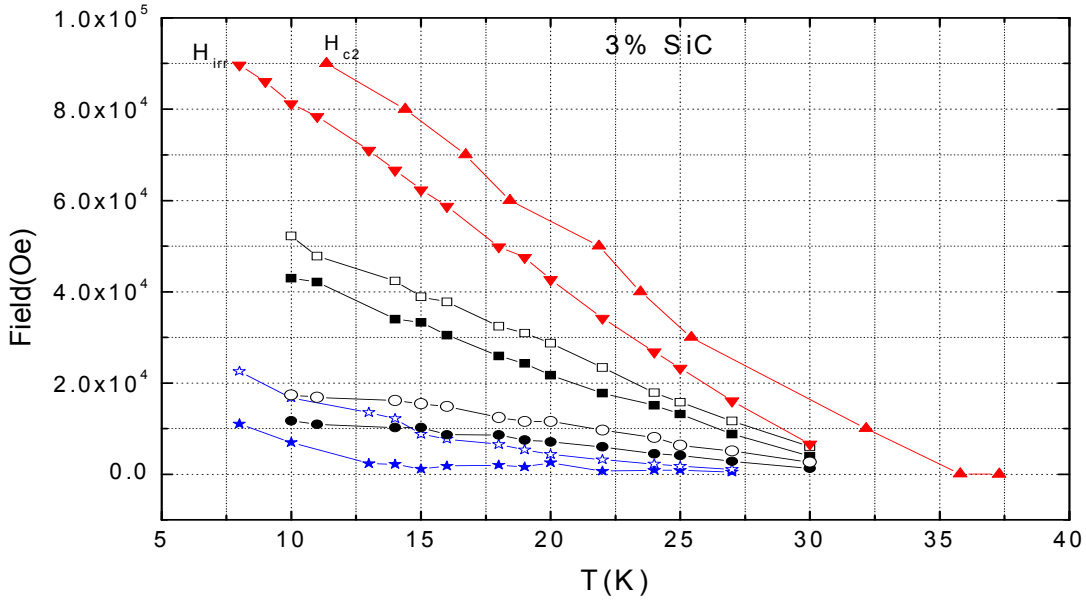


**Figure 4.5** $H_{irr}$ and $H_{c2}$ together with regimes of findings of different $J_c(B)$ relations for $MgB_2$/Nb wire with 3% SiC addition. Upper (○) and lower (●) limit for $J_c \sim B^{-1}$range, upper (□) and lower (■) limit for $J_c \sim B^{-3}$ range and $B_{sb}$ (★) and $B_{lb}$ (☆).

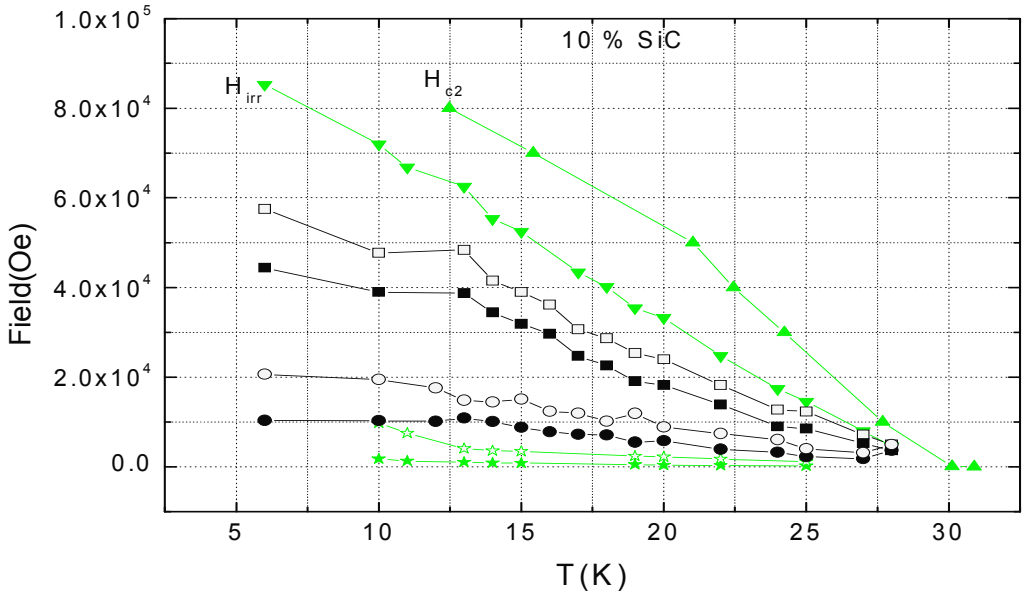


**Figure 4.6** $H_{irr}$ and $H_{c2}$ together with regimes of findings of different $J_c(B)$ relations for $MgB_2$/Nb wire with 10% SiC addition. Upper (○) and lower (●) limit for $J_c \sim B^{-1}$range, upper (□) and lower (■) limit for $J_c \sim B^{-3}$ range and $B_{sb}$ (★) and $B_{lb}$ (☆).

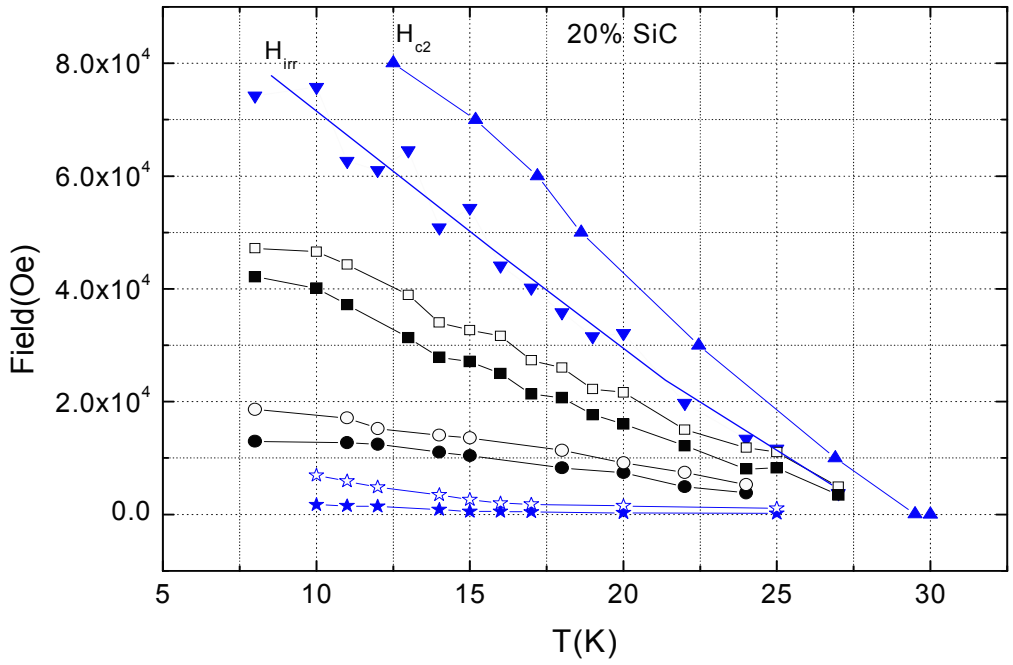


**Figure 4.7** $H_{irr}$ and $H_{c2}$ together with regimes of findings of different $J_c(B)$ relations for $MgB_2$/Nb wire with 20% SiC addition. Upper (○) and lower (●) limit for $J_c \sim B^{-1}$range, upper (□) and lower (■) limit for $J_c \sim B^{-3}$ range and $B_{sb}$ (★) and $B_{lb}$ (☆).

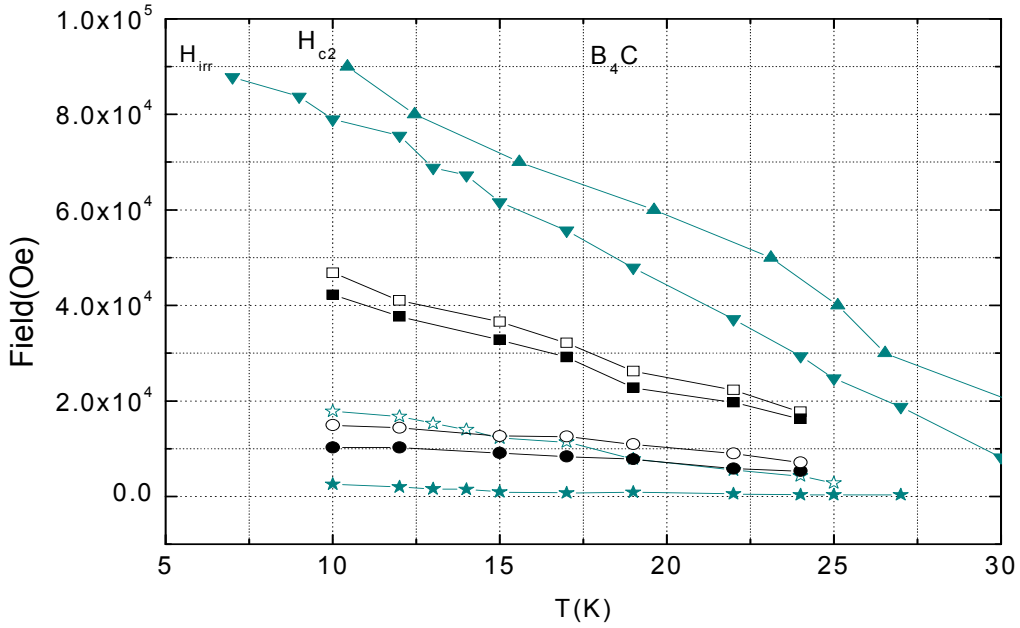


**Figure 4.8** $H_{irr}$ and $H_{c2}$ together with regimes of findings of different $J_c(B)$ relations for $MgB_2$/Nb wire with 10% $B_4C$ addition. Upper (○) and lower (●) limit for $J_c \sim B^{-1}$range, upper (□) and lower (■) limit for $J_c \sim B^{-3}$ range and $B_{sb}$ (★) and $B_{lb}$ (☆).

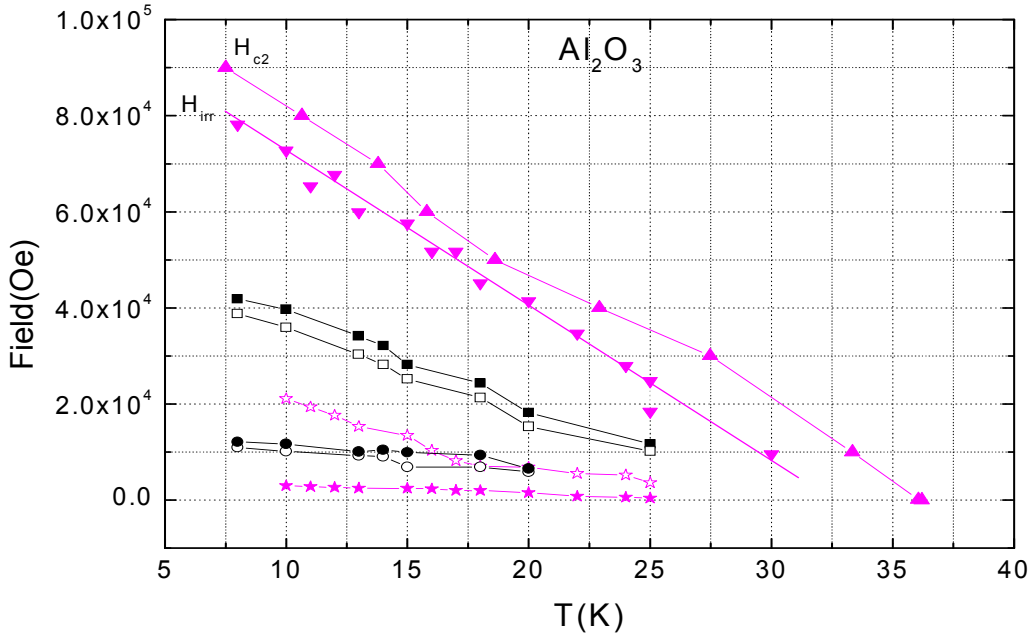


**Figure 4.9** $H_{irr}$ and $H_{c2}$ together with regimes of findings of different $J_c(B)$ relations for $MgB_2$/Nb wire with 0% SiC addition. Upper (○) and lower (●) limit for $J_c \sim B^{-1}$range, upper (□) and lower (■) limit for $J_c \sim B^{-3}$ range and $B_{sb}$ (★) and $B_{lb}$ (☆).

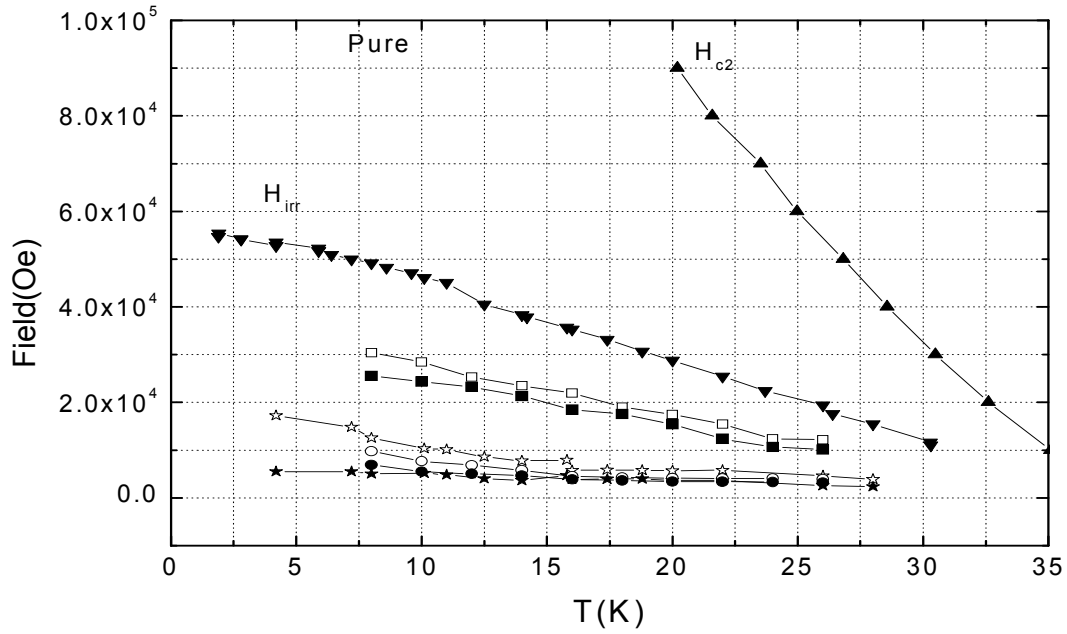


**Figure 4.10** $H_{irr}$ and $H_{c2}$ together with regimes of findings of different $J_c(B)$ relations for pure $MgB_2$ bulk sample. Upper (○) and lower (●) limit for $J_c \sim B^{-1}$range, upper (□) and lower (■) limit for $J_c \sim B^{-3}$ range and $B_{sb}$ (★) and $B_{lb}$ (☆).

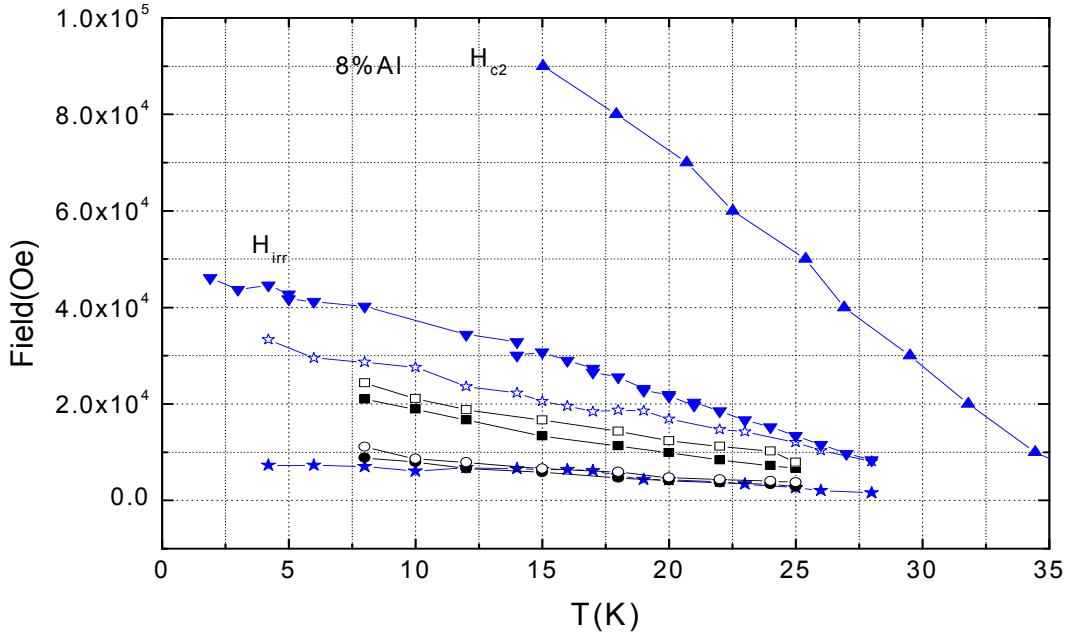


**Figure 4.11** $H_{irr}$ and $H_{c2}$ together with regimes of findings of different $J_c(B)$ relations for $MgB_2$ bulk sample with Al addition. Upper (○) and lower (●) limit for $J_c \sim B^{-1}$range, upper (□) and lower (■) limit for $J_c \sim B^{-3}$ range and $B_{sb}$ (★) and $B_{lb}$ (☆).

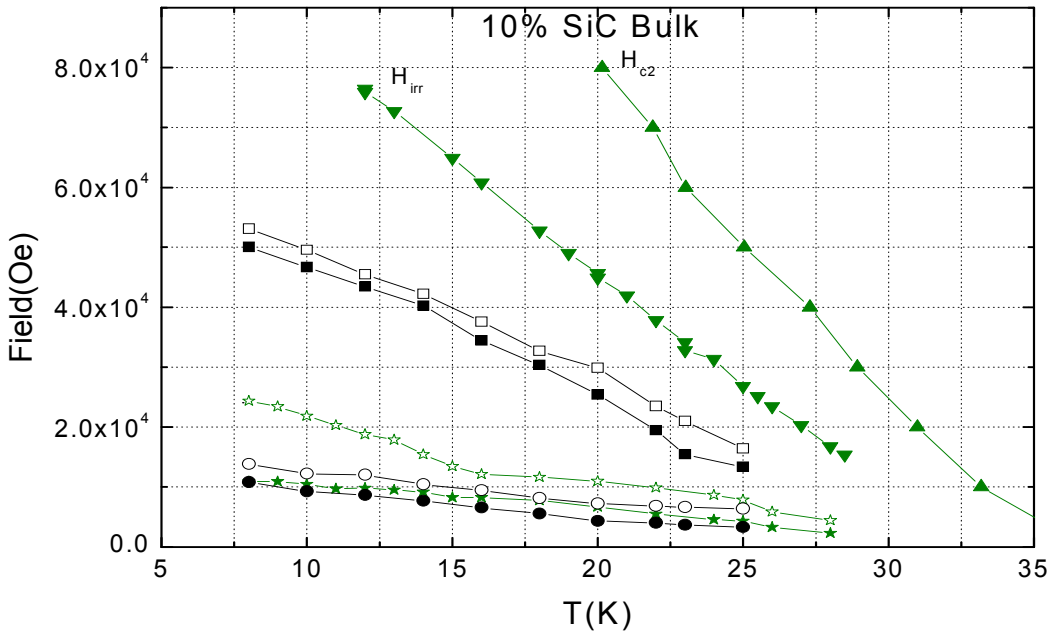


**Figure 4.12** $H_{irr}$ and $H_{c2}$ together with regimes of findings of different $J_c(B)$ relations for $MgB_2$ bulk sample with SiC addition. Upper (○) and lower (●) limit for $J_c \sim B^{-1}$range, upper (□) and lower (■) limit for $J_c \sim B^{-3}$ range and $B_{sb}$ (★) and $B_{lb}$ (☆).

Supported is this result by the fact, that according to the expectation the range where a $B^{-3}$ dependence of $J_c$ is found, is always present at higher fields. This region, which indicates 3D pinning of large flux bundles goes up to ~60% of the corresponding irreversibility field $B_{irr}$.

From the temperature dependence of $B_{sb}$ information about the pinning mechanism can be obtained. According to Griessen et al [Gri94] $B_{sb}(T)$ should follow in case of $\Delta T_c$ pinning

$$B_{sb} \backsim B_{sb}(0)\left(\frac{1-t^2}{1+t^2}\right)^{2/3} \qquad 4.3$$

and in case of $\Delta l$ pinning

$$B_{sb} \backsim B_{sb}(0)\left(\frac{1-t^2}{1+t^2}\right)^{2} \qquad 4.4$$

where $t = T/T_c$.

In Figs. 4.13 and 4.14 the temperature dependence of $B_{sb}$ for the different samples are given in comparison with the predicted tendency for $\Delta l$ and $\Delta T_c$ pinning.

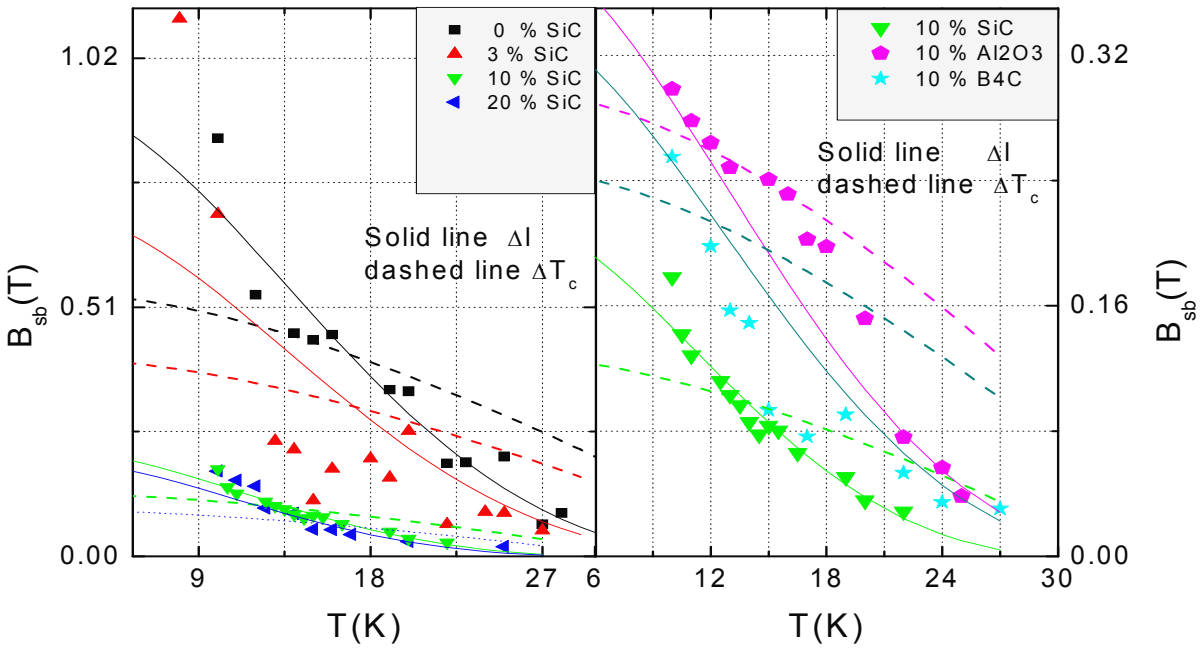


**Figure 4.13 Temperature dependence of $B_{sb}$ for $MgB_2$/Nb wires with and without additions in comparison with predictions for $\Delta l$ (solid line) and $\Delta T_c$ (dashed line) pinning.**

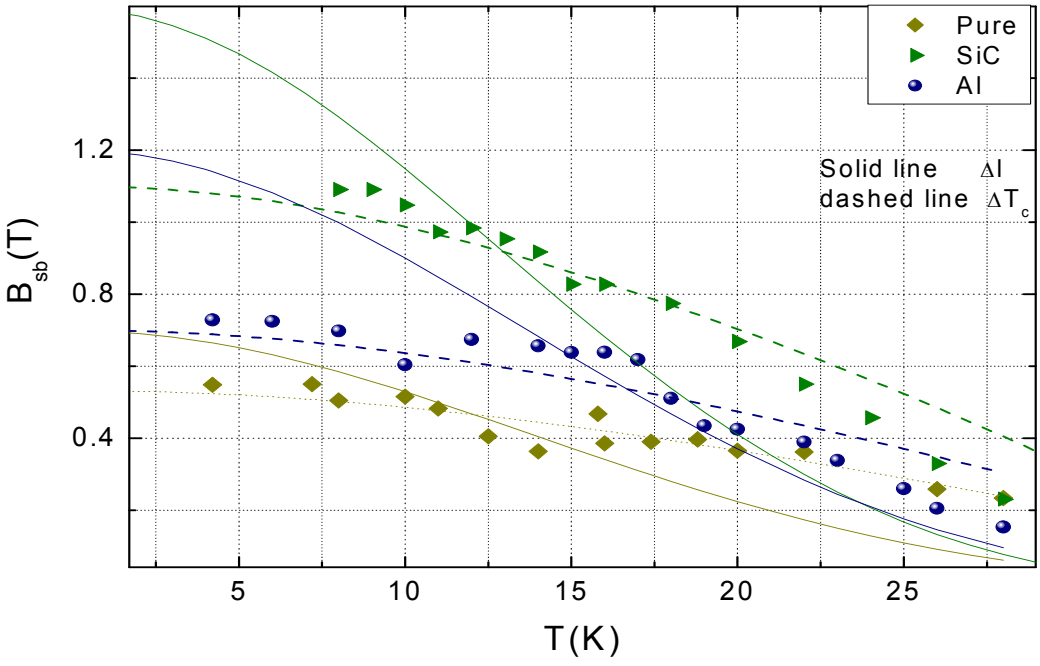


**Figure 4.14 Temperature dependence of $B_{sb}$ for $MgB_2$ bulk samples with and without additions in comparison with predictions for $\Delta l$ (solid line) and $\Delta T_c$ (dashed line) pinning.**

In case of the $MgB_2$/Nb wires (Fig. 4.13) the temperature dependence of $B_{sb}$ resembles more the one corresponding to Δ*l* pinning, while in case of the bulk samples the pinning seems to be more like $\Delta T_c$.

### 4.1.2 Temperature dependence of critical current density

Another way to distinguish between $\Delta T_c$ and Δ*l* pinning is by analysis of the temperature dependence of $J_c$. According to collective pinning theory [Gri94a] for single vortex creep $J_c$ should follow in case of $\Delta T_c$ pinning

$$J_c(t) = J_c(0)(1-t^2)^{7/6}(1+t^2)^{5/6} \qquad 4.5$$

and in case of Δl pinning

$$J_c(t) = J_c(0)(1-t^2)^{5/2}(1+t^2)^{-1/2} \qquad 4.6$$

where $t = T/T_c$.

$J_c(T)$ curves were obtained at 1, 4 and 6 T from the field dependence of $J_c$ for all measured samples which were normalized to $J_c$ at 0 K by making extrapolation to $T = 0$ and similarly the corresponding temperatures were normalized to $T_c$. The results of normalized $J_c$ as a function of normalized temperature are shown in Figs. 4.15 and 4.16 along with the expected curves for $\Delta T_c$ and Δ*l* pinning. In case of bulk samples $J_c(T)$ curves at 0.5 T were also determined. It can be seen that the dominant pinning mechanism is more close to Δ*l* pinning in wires. Whereas for 0.5 T $J_c(T)$ is also nearer to the Δ*l* curve, the shape of curves resembles more the one of the $\Delta T_c$ curve. In all cases the higher the field, the farer away are the $J_c(T)$ curves from the expected range between the two theoretical curves. The reason for this is, that with increasing field the prediction, that equations (4.5) and (4.6) are valid for single vortex creep, is lost.

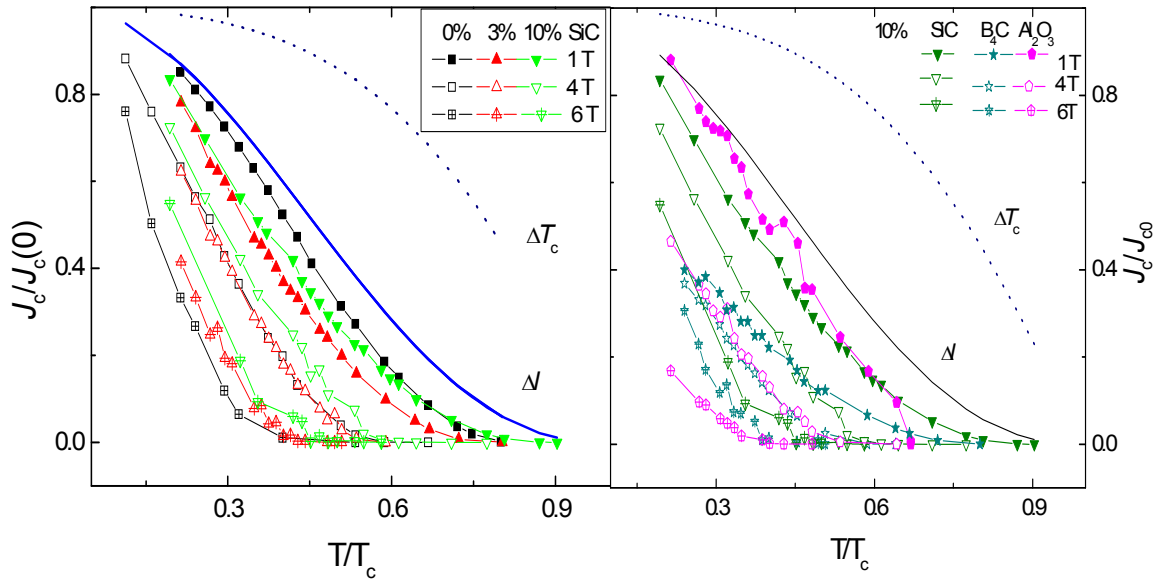


**Figure 4.15 Temperature dependence of normalized $J_c$ for $MgB_2$/Nb wires with different additives in comparison with predictions for $\Delta l$ (solid lines) and $\Delta T_c$ (dotted lines) pinning.**

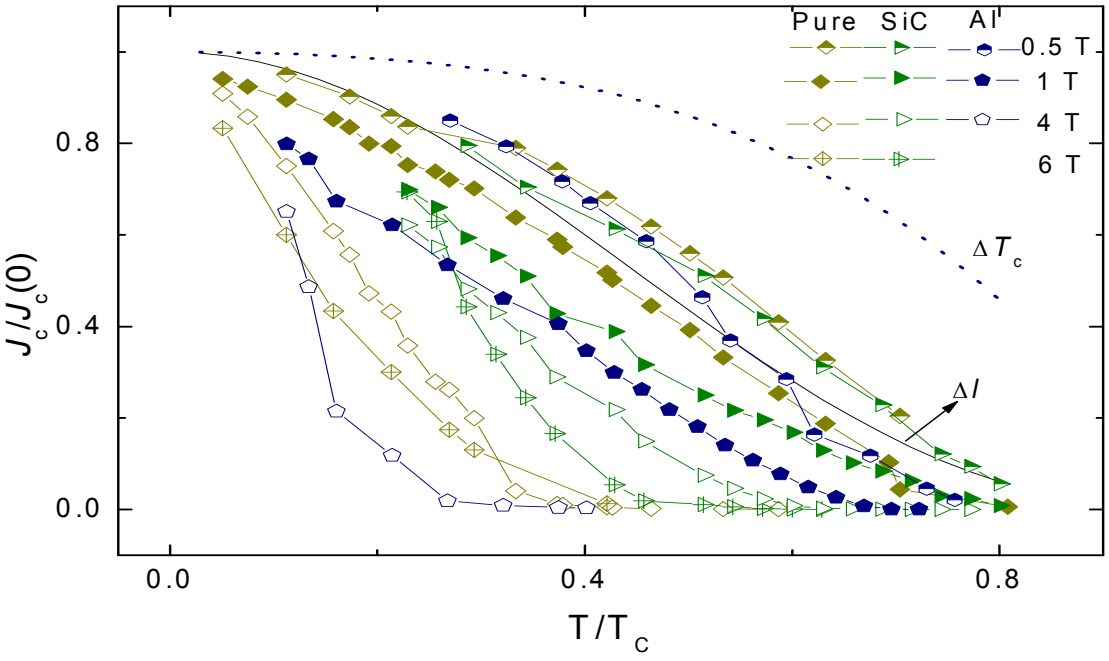


**Figure 4.16 Temperature dependence of normalized $J_c$ for $MgB_2$ bulk samples with and without additives in comparison with predictions for $\Delta l$ (solid lines) and $\Delta T_c$ (dotted lines) pinning.**

Qin et al [Qin02] have found a dominance of $\Delta T_c$ pinning in case of $MgB_2$ samples. The same result was obtained by Prischepa et al [Pri03] for measurements on $MgB_2$ thin films, *in situ* deposited by sputtering. In contrast to this Xu et al [Xu03] have obtained $J_c/J_c(0)$ versus $T/T_c$ curves, which are just inbetween the two types of pinning in their investigation of epitaxial $MgB_2$ thin films. Yuan et al [Yua05] have investigated bulk $MgB_2$ samples doped with carbon and synthesized either under ambient pressure as well as under high pressure. They found $\Delta l$ pinning at low and $\Delta T_c$ pinning at high temperature in case of high pressure prepared samples where in the ambient pressure only $\Delta T_c$ pinning is found in the whole temperature range. There is also a report on polycrystalline $MgB_2$ supporting two different pinning mechanisms dominant either at low or high fields or acting in parallel in whole temperature and field range [Shi06].

From the analyses of critical current density in terms of field and temperature dependence, it can be concluded that the $MgB_2$/Nb wires show behavior more close to $\Delta l$ pinning, while the bulk samples give indications to have $\Delta T_c$ pinning from the $B_{sb}(T)$ analysis and $\Delta l$ pinning at high and may be $\Delta T_c$ pinning at low fields on the basis of the $J_c(T)$ analysis, which indicates that the bulk samples change the pinning mechanism at a field higher than $B_{sb.}$

## 4.2 Pinning Force

The flux lines can interact with pinning centers in two ways. If the size and spacing of pinning centers is larger than the penetration depth λ of the superconductor, an interaction takes place known as magnetic interaction [Dew74]. However if the size or spacing of pinning centers is smaller than λ, the resulting interaction is known as core interaction. In case of core interaction Dew-Hughes [Dew74] has proposed expressions for flux pinning describing the field dependence of pinning force $F_p$ for different types of interactions under the assumption of strong pinning. They can be generalized by

$$\frac{F_p}{F_{\max}} \propto h^{P_1}(1-h)^{P_2} \qquad 4.7$$

with $h = H/H_{c2}$. In case of point, surface, or volume pinning this reduces to (s. Table 1.2)

$$\frac{F_p}{F_{max}} \propto h(1-h)^2 \qquad \text{maximum at } h = 0.5 \qquad 4.8$$

$$\frac{F_p}{F_{max}} \propto h^{0.5}(1-h)^2 \quad \text{maximum at } h = 0.2 \qquad 4.9$$

$$\frac{F_p}{F_{max}} \propto (1-h)^2 \quad \text{maximum at } h = 0.33 \qquad 4.10$$

Because pinning takes place only below the irreversibility line, $H_{irr}$ was used instead of $H_{c2}$ for the normalization of the field ($h = H/H_{irr}$). The obtained values for the exponents $P_1$ and $P_2$ for two typical temperatures together with the field of the maximum are given in Table 4.2.

It can be noted from the values of the exponents that the pinning mechanism is nearest to grain boundary pinning as described by expression (4.9) and also found in $Nb_3Sn$ [Dew87]. The same is clear if looking on the position of the maximum, which is for all samples near or below $H/H_{irr} = 0.2$.

**Table 4.2 Exponents obtained from fitting the field dependence of the pinning forces by equation (4.7) and field *h* at which the maximum is observed for two typical temperatures for $MgB_2$ wire and bulk samples.**

| sample | maximum 10 K | $P_1$ 10 K | $P_2$ 10 K | maximum 25 K | $P_1$ 25 K | $P_2$ 25 K |
|---|---|---|---|---|---|---|
| 0% SiC | 0.16 | 0.71 | 2.72 | 0.17 | 0.66 | 2.34 |
| 3% SiC | 0.17 | 0.49 | 2.02 | 0.24 | 0.53 | 1.62 |
| 10% SiC | 0.19 | 0.46 | 1.67 | 0.32 | 0.53 | 1.00 |
| 20% SiC | 0.21 | 0.42 | 0.80 | 0.32 | 0.49 | 0.61 |
| 10% $B_4C$ | 0.16 | 0.53 | 2.32 | 0.22 | 0.54 | 1.77 |
| 10% $Al_2O_3$ | 0.15 | 0.60 | 2.65 | 0.20 | 0.61 | 2.63 |
| Pure | 0.15 | 0.46 | 2.01 | 0.19 | 0.37 | 1.69 |
| Al | 0.21 | 0.83 | 2.81 | 0.24 | 0.50 | 2.08 |
| SiC | 0.14 | 0.44 | 2.05 | 0.20 | 0.43 | 1.62 |

This excludes both point and volume pinning, where the maximum should be at 0.5 or 0.33, respectively. The same flux pinning characteristic was observed in similar investigations on pure $MgB_2$ bulk samples [Lar01, Sus07] with some deviations at higher fields. Larbalestier et al [Lar01] have attributed the deviations to be due to weaker superconducting phases, while Susner et al [Sus07] concluded inhomogeneity and anisotropy to be the reason for the observed deviations. Similar analyses on $MgB_2$ films resulted in a $h(1\text{-}h)^2$ dependence, which is typical for point like normal core pinning [Pri03].

For the samples under study it is observed that $P_1$ and $P_2$ decreases with increasing SiC concentration in $MgB_2$/Nb wires both at 10 and 25 K. In case of the $MgB_2$/Nb wires with $B_4C$ and $Al_2O_3$ addition and the bulk sample with Al substitution $P_2$ values higher than expected in case of pure grain boundary pinning are found. For all samples the $P_2$ value is lower at 25 K than at 10 K. Also the value of the maximum is found to be higher at 25 K than at 10 K. The observed differences in the exponents and their temperature dependence may be due to the inhomongeneity and weak superconducting phases as a result of substitutions. Deviations from the 'pure' behavior according to the relations given by Dew-Huges [Dew74] (Table 1.2) can be present, if more than one pinning mechanism is operative in the samples. Due to the complex microstructure of the investigated samples this is not unexpected. It should be mentioned that for the pure bulk sample the exponents are very near to the ideal case for grain boundary pinning. Only the peak is shifted by approximately 25% to lower fields, which might be due to the fact, that in this analysis $B_{irr}$ was used instead of $B_{c2}$. Interestingly the same is true for the wire with 3% SiC addition. This is the sample which shows best performance of all the wires concerning the critical current density. The fact that the scaling is not as good in wires as in the bulk samples, and becomes worse with increasing addition of foreign phases, indicates that pinning becomes more complex. There is also relation not only to the nanoscaled additions, but also to the appearance of the secondary phases, identified in the X-ray investigations (MgO and $Mg_2Si$ see Table 3.1). The samples with no secondary phases (wire with 0% addition and with 10% $Al_2O_3$ substitution) as well as the wire with 3% SiC, which has only 4% secondary phase, are also those with best scaling and nearest to pure grain boundary pinning. Hence the observed change in the exponents with particle addition may be attributed to the appearance of additional pinning centers or to a changed pinning mechanism.

Figs. 4.17 and 4.18 show the normalized pinning force as a function of reduced field at 10 K for all samples together with the theoretical curves for grain boundary pinning. Deviations from grain boundary pinning behavior can be clearly seen.

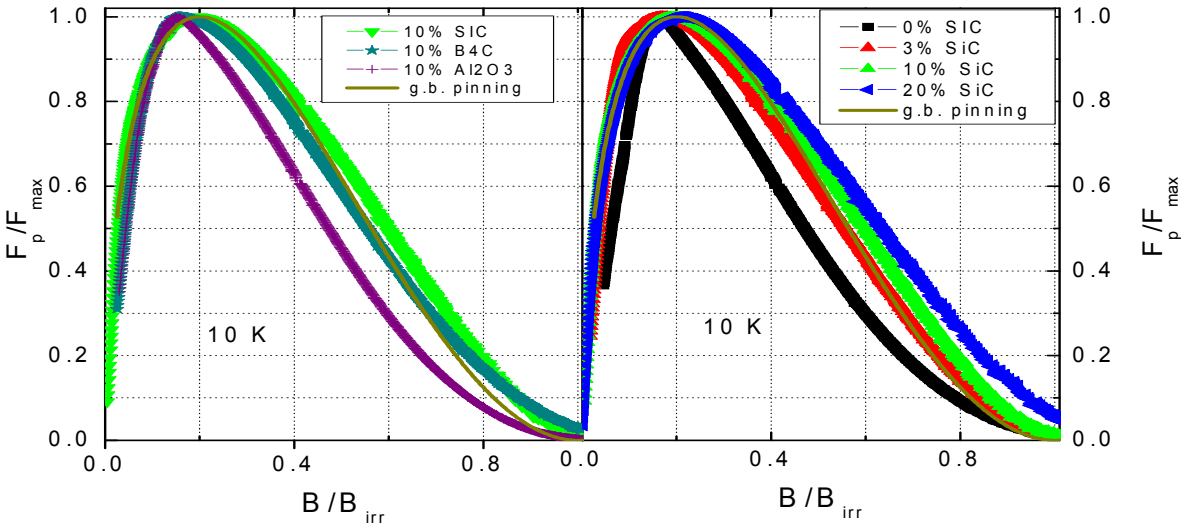


**Figure 4.17 Normalized pinning force versus reduced field for wires compared with theoretical curves for grain boundary pinning.**

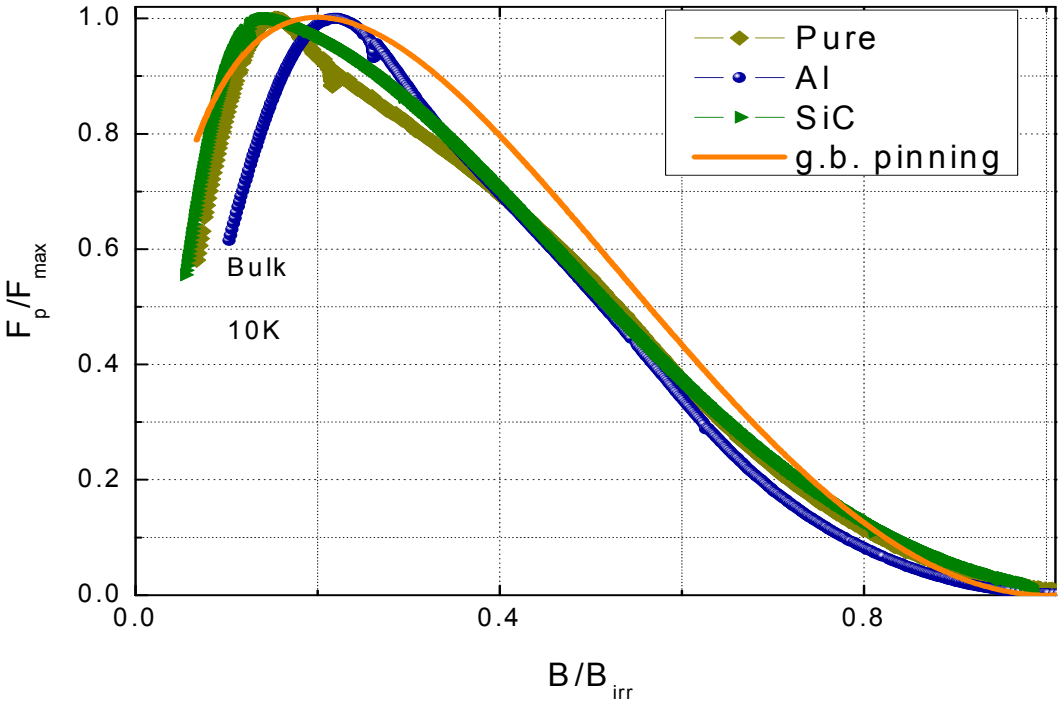


**Figure 4.18 Normalized pinning force versus reduced field for bulk samples with theoretical curves for grain boundary pinning.**

## 4.3 Relaxation measurements

### 4.3.1 Mean effective activation energy

Mean effective activation energies obtained from the relaxation data by making use of the Anderson model [And64] are analyzed in terms of temperature, field and critical current density dependence to study the complex nature of flux dynamics in $MgB_2$.

As can be seen in Figs. 3.46-3.48, the mean effective activation energy increases with temperature showing a peak and then decreases as a result of further increase in temperature in all the measured samples at both 1 and 3 T with exception of wire with 0% SiC addition where due to scatter in data at low temperature, the increasing part is not visible. The rising part is only short in wires as the measurements below 8 K could not be analyzed due to flux jumps while in bulk samples this part is visible at both fields. The obtained peaks are rather flat which is also seen in the temperature dependence of the normalized creep rate *S* Fig.4.19. Up to 20 K *S* shows weak temperature dependence and lower values at 1 T, whereas this increase starts at much lower temperature for 3 T. This indicates again that the mean effective pinning barrier is larger at low field and low temperature.

This weak $S(T)$ dependence at low field was also reported in other works [Mar04, Wen01, Jin03, Fen03, Mum01].

Martinez et al [Mar04] have investigated undoped and SiC doped $MgB_2$ wires. They find that *S* is much lower at 1.5 and 3 T for the doped compound whereas it is nearly the same for 4 T.

Explaining the flux dynamics of $MgB_2$ bulk samples, Wen et al [Wen01] have concluded that the pinning potential well is so deep in $MgB_2$ that besides thermal activations, quantum fluctuation and quantum tunnelling may become important. From magnetic measurements they find non vanishing dynamic creep rate at lowest temperature which supports this assumption. A non vanishing normalized creep rate at T = 0 was also found by Jin et al [Jin03] on high pressure bulk

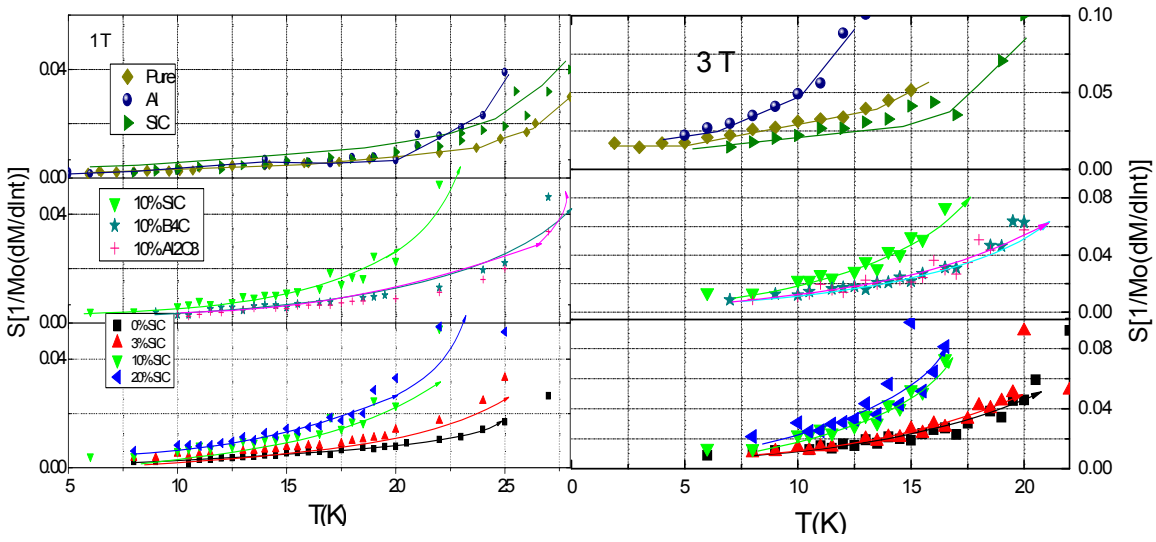


**Figure 4.19 Normalized relaxation rate (S) as a function of temperature for $MgB_2$ wire and bulk at 1 and 3 T.**

samples. They indicate that this can not only be due to quantum tunnelling but also be governed by the fact that $MgB_2$ is a two gap superconductor.

On the other hand Mumtaz et al [Mum01] have discussed the low relaxation rate up to 20 K. They argue that quantum effects are highly unlikely at such high temperatures. The effective activation energy has always been reported to increase with temperature in high temperature superconductors where the relaxation rate is also found to be an order of magnitude larger than in $MgB_2$. The fact that the relaxation rates found in $MgB_2$ at low field and temperature are much smaller than for high temperature superconductors, suggests a much stronger pinning in $MgB_2$.

### 4.3.2 Activation energy distribution

The model of Hagen et al [Hag90] to determine activation energy distributions from relaxation measurements was applied to interpret pinning in pure and SiC doped $MgB_2$ bulk samples at high field by Martinez et al [Mar04].

The centre of gravity found in $m(U_0)$ Figs. 3.50 to 3.52 corresponds to the mean effective activation energies determined within the Anderson theory Figs. (3.47-3.49). Therefore the difference in $<U>$ for different samples should also be seen as a shift of their respective activation energy distribution functions. Such agreements can be seen in most of the samples with the exception of the 3% SiC wire, where the peak is lower than expected, but due to the different shape of the distribution function for this compound the centre of gravity is as expected, very near to the one of the 0% SiC sample.

The used function is normalized to 1, therefore the corresponding area under the curve should give a value close to 1. The areas determined from the respective distribution curves for all samples are given in Table 4.3 along with the corresponding maxima. The obtained values of area are considerably small at 1 T (7-26%) while at high field (3 T) the range (37-83%) is more reasonable. This means that at high fields the results obtained using this model are more reliable than at low fields.

**Table 4.3 Characteristic parameters of the activation energy distribution for the investigated samples.**

| | 1 T | | 3 T | |
|---|---|---|---|---|
| samples | area | peak energy (meV) | area | peak energy (meV) |
| 0% SiC | 0.09 | 48 | 0.43 | 42 |
| 3% SiC | 0.14 | 49 | 0.38 | 41 |
| 10% SiC | 0.09 | 42 | 0.58 | 36 |
| 20% SiC | 0.26 | 34 | 0.73 | 31 |
| 10% $B_4C$ | 0.11 | 45 | 0.64 | 42 |
| 10% $Al_2O_3$ | 0.09 | 53 | 0.37 | 45 |
| Pure | 0.21 | 39 | 0.83 | 25 |
| Al | 0.07 | 46 | 0.74 | 20 |
| SiC | 0.14 | 77 | 0.42 | 40 |

### 4.3.3 Energy-current relation

Although the Hagen-Griessen model gives information about a possible distribution in the energy of pinning centers but, it is still based on the Anderson theory which is known to be too simple as it assumes a linear $U(J)$ dependence. As Maley et al [Mal90] have shown the real shape of $U(J)$ can be obtained from relaxation measurements without any prior assumption. The obtained results can be discussed on the basis of different models for the $U(J)$ dependence. E.g for high temperature superconductors a logarithmic $U(J)$ dependence was proposed by Zeldov et al [Zel90] from resistivity measurements. A more general equation was suggested by Feigel'man et al [Fei90] on basis of collective pinning theory. With the assumption that $J<<J_c$, the proposed equation is given by

$$U = U_c\left[\left(\frac{J_c}{J}\right)^{\mu} - 1\right] \qquad 4.10$$

where $U_c$ is the activation energy for $J = J_c$. The exponent $\mu$ depends upon the dimensionality and its value can describe the particular flux pinning regime in the superconductor. For three dimensional pinning (3D), the value of $\mu$ should be 1/7 for single vortex (sv), 3/2 for small flux bundles (sfb) and 7/9 for large flux bundles (lfb) pinning [Fei89]. In case of two dimensional pinning (2D), $\mu$ is expected to be 9/8 in the single vortex (sv) and 1/2 in the collective vortex (cv) pinning regime [Fei90].

The value of $\mu$ can be determined using equation 4.10 by taking the slope of the $U(J)$ curve in a double logarithmic representation.

The $U(J)$ curves (Figs. 3.53-3.55) obtained by the method given by Maley et al [Mal90] were analyzed in terms of collective pinning theory in two ways (Figs 4.20 to 4.22). First it was assumed that pinning is 3D, and the ranges where the appropriate values for $\mu$ can be found are indicated as bars in the right figures. Afterwards the same procedure was performed assuming that the pinning is 2D. These results are shown in the left figures.

As can be seen the bars from the 2D analysis covers a slightly larger range than those from 3D analysis for all measured samples, which points towards two dimensional pinning mechanisms in these samples. For the $J_c$ analyses of these samples, both 3D and 2D pinning were found, but 3D was shown to explain the $J_c$ behavior in a much larger region than 2D pinning. The two dimensional pinning is usually found in layered superconductors for which the coherence length is smaller than the distance between superconducting layers resulting in a decoupling of the flux lines into pancakes. But for $MgB_2$ the coherence length is found to be large (s. table 1.1) and hence 3D pinning is expected.

One problem in this analysis is the obtained high value of *C* (Table 3.4). Martinez et al. [Mar04] have obtained *C* = 50 in their investigation on Ni. Sheathed undoped and SiC doped $MgB_2$ at 3 T, while Jin et al [Jin03] report on *C* values of 400, 130 and 50 for 0.5, 1 and 1.5 T, respectively.

Such high *C* values have never been reported in high temperature superconductors. The shift of *C* value to a smaller value with increasing field, points to the fact that the pinning mechanisms may be different at low and high fields.

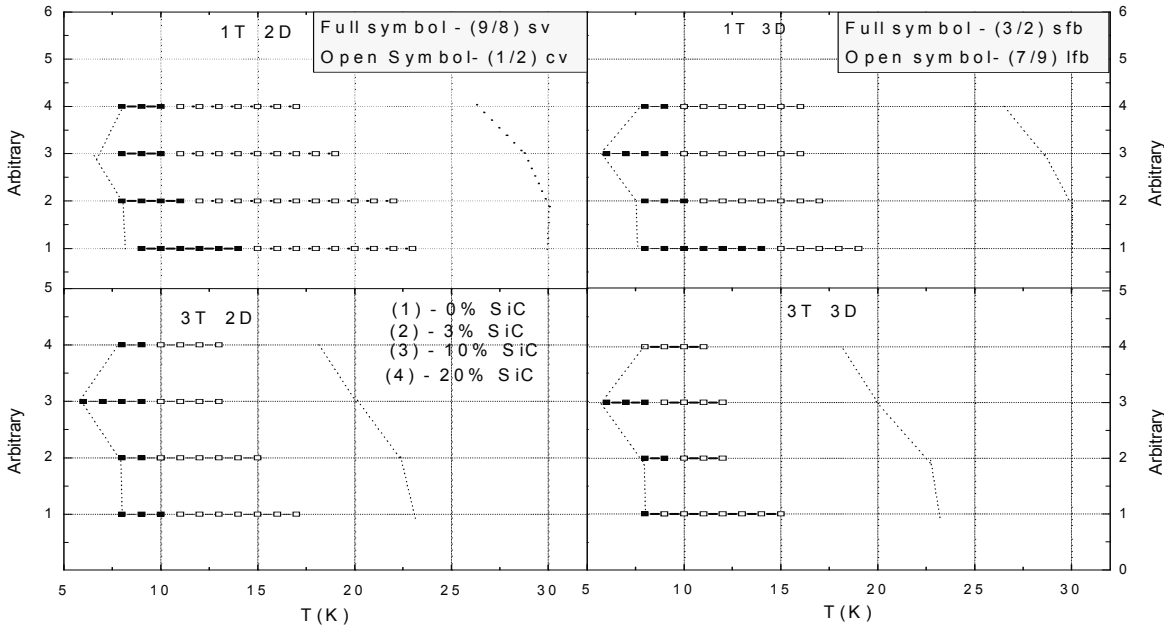


**Figure 4.20 Analysis of *U*(*J*) curves in terms of collective pinning theory for $MgB_2$/Nb wires with different SiC additions at 1 T and 3 T in the measured temperature range. Full (open) symbols denote the temperature range where the exponent corresponding to single (collective) vortex pinning in case of a 2D (left) and corresponding to small (large) flux bundle pinning in case of a 3D (right) analysis. The dotted lines indicate the investigated temperature intervals.**

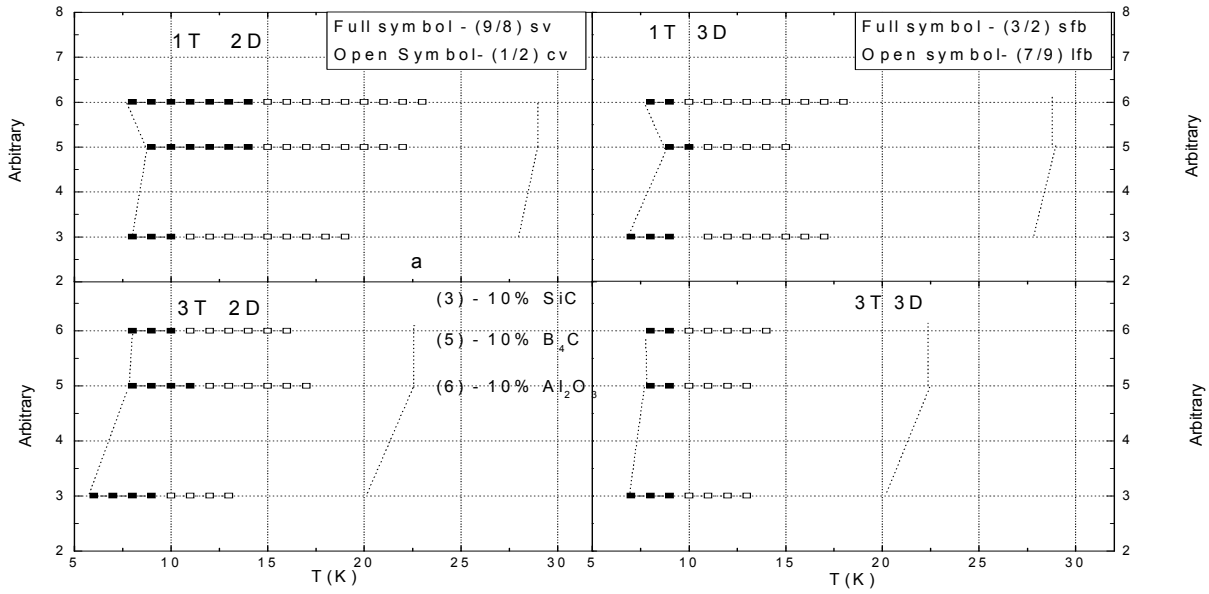


**Figure 4.21 Analysis of *U*(*J*) curves in terms of collective pinning theory for $MgB_2$/Nb wires with different additives but same concentration at 1 T and 3 T in the measured temperature range. Full (open) symbols denote the temperature range where the exponent corresponding to single (collective) vortex pinning in case of a 2D (left) and corresponding to small (large) flux bundle pinning in case of a 3D (right) analysis. The dotted lines indicate the investigated temperature intervals.**

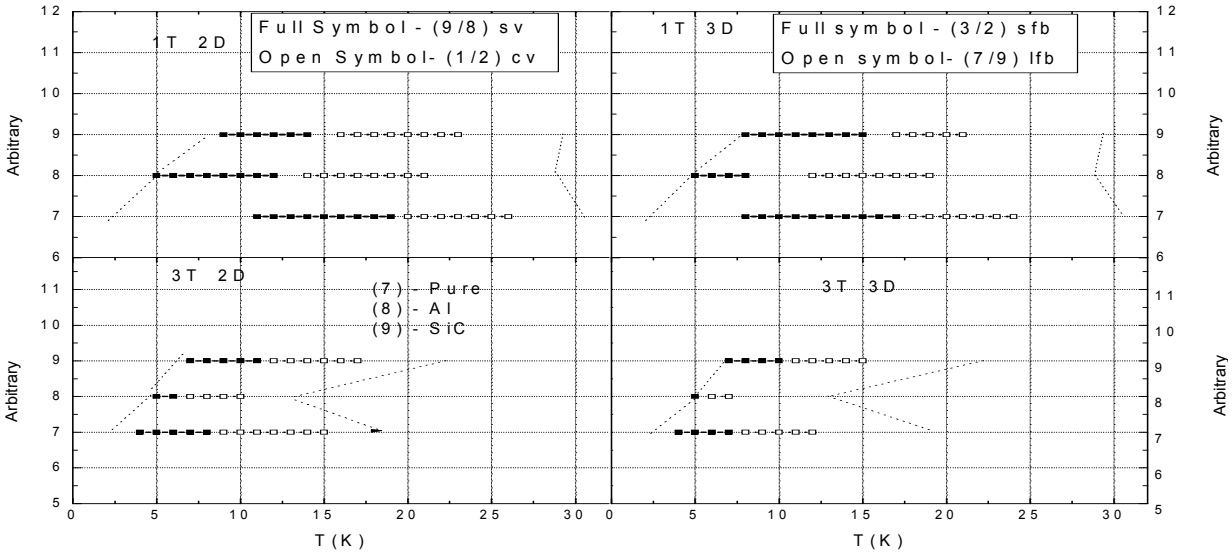


**Figure 4.22 Analysis of *U*(*J*) curves in terms of collective pinning theory for $MgB_2$/Nb bulk samples with and without different additions at 1 T and 3 T in the measured temperature range. Full (open) symbols denote the temperature range where the exponent corresponding to single (collective) vortex pinning in case of a 2D (left) and corresponding to small (large) flux bundle pinning in case of a 3D (right) analysis. The dotted lines indicate the investigated temperature intervals.**

## 4.4 Summary

Nb-sheathed $MgB_2$ wires with different additions to improve the critical current density for possible application were investigated by dc magnetic measurements and compared to results on bulk samples. Concerning the wires, one series with SiC inclusions in the concentration range around 10 wt%, where literature reports for bulk samples maximum performance, was prepared. In a second series the influence of different additives ($B_4C$, $Al_2O_3$, SiC) with the same concentration (10 wt%) was investigated. Finally, the results of the wires were compared with bulk samples, one without inclusions, one with 8 wt% Al, and one with 10 wt% SiC.

Putting all results together the following picture is obtained. Highest $T_c$ is obtained for the pure bulk sample (38 K). For the wire without addition $T_c$ is 1 K lower. Inclusion of nonsuperconducting phases reduce $T_c$. For the wires with increasing SiC concentration transition temperature drops drastically. This decrease is larger than usually found for SiC substituted bulk samples (e.g. for the 10 wt% SiC $T_c$ = 35 K, 31 K for bulk and wire, respectively). Also the width of the transition, which is a measure of sample homogeneity, increases with increasing concentration of the additives. This is accompanied by the fact, that in the wires with substitution an increasing amount of secondary phases (mainly $Mg_2Si$) is found in the X-ray investigations. Whereas the *a* – parameter is little bit smaller than reported for bulk samples [Dou02], the *c* – parameter is much larger (~3.5 instead of ~3.1 Å). Nevertheless the *a*-parameter is slightly lower for the wires with SiC additives, indicating, that C is incorporated in the matrix. Due to the preparation process the density of the wires is higher than of the bulk samples. The microstructure looks more homogenous in the wires. The average grain size is approximately the same for all wires (~10 µm) and slightly larger for the bulk samples.

Critical current densities were determined from the hysteresis loops by the Bean model, assuming that the samples behave nongranular, that means that the sample dimension is the relevant for the supercurrent flow. There are several restrictions concerning the field and temperature range in which the thus obtained current densities can be analyzed. On the one hand some of the samples show flux jumps up to ~1 T, on the other hand it cannot be assumed, that the samples behave in the full field range nongranular. According to Horvat et al [Hor04] a lower limit for nongranular behavior was found ($B_t$ < 1 T). At the high fields there is a gradual change from nongranular to granular behavior. If $J_c$ for the highest fields is analyzed assuming granular behavior, the strong decrease of $J_c$ at high fields, which is not present in direct transport measurements can be compensated. Therefore analyses of critical current densities are only performed for temperatures above the region where flux jumps appear and in fields above $B_t$. At high fields results have to be

taken with caution, because the change to granular behavior appears gradual and could therefore not be corrected.

In contrast to bulk superconductors, where 10% SiC substitution is reported to show best performance, for the wires the 3% SiC compound turns out to be the best. As for bulk samples at low temperatures and low fields the wire without addition shows highest $J_c$ but strongest field dependence. Therefore a crossover appears at higher fields where the 3% and at even higher fields the 20% sample becomes better. In contrast to this at high temperatures the 0% sample has for all fields highest $J_c$. Comparing the wires with same concentration but different additives, at low temperatures the wire with $Al_2O_3$ is best at low fields, whereas at high fields the wire with $B_4C$ shows highest $J_c$. For the bulk samples the SiC added one is much better than the pure and the Al substituted compound for all fields and temperatures. The Al substituted bulk is only at lower fields better than the pure one. Comparing pure samples the wire shows better performance than the bulk sample. For 10% SiC addition the bulk sample gives higher $J_c$ values. As in bulk samples the improvement in $J_c$ by addition of SiC is very strong in contrast to the wire, where already the sample without SiC has relative high critical current density, it can be concluded that the wiring process alone improves critical current density strongly. The additives therefore only slightly change $J_c$.

This is also seen in the irreversibility line. At low temperatures the wire with 3%, at high temperature the one without additives is best. Substitution of 10% $B_4C$ is as good as the 3% SiC wire at low temperatures and as good as the 0% wire at high temperatures. For the bulk samples 10% SiC addition gives same high irreversibility line as 3% SiC addition in the wires. Whereas the additives have not very large influence in the wire samples, the influence of the 10% SiC addition in the bulk has a drastic effect. Substitution of Al into the bulk shifts the irreversibility line to even lower values than for the pure bulk.

The upper critical field is not largely influenced by the substitutions. It is highest for the pure bulk sample. Concerning the wires again the sample with 3% SiC addition is best.

To get information about the pinning mechanisms, the critical current density was analyzed in different ways. From the pinning force it can be concluded that grain boundary pinning seems to be the main mechanism. But it has to be taken into account that the scaling which is demand in this analysis is not perfect. Deviations from scaling are larger in wires than in bulk. With increasing SiC addition the scaling becomes worse. Best scaling is found for the $Al_2O_3$ substituted wire. This is the sample where no secondary phases are found in the X-ray investigation. The increasing deviation from scaling can be due to a larger spread in different pinning centers.

The field dependence of the critical current density was analyzed using both models for strong and weak pinning. It turns out that best description is given by weak pinning

models, where a 3D pinning scenario seems to be more plausible than a 2D one, because the expected field dependences are found in a larger temperature and field range. There is a rather large range of small flux bundle pinning which changes to large flux bundle pinning at higher fields. Single vortex pinning is if present below the field $B_t$ and can therefore not be found. From the temperature dependence of the field, where small flux bundle pinning sets in, it follows that pinning is more likely of $\Delta l$ type for the wires, while in the bulk samples a $\Delta T_c$ pinning seems to be more probable. A similar picture is obtained from the analyses of the temperature dependence of $J_c$, with the exception that for all samples $\Delta l$ pinning is more likely.

The mean effective activation energies <*U*> obtained from the relaxation measurements have values which are nearly a factor of ten higher as those found in the high $T_c$ cuprates. After a rather flat maximum <*U*> decreases with temperature. This is also in contrast to the high $T_c$ materials where a strong increase is present in most of the temperature range. This indicates that the distributions of activation energies are much narrower in the investigated samples.

For the wires with SiC inclusions the mean effective activation energy decreases with concentration both at 1 and 3 T. In case of the 10% substituted samples with different additions, $Al_2O_3$ give highest values. SiC gives the lowest <*U*>. For the bulk samples at low temperatures the pure sample is better, in contrast to 3 T, where the SiC substituted compound is best. As expected the wire with no additions has higher activation energy than the pure bulk sample. But after inclusion of 10% SiC the bulk shows higher <*U*> values than the wire. With increasing field <*U*> decreases much faster in case of the bulk samples compared to the wires. As expected from the temperature dependence of <*U*> the determined activation energy distributions are rather narrow. They all have very similar shape with one pronounced peak around 30 to 50 meV. Only for the pure bulk sample and the bulk sample with Al addition the peak is found at lower values. These findings are in good agreement with the results of the mean effective activation energy, but it has to be mentioned that at 1 T the area under the distribution function, which should be 1 is much lower. At 3 T areas are more reasonable.

The analysis of the *U*(*J*) curves in terms of collective pinning theory favors more 2D pinning than 3D pinning. This would support the finding of the grain boundary pinning as main mechanism as derived from the analysis of the pinning force. Care has to be taken concerning this analysis, because unphysical high values are obtained for the parameter *C* which is used in the determination of the *U*(*J*) curves. Values above 50 are not compatible with the expected flux line dynamics. Again the results for 3 T are more valuable as here *C*

values near to 50 are found, whereas at 1 T much to high values (180) are necessary to find smooth *U*(*J*) curves.

# References

[An01] J. M. An and W.E. Pickett. Phys. Rev. Lett. **86** (2001) 4366

[And62] P.W. Andersen Phy. Rev. Lett. **9**, 309(1962)

[And64] P.W. Andersen Y. B. Kim: Rev. Mod. Phys. **36**, 39(1964)

[Bea62] C. P. Bean , Phy. Rev Lett. **8** (1962) 250

[Bea64] C. P. Bean , Phy. Rev Lett. **36** (1964) 31

[Bea69] M. R. Beasley R. Labusch, and W. W. Webb, Phys. Rev. **181** (1969) 682

[Bla94] G. Baltter, M. V. Feigel'man, V.B. Geshkenbein, A.I. Larkin, V. M. Vinokur, Rev. Mod. 66 (1994) 1125

[Bou01] F. Bouquet, R. A. Fisher, N. E. Philips, D. G. Hinks and J. D. Jorgensen. Phy. Rev. Lett. **87** 2001) 047001

[Bou01b] F. Bouquet, Y. Wang, R. A. Fisher, D. G. Hinks, J. D. Jorgensen, A. Junod and N. E. Philips. Europhys. Lett. **56** (2001) 856

[Bud01a] S. L. Bud'ko, C. Petrovic, G. Lapertot, C. E. Cunningham, P. C. Canfield, M. H. Young and A. H. Larseda Phy. Rev. B. **63** (2001) 220503

[Bud01b] S. L. Bud'ko, G. Lapertot, C. Petrovic, C. E. Cunningham, N. Anderson and P. C. Canfield. Phy. Rev. Lett. **86** (2001) 1877

[Bur89] J. K. Burdet and G. J. Miller, Chem. Mater. **2**, 12 (1989)

[Buz01] C. Buzea and T. Yamashita Super. Science and Tech. **14** R115(2001)

[Cam72] A. M. Campell and J. E. Evetts Adv. Phys. **21** (1972) 199

[Can01] P. C. Canfield, D. K. Finnemore, S. L. Budko, J. E. Osten, G. lapertot, C. E. Cunningham and C. Petrovic, Phy. Rev. Lett. **86** (2001) 2423

and C. Petrovic, Phy. Rev. Lett. **86** (2001) 2423

[Che89] D. X Chen, R. B. Goldfarb, J. Appl. Phy. **66** (1989)2489

[Cyr91] M. Cyrot and D. Pavuna, Intrudction to Superconductivity and high $T_c$ material. World Scientific Publishing Singapore.

[Dew74] Dew-Hughes, Phil. Mag. **30** (1974) 293

[Dew87] Dew-Hughes, Phil. Mag. **55** (1974) 459

[Dou01] S. X. Dou, X. L. Wang, J. Horvat, D. Milliken, A. H. Li, K. Konstantinov, E. W. Collings, M. D. Sumtion and H. K. Liu. Physica C **361** (2001) 79-83

[Dou01] S. X. Dou, S. Soltanian, J. Horat, W. L. Wang, S. H. Zhou, M. Lonescu, H. K. Liu, P. Munroe and M. Tomsic, Appl. Phys. Lett. **81** (2002) 3419

[Dou01] S. X. Dou, V. Braccini, S. Soltanian, R. Klie, Y. Zhu, S. Li, X. L. Wang and D. Larbalestier, Cond-mat/0308265 (2003)

[Dou05] S. X. Duo, A. V.Pan, M. J. Qin and T. Silver. Frontiers in Superconducting Materials Materials 2005 Springer Verlang

[Eis07] M. Eisterer, Supercond. Sci. and Tech. **20** (2007) R47

[Fei89] M. V. Feigel'man V. B. Geshkenbein, A. I. Larkin and V. M. Vinkur, Phys. Rev. Lett. **63**, 2303(1989)

[Fei90] M. V. Feigel'man, V. B. Geshkenbein and A. I. Larkin, Physica C **167**,177(1990)

[Fen03] Y. Feng, G. Yan, Y. Zhao, A. K. Pradhan, C. F. Liu, P. X. Zhang and L. Zhou, Cond-Mat 15 (2003) 6395-6402

[Fri63] J. Friedal, P. G. de Gennes and J. Matricon, Appl. Phys. Lett. **2** (1963) 119

[Glo01] B. A. Glowacki, M. Majoros, M. Vickers, J. E. Evetts, Y. Shi, I. McDougall, Sup. Sci. Tech. **14** (2001) 193

[Gon01] A.F. Goncharov, V.V. Struzhkin, E. Gregoryanz, H.K. Mao, R.J. Hemley, G.lapertot,

S.L. Budko, P.C. canfield and I.I. Mazin, Cond-Mat/0106258 (2001)

[Gol01] W. Goldacker, S. I. Schlachter, S. Zimmer, and H. Reiner, Supercond. Sci. Tech. **14** (2001) 787

[Gra03] G. Grasso, A. Malagoli, M. Modica, A. Tumino, C. Ferdeghini, A. S. Siri, C. Vignola, L. Martini, V. Previtali and G. Volpini, Sup. Sci. Tech. 16 (2003) 271

[Gri94] R. Griessen, Wen Hai.hu, A. J. J. Van Dalen, B. Dam, J. Rector and H. G. Schnack, Phy. Rev. Lett. 72 (1994) 1920

[Gri94a] Griessen, Wen Hai.hu, A. J. J. Van Dalen, J. Rector, H. G. Schnack, S. Libbrecht, E. Osquiguil and Y. Bruynseraede, Phy. Rev. Lett. 72 (1994) 1910

[Hag89] C. W. Hagen, R. P. Griessen and E. Salomons, Physica C **157**(1989) 199

[Hag89b] C. W. Hagen and R. P. Griessen, PRL. 62(1989) 2857

[Hag90] C. W. Hagen and R. P. Griessen, Studies of High Temperature Superconductors. Vol. **3**, ed. A. V. Narlikar, Nova Science Publishers Ny. (1990) 159

[Hin01] C. Hinks and J. D. Jorgensen. Nature **411** (2001) 457

[Jin01] R. Jin, M. Paranthaman, H. Y. Zhai, H. M. Christen, D. K. Christen and D. Mandrus. Cond-Mat/010441 (2001)

[Hor04] J. Horvat, S. Sultanian, A. V. Pan and X. L. Wang Jour. App. Phy. No. 8 . Vol. **96** (2004)4242

[Jin01b] Jin. S et al. Nature **411** (2001) 563

[Jin03] Hao Jin, Hai-Hu Wen, Hai-Peng Yang. Zhi-Yong Liu, Zhi-An Ren, Guang-Can Che and Zhong-Xian Zhao, Appl. Phy. Lett. **83** (2003) 13

[Jon54] M.E. Jones and R.E. Marsh ,JACSAT **76** (1954) 1434

[Jor01] J. D. Jorgensen,D.G. Hinks and S.Shorts , Phys. Rev. B **63** (2001)224522

[Jos01] A. G. Joshi, C. G. S. Pillai, P. Raj and S. K. Malik, Sol. Stat. Com. **118** (2001) 445

[Kar01] J. Kartus, I.I. Mazin, K.D. Belaschenko, V.P. Antropov and L.L. Boyer, Phys. Rev. Lett. **86** (2001) 4656.

[Kara01] G. Karapetrov, M. Iavarone, W. K. Kwok, G. W. Crabtree and D. G. Hinks, Phys. Rev. Lett. **86** (2001) 4374

[Kes04] S. Keshavarzi, M. J. Qin, S. Soltanian, H. K. Liu, S. X. Dou, Physica C **601** (2004) 408

[Kot01] H. Kotegawa, K. Ishida, Y. Kitaoka, T. Muranaka and J. Akimitsu, Phys. Rev.Lett. **87** (2001) 127001

[Kov02] Kovac P et al. Supercon. Sci. Tech **15** (2002) 1340

[Kov03] Kovac P et al. Supercon. Sci. Tech **16** (2003) 292

[Kov06] P. Kovac, I. Husek, T. Melisek, M. Kulich and V. Strbik, Supercon. Sci. Tech **19** (2003)600

[Kus02] I. Kušević, Ž. Marohnić, E. Babić, Đ. Drobac, X. L. Wang, S. X. Dou, Sol. Sat. Com. **122** (2002) 347

[Lar01] D. C. Larbalestier et al Nature (London) **410**, 186 (2001)

[Lar79] A. I. Larkin, and Yu. N. Ovchinnikov, Jour. Low. Temp. Phy. **34** (1979) 409 012509

[Lee01] S. Lee, H. M0ri, T.Masui, Y. Eltev, A. Yamamoto, and S. Tajima, J. Phys. Rev. B **63** (2001)

[Lee01a] S. Lee, H. Mori, T.Masui, Y. Eltev, A. Yamamoto, and S. Tajima, J. Phys. Rev. B **63** (2001) 012509.

[Liu01] A.Y.Liu, I.I. Mazin and J. Kortus, Phys. Rev. Lett. **87** (2001) 087005.

[Mal90] M. P. Maley, J. O. Willis, H. Lessure, and M. E. McHenry, Phy. Rev. B **42** (1990) 2639

[Mar04] E. Marinez and R. Navarro, Appl. Phy. Lett. **85** (2004) 8

[Maz03] I.I. Mazin a, V.P. Antropov Physica C **385** (2003) 49–65

[Mum01] A. Mumtaz, W. Setyawan and S. A. Shaheen, Phy. Rev. B **65** (2001) 020503(R)

[Mur05] T. Muranaka, Y. Zenitani, J. Shimoyama and J.Akimitsu Frontiers in Superconducting Materials 2005, Springer.Verlang

[Nag01] J .Nagamatsu, N. Nakagawa, T. Muranaka, Y. Zenitani and J.Akimitsu, Nature **410**, 63 (2001)

[Nee05] Neeraj Khara, D. P. Singh, and A.K Gupta, Jour. Appl. Phy. **97** (2005) 076103

[Nis01] E. Nishiburi, M.Takata, M.Sakata, H.Tanaka, T.Muranaka and J.Akimitsu, J.Phys.Soc. Jpn. **70** (2001) 2252

[Oik02] K. Oikawa, T.Kamiyama,T.Mochiku,H.Takeya, M.Furuyama, S.Kamisawa, M.Arai, and K.Kadowaki, J.Phys.Soc. Japan. **71** (2002)L795

[Pra01] K. Prassides, Y.Iawasa, T.Ito, D.H.Chi, K.Uehara, E. Nishibori, M.Takata, M.Sakata, Y.Ohishi, O.Shimomura, T.Muranaka and J.Akimitsu, Phys. Rev. B **64** (2001) 012509

[Pri03] S. L. Prischepa, M. L. Della Rocca, L. Maritato, M. Salvato, R. Di Capua, M. G. Maglione and R. Vaglio, Phy. Rev. B **67** (2003) 024512.

[Qin02] M. J. Qin, X. L. Wang, H. K. Liu and S. X. Dou, Phys. Rev. B 65 (2002) 132508

[Reg01] M. A. Regan, T. He Hayward, S. M. Loureiro, and R. J. Cava, cond-mat/0106585 (2001)

[Sch01] S. Schlachter, W.H. Fietz, K. Grube and W. Goldacker, Advances in gryogenic engineering: Proceeding of ICMC, **48** (2002) 809 Cond.Mat/0107205(2001)

[Sch06] S. I. Schlachter, A. Frank, B. Rinsdorf, H. Orsschulko, B. Obst, B. Liu, W. Goldacker, Physica C 445-448 (2006) 777-783

[Sha01] A. Sharoni, I. Felner and O. Millo, Phys. Rev. B **63** (2001) 220508(R)

[Shi06] Z. X. Shi, J. Wang, H. Lv, T. Tamegai, Physica C **449** (2006) 104-108

[Sol01] Soltanian S et al. Physica C **361** (2001) 84

[Sol03] S. Soltanian, J. Horat, X. L. Wang, P. Munroe, S. X. Dou, Physica C **390** (2003) 185.

[Suo01] Suo H L et al. Appl. Phys. Lett **79** (2001) 3116

[Sou03] S. Souma, Y. Machida, T. Sato, T. Takahashi, H. Matsui, S. –C. Wang, H. Ding, A. Kaminski, J. C. Campuzano, S. Saaki and K. Kadowaki, Nature **423** (2003) 65

[Suh80] H. Suhl, B.T. Matthias and L.R. Walker, Phys. Rev. Lett. **45** (1980) 1352

[Sum04] M. Sumption, M. Bhatia, S. X. Dou, M. Tomsic, L. Arda, M. Ozdemir, Y. Hascicek and E. W. Collings, Supercond. Sci. Tech. **17** (2004) 1180

[Sus07] M. A. Susner, M. D. Sumption, M. Bhatia, X. Peng, M. J. Tomsic, M. A. Rindfleisch, E. W. Collings, Physica C **456** (2007) 180-187

[Tin88] M. Tinkham, Phy. Rev. Lett. **61** (1988) 1658

[Tak02] Y.Takano, H.Takeya, H. Fujii, H. Humakura, T. Hatanu and K. Togano, Appl. Phys. Lett. **78**, 2914 (2001)

[Tan91] K. Tanigaki, T. W. Ebbesen, S. Saito, J. Mizuki, J. S. Tsai, Y. Kubo and S. Kuroshima, Nature **352** (1991) 814

[Tsu01] S. Tsuda, T. Yokoya, Y. Takano, H. Kito, A. Matsushita, F. Yin, J. Itoh, H. Harima and S. Shin, Phys. Rev. Lett. **91** (2003) 127001

[Tsu03] S. Tsuda, T. Yokoya, T. Kiss, Y. Takano, K. Togano, H. Kito, H. Ihara and S. Shin, Phys. Rev. Lett. **87** (2003) 177006

[Tuo88] M. Tuominen, A. M. Golgman, M. L. McCartney, Physica C 153-155, **324** (1988)

[Vin95] V. M. Vinokur, P. H. Kes, and A. E. Koshelev, Physica C **248** (1995) 179

[Vog01] T. Vogt, G. Schneider, J. A. Hriljac, G. Yang and J. S. Abell, Phys. Rev. B **63** (2001) 220505(R)

[Wan01] Y. Wang, T. Plackowski and A. Junod. Physica C **355** (2001) 179

[Wan01b] Wang X L et al. Physica C **361** (2001) 149

[Wan04] X. L. Wang, Q. W. Yau, J. Horvat, M. J. Qin and S. X. Dou, Supercon. Sci. Tech. 17 No 3 (2004) L21

[Wen01] H. H. Wen, S. L. Li, Z. W. Zhao, H. Jin, Y. M. Ni, Z. A. Ren, G. C. Che, Z. X. Zhao, Physica C **363** (2001) 170- 178

[Won67] V. K. Wong and C.C. Sung, Phys. Rev.Lett. **19** (1967) 1236

[Wu04] L. Wu, Y. Zhu, T. Vogt, H. Su and J. Davenport, Phys. Rev. B **69** (2004) 064501.

[Xu01] M. Xu, H. Kitazawa, Y. Takano, J. Ye, K. Nishida, H. Abe, A. Matsushita and G. Kidu. Cond-Mat./0105271 (2001)

[Xu03] S. Y. Xu, Qi Li, E. Wertz, Y. F. Hu, A. V. Pogerebnyakov, X. H. Zeng, X. X. Xi and J. M. Redwig, Phy. Rev. B **68**, (2003) 224501

[Yau05] G. Yuan, X. Xu, Z. Wang, D. Lu, X. Jin, Sol. Stat. Com. **135** (2005) 352-355

[Yil01] T. Yildirim, *et al*., Phys. Rev. Lett. **87**, 37001 (2001)

[You03] R. A. Young, Editor, The Rielveldoa, Oxfor University Press, Oxford (2003)

[Zel90] E. Zeldov, N. M. Amer, G. Koren, A. Gupta, M. W. McElfresh and R. J. Gambino, Appl. Phys. Lett. **56**, 680 (1990)

# CURRICULUM VITAE


## Saleh MOHAMMAD

**Village Dagi Tehsil and Distt Swabi Pakistan**

**Date of birth: 15 April 1969**

**Telephone No: +92-0-938-311159**

**Full clean driving licence**

**Email: saleh.dagiwal@gmail.com**


## CAREER PROFILE

- An enthusiastic experimental Physicist committed to a career in teaching and research.
- An excellent communicator with experience in teaching.

## EDUCATION & QUALIFICATIONS

**Dec 2003 – to date** **Doctor of Technical Science PhD (In progress)**

**Institute of Solid State Physics**

**Vienna University of Technology**

- Modules include courses on Low Temperature Physics, Magnetic Relaxation Processes, Magnetism in the Solid State, Electron Beam Techniques for Nano-analysis
- Project "**Influence of Non-Superconducting Additions on the Pinning Behavior in MgB2 Wires and Bulk samples -a Comparative Study**"

**April 1990 – June 1992** **MSc Physics (Grade B)**

**University of Peshawar**

- Modules include Courses on Classical Physics, Solid State Physics, Nuclear Physics, Modern Physics, Quantum Physics, Basic Electronics, Mathematical Physics, Thermodynamics, Statistical Mechanics.

- Final Year project “Preparation of Superconducting Material”

**Sept 1987 – June 1989** **BSc ( Grade B)**

**Govt College Swabi**

- Physics, Applied Mathematics, Pure Mathematics

---

## EMPLOYMENT

**Oct 1992 – Sept 1995** **Lecturer Physics**

**PAF College Risalpur NWFP PAKISTAN**

- Responsible to teach physics to HSSC classes
- Physics Laboratory In-charge

**Oct 1995 – Nov 2003** **Lecturer Physics**

**PPS College Peshawar**

- Teaching Physics to HSSC Classes
- House In-charge
- Physic Laboratory In-charge

## Referees:

Ao. Prof. Dr. Michael REISSNER

Institute of Solid State Physics

Vienna University of Technology

Austria

Tel: +43-1-58801-13772

Email: reissner@ifp.tuwien.ac.at

Dr. Shah Khusro

Computer Science Department

University of Peshawar

Pakistan

Tel: +92-3443445008

Email: shah_khusro@yahoo.com